Wegener Center for Climate and Global Change
University of Graz

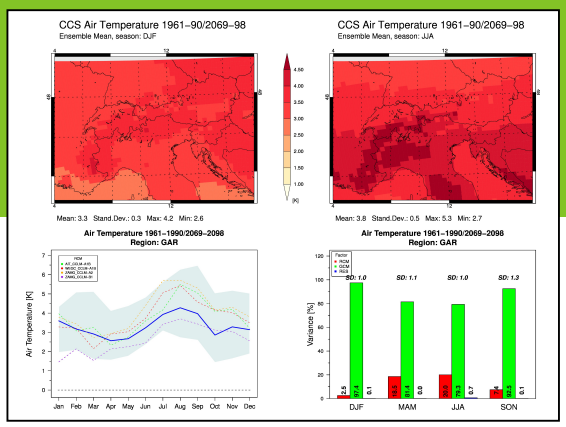

Scientifc Report No. 50-2013

Expected Climate Change and its Uncertainty in the Alpine Region

Extended Uncertainty Assessment of the reclip:century and ENSEMBLES Multi-Model Dataset

G. Heinrich, A. Gobiet, H. Truhetz, T. Mendlik

May 2013

Kindly supported by the Austrian Climate Research Program (ACRP), Klima- und Energiefonds der Bundesregierung, project number A963768

The **Wegener Center for Climate and Global Change** combines as an interdisciplinary, internationally oriented research institute the competences of the University of Graz in the research area „Climate, Environmental and Global Change“. It brings together, in a dedicated building close to the University central campus, research teams and scientists from fields such as geo- and climate physics, meteorology, economics, geography, and regional sciences. At the same time close links exist and are further developed with many cooperation partners, both nationally and internationally. The research interests extend from monitoring, analysis, modeling and prediction of climate and environmental change via climate impact research to the analysis of the human dimensions of these changes, i.e., the role of humans in causing and being effected by climate and environmental change as well as in adaptation and mitigation. (more information at www.wegcenter.at)

The present report is the result of work package 4, task 4.2, of the project “Research for Climate Protection: Century Climate Simulations (reclip:century 2)” (reclip.ait.ac.at/reclip_century), funded by the Austrian Climate Research Program (ACRP), project number A963768 and completed in September 2012.

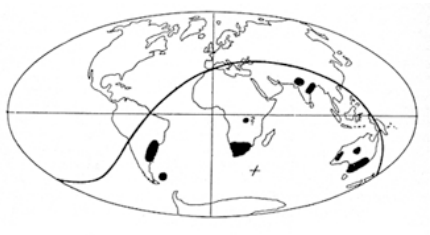

Alfred Wegener (1880-1930), after whom the Wegener Center is named, was founding holder of the University of Graz Geophysics Chair (1924-1930) and was in his work in the fields of geophysics, meteorology, and climatology a brilliant, interdisciplinary thinking and acting scientist and scholar, far ahead of his time with this style. The way of his ground-breaking research on continental drift is a shining role model — his sketch on the relationship of the continents based on traces of an ice age about 300 million years ago (left) as basis for the Wegener Center Logo is thus a continuous encouragement to explore equally innovative scientific ways: *paths emerge in that we walk them* (Motto of the Wegener Center).

Wegener Center Verlag • Graz, Austria

ISBN 978-3-9503112-7-3

May 2013

Contact: Georg Heinrich
g.heinrich@uni-graz.at

Wegener Center for Climate and Global Change
University of Graz
Brandhofgasse 5
A-8010 Graz, Austria
www.wegcenter.at

Introduction I-4

I Update of the reclip:century 1 uncertainty analysis I-5

I-1 Climate Model Data and Study Regions I-5

I-2 Missing Data Reconstruction I-6

I-3 Representation of Uncertainty I-7

I-4 Results I-8

I-4.1 Air Temperature I-8

I-4.2 Precipitation Amount I-9

I-4.3 Global Radiation I-11

I-4.4 Relative Humidity I-12

I-4.5 Wind Speed I-14

I-5 Summary I-15

Appendix I I-17

II Extended RCM projections for Europe based on ENSEMBLES and CMIP3 ..... II-38

II-1 Introduction II-38

II-2 Climate Model Data and Study Regions II-40

II-3 Missing Data Reconstruction Methods II-41

II-3.1 Additive Methods II-41

II-3.2 Scaling Methods II-42

II-4 Design of the Cross-Validation and Statistical Analysis II-43

II-4.1 Cross-Validation II-43

II-4.2 Statistical Analysis II-44

II-5 Results of the Cross-Validation II-45

II-6 Revision of expected regional climate change and its uncertainty over Europe II-49

II-7 Summary and Conclusions II-52

Appendix II II-54

References II-64

Introduction

Future projections of regional climate are subject to different sources of uncertainties stemming from the natural variability of the climate system, from unknown future greenhouse gas (GHG) emissions, from errors and simplifications in global climate models (GCMs), and from the dynamical downscaling with regional climate models (RCMs). In Heinrich and Gobiet (2011b), a more detailed discussion of the individual uncertainty components is provided.

The resulting uncertainties in regional climate scenarios can be assessed by analysing an ensemble of climate simulations, which adequately samples the various sources of uncertainty. In this report, we assess the uncertainty of the 10 km high resolution climate simulations for the Alpine region produced in the projects reclip:century 1 and reclip:century 2 (Loibl et al. 2011) by putting them into the context of the most recent and most comprehensive ensemble of RCM projections for Europe from the EU FP6 Integrated Project ENSEMBLES (http://www.en-sembles-eu.org/).

In phase 1 of reclip:century, the basic uncertainty estimation was set up (Heinrich and Gobiet 2011b). Based on variance decomposition methods (Déqué et al. 2007) the uncertainties of seasonal mean air temperature and precipitation climate change signals for the mid-century in various Alpine climate sub-areas were investigated. In phase 2 of the project, we aim at updating the uncertainty estimation by extending the analysis from mid to end of the 21st century. In addition, we extend the uncertainty analysis to the entire set of "key climate variables" for climate change impact research: air temperature, precipitation, global radiation, relative humidity, and wind speed. Furthermore, we develop and investigate methods in order to combine uncertainty from the coarser scale GCM projections of CMIP3 (Meehl et al., 2007) with fine-scale uncertainty of the ENSEMBLES RCM projections.

The report is structured in two parts. In part I, we provide an update of the uncertainty estimation conducted in the first part of reclip:century by extending the analysis until the end of the 21st century and by incorporating global radiation, relative humidity, and wind speed in addition to air temperature and precipitation. In part II of the report, we assess and compensate the GCM sampling bias in expected regional climate change and the associated uncertainty of the ENSEMBLES RCM projections by combining them with the full set of the CMIP3 GCM ensemble.

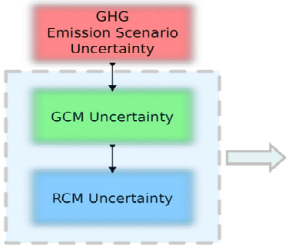

	ARPEGE	BCM	CGCM3	ECHAM5-r3	HadCM3Q0	HadCM3Q3	HadCM3Q16	IPSL	*8 GCMs*
C4I_RCA	1.79	0.69	1.64	1.17	2.40	1.95	2.02	1.63	*1*
CNRM_RM4.5	2.12	1.01	1.96	1.49	2.72	2.27	2.34	1.95	*1*
CNRM_RM5.1	1.74	0.64	1.59	1.11	2.34	1.90	1.97	1.58	*1*
DMI_HIRHAM	1.50	0.47	1.37	0.87	2.13	1.68	1.75	1.36	*3*
ETHZ_CLM	1.79	0.70	1.65	1.17	2.40	1.95	2.03	1.64	*1*
GKSS_CLM	1.74	0.64	1.59	1.12	2.35	1.90	1.97	1.58	*1*
ICTP_RegCM	1.78	0.68	1.63	1.16	2.39	1.94	2.01	1.62	*1*
KNMI_RACMO	2.06	0.96	1.91	1.44	2.67	2.22	2.29	1.90	*1*
METNO-HIRHAM	1.64	0.81	1.49	1.02	2.18	1.80	1.88	1.48	*2*
METO-HC_HadRM3	2.10	1.00	1.95	1.48	2.79	2.17	2.34	1.94	*3*
MPI_REMO	1.92	0.82	1.77	1.30	2.53	2.08	2.16	1.76	*1*
OURANOS_CRCM	2.19	1.09	2.04	1.57	2.80	2.35	2.43	2.03	*1*
SMHI_RCA	1.93	0.71	1.78	1.33	2.53	2.18	2.16	1.77	*3*
UCLM_PROMES	1.83	0.73	1.68	1.21	2.44	1.99	2.07	1.67	*1*
VMGO_RRCM	1.48	0.38	1.33	0.85	2.08	1.64	1.71	1.32	*1*
15 RCMs	*3*	*3*	*1*	*5*	*5*	*2*	*2*	*1*	***22***

Fig. 1 The GCM-RCM simulation matrix of the 25 km of the EU FP6 Integrated Project ENSEMBLES. The orange and green highlighted cells are the available simulations until 2050 and 2100, respectively. The values indicate the simulated and reconstructed changes in summer air temperature for the Greater Alpine Region.

I Update of the reclip:century 1 uncertainty analysis

I-1 Climate Model Data and Study Regions

In reclip:century, a mini-ensemble of four RCM simulations until the end of the 21st century was produced (Loibl et al. 2011). The simulation domain covers the entire Alpine region and the RCMs were driven with a very high horizontal resolution of only 10 km. The ensemble consists of four RCM simulations with CCLM: AIT-CCLM which is driven by the GCM HadCM3 and forced by the A1B emission scenario, WEGC-CCLM which is driven by the GCM ECHAM5 run 2 and forced by the A1B emission scenario, and two ZAMG-CCLM simulations which are driven by the GCM ECHAM5 run 2 and forced by the A2 and B1 emission scenarios. Therefore, some spread due to the future GHG emission scenario is spanned by the WEGC and ZAMG simulations (same GCM and RCM, different emission scenarios) and uncertainty due to the driving GCM is partly spanned by the WEGC and AIT simulations (same RCM and emission scenario, different GCMs with very different characteristics). Uncertainty due to natural variability is only implicitly regarded by using different GCMs and uncertainty due to the formulation of RCMs is not covered (only CCLM is used). This means, that three of the four major uncertainty components are covered to some degree by the reclip:century ensemble.

This mini-ensemble is supplemented by further RCM simulations from the ENSEMBLES project. In ENSEMBLES, a set of 22 (15) high resolution RCM simulations for entire Europe until the mid (the end) of the 21st century has been produced (Fig. 1). The simulations have a horizontal grid spacing of about 25 km and the lateral boundary conditions (LBCs)were provided by eight different GCMs. Due to limited computational resources, not all possible GCM-RCM combinations could be realised in ENSEMBLES. The simulation matrix mainly addresses uncertainty in LBCs (choice of the driving GCM) and RCM uncertainty which is not covered by the reclip:century ensemble (van der Linden and Mitchell 2009). Uncertainty due to natural variability is again only implicitly regarded by using different GCMs. Concerning future GHG emissions, only the A1B emission scenario (Nakicenovic et al. 2000) was used. Therefore, three of the four major uncertainty components are covered by the ensemble. A rough estimate to which extent the overall uncertainty is underestimated by only using

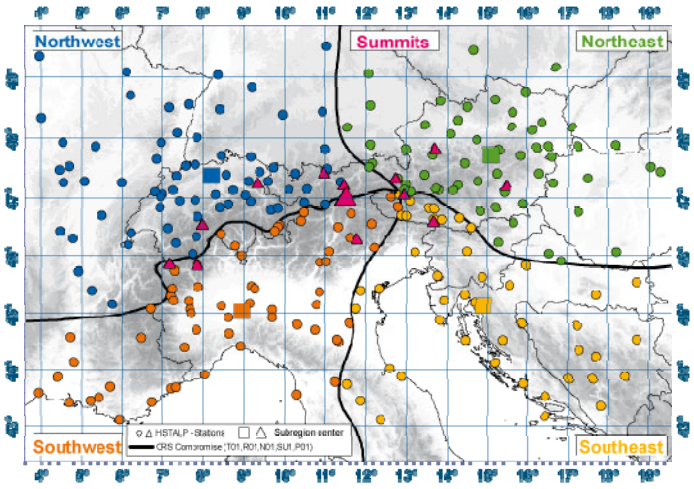

Fig. 2 The regions studied. The left panel depicts the four HISTALP regions GAR-Northwest, GAR-Northeast, GAR-Southwest, and GAR-Southeast (picture taken from www.zamg.ac.at/histalp/). The right panel shows the eight European subregions used for the extension of the uncertainty analysis to unknown GCMs.

one emission scenario can be obtained from Prein et al. (2011). The relative contribution of emission scenario to overall uncertainty until the mid of the 21st century is very small (below 6 %) for both air temperature and precipitation amount. Until the end of the 21st century, this fraction increases for air temperature to about 35 %, but remains very small for precipitation (Prein et al. 2011).

The analysis of the reclip:century simulations with respect to the A1B uncertainty range of the ENSEMBLES simulations aims at facilitating the interpretation of the reclip:century simulations and indicating their position within the A1B uncertainty range. As study domain, the Greater Alpine Region (GAR) and four subregions within the GAR are investigated (Fig. 2). In order to provide comparable results between the mid and the end of the 21st century, we restrict our analysis to the 15 ENSEMBLES simulations extending until the end of the 21st century for both time horizons. Results based on the full ensemble until 2050 for air temperature and precipitation amount can be found in Heinrich and Gobiet (2011b).

I-2 Missing Data Reconstruction

The GCM-RCM simulation matrix of ENSEMBLES shown in Fig. 1 reveals that a large fraction of RCMs was forced by the GCM ECHAM5-r3 until the end of the 21st century (5 out of 15 simulations). Therefore, this particular GCM is overweighed compared to the other GCMs and even simple estimates for expected climate change and its uncertainty such as ensemble mean or variability are potentially biased towards the climate response of ECHAM5-r3. In order to avoid biased estimates, the missing climate change signals (CCSs) of Fig. 1 are reconstructed following Déqué et al. (2007) as in the first phase of reclip:century. The reconstruction method is embedded in the framework of an analysis of

variance (ANOVA), neglecting the highest interaction term in order to reconstruct the actual missing value. The reconstruction algorithm writes in case of the ENSEMBLES simulation matrix as follows:

$$\Delta X_{ij} = \Delta X_{i\bullet} + \Delta X_{\bullet j} - \Delta X_{\bullet\bullet} = \Delta X_{\bullet\bullet} + (\Delta X_{i\bullet} - \Delta X_{\bullet\bullet}) + (\Delta X_{\bullet j} - \Delta X_{\bullet\bullet}) \qquad (1)$$

where ΔX denotes the CCS of a RCM for a specific subregion, i the index of the RCM and j the index of the driving GCM. The dot operator denotes averaging across the according indices. The reconstruction algorithm can be intuitively understood: consider RCM1 driven by a set of GCMs and RCM2 driven by the same GCMs except one. This missing value is then reconstructed by adding the mean difference between RCM2 and RCM1 to RCM1. Since the reconstruction of the missing values depends on the grand mean of the entire GCM-RCM matrix, 100 iterations are performed.

I-3 Representation of Uncertainty

Uncertainties of the projected changes are quantified by different measures. The multi-model mean and the median are provided as measures of central tendencies. The 10th and 90th percentiles are used to indicate the range of the projected changes (i.e. 80 % of the projected changes are within this range). As a non-parametric uncertainty measure, we calculate the ensemble accordance which is defined as the percentage of models which show the same sign of change as the multi-model mean.

I-4 Results

I-4.1 Air Temperature

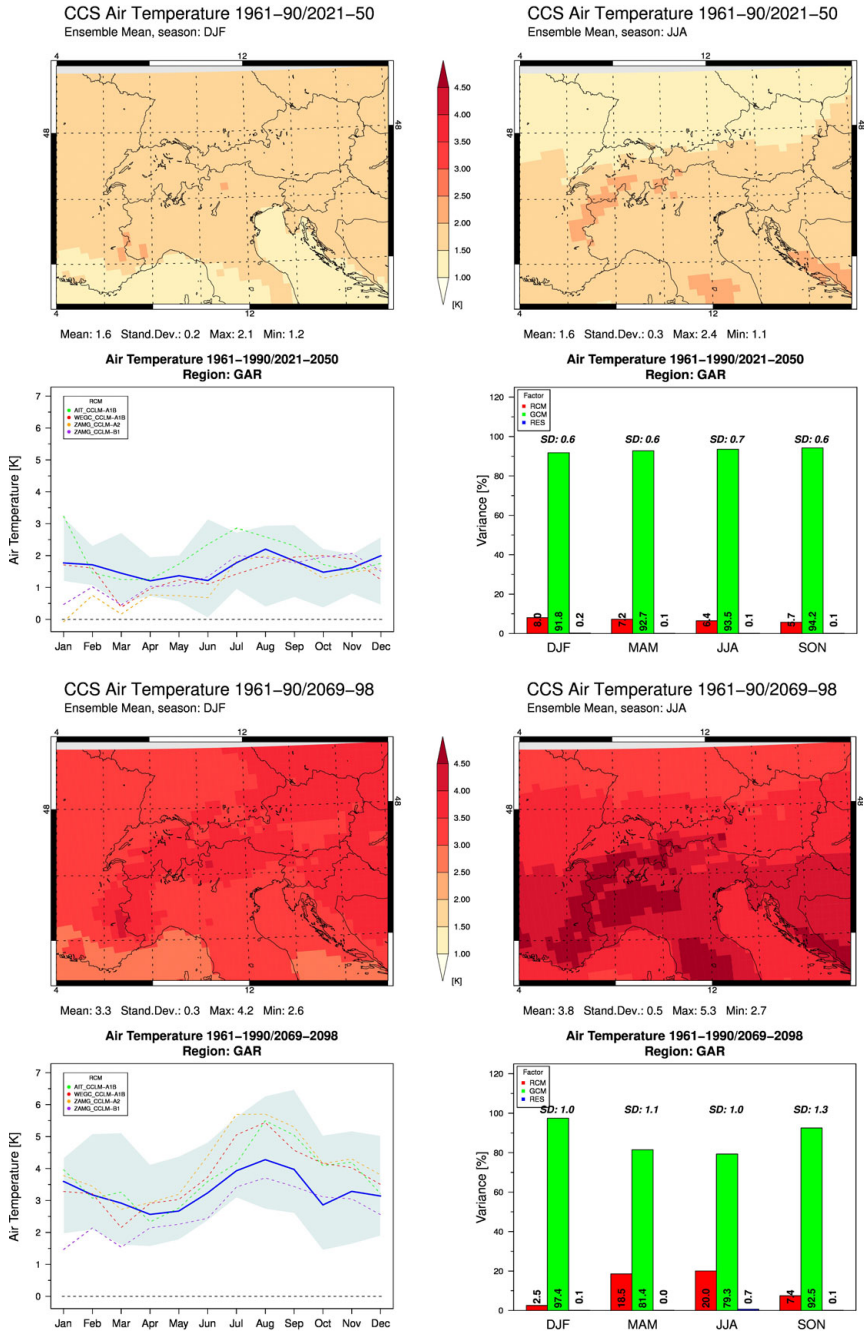

Fig. 3 Projected changes of air temperature in the GAR until the mid (upper four panels) and the end (lower four panels) of the 21st century for the 15 ENSEMBLES simulations. In each block, the upper left and right panels display the changes in DJF and JJA, respectively. The lower left panel shows the annual cycle of the expected changes as thick blue line (50th percentile of the reconstructed CCSs) and the according uncertainties as blue shaded area (range between 10th and 90th percentile of the reconstructed CCSs). The lower right panel shows the results of the ANOVA based on the reconstructed CCSs.

Fig. 3 depicts spatial maps of the multi model mean changes until the mid and the end of the 21st century for air temperature in DJF and JJA for the GAR concerning the original CCS matrix. Furthermore, the annual cycle of the spatial average and the results of the ANOVA concerning the reconstructed CCS matrix are shown. Fig. 3, Fig. A 1, and Fig. A 2 in Appendix I show that the projected changes of 2-m air temperature are positive for entire Europe in all seasons. Regionally, the largest responses are obtained for the north-eastern parts of Europe in winter and for the southern parts of Europe in summer. These differences can be largely explained by the modest warming of the Northern Atlantic, influencing the maritime climate of Western Europe in combination with altered snow-albedo feedback mechanisms in Northern and Eastern Europe (e.g., Rowell, 2005). The high summer temperatures in the south can be related to an earlier and more rapid reduction of soil moisture in spring (e.g. Wetherald and Manabe, 1995; Gregory et al., 1997). The spatial averages of the multi-model mean change for the GAR are seasonally varying between +1.2 K (+2.7 K) in MAM and +1.6 K in JJA and DJF (+3.8 K in JJA) until the mid (end) of the 21st century. A stronger warming along the Alpine ridge is indicated which is highly pronounced in JJA at the end of the 21st century. All models agree in a positive temperature change (warming) in all seasons for both time horizons. Fig. 3 and Fig. A 11 reveal a summer peak of the annual cycle of the reconstructed CCSs which is stronger pronounced until the end of the 21st century. However, the according uncertainties are generally larger for the long-term projections. The reclip:century ensemble is subject to emission scenario uncertainty which is manifested in a large spread of the ensemble until the end of the 21st century and the largest difference is obtained between the A2 and B1 driven ZAMG-CCLM simulations. The ANOVA for the reconstructed ENSEMBLES CCS matrix (Fig. 3 and Fig. A 16) reveals that the choice of the GCM has the largest effect on the total variation concerning both time horizons, all seasons, and sub regions. However, the RCM contribution to overall uncertainty slightly increases until the end of the 21st century mainly in MAM and JJA, and peaks up to 38.2 % for GAR-Northeast in JJA.

I-4.2 Precipitation Amount

Fig. 4 depicts spatial maps of the multi model mean changes until the mid and the end of the 21st century for precipitation in DJF and JJA for the GAR concerning the original CCS matrix. Furthermore, the annual cycle of the spatial average and the results of the ANOVA concerning the reconstructed CCS matrix are shown. The according CCS is calculated as relative difference with respect to the reference period. For Europe, the changes clearly indicate a bipolar north-south pattern with reduced precipitation over southern Europe in summer and increasd precipitation over northern Europe in winter (Fig. A 3). Areas with reduced precipitation show a northward shift from winter to summer which is identified as the European Climate change Oscillation (ECO) and can be related to a seasonal dependent northward shift of the mid-latitude storm track (Giorgi and Coppola, 2007). Fig. 4 and Fig.

A 4 show that the spatial average multi-model mean in the GAR is seasonal varying between -4.1 % (-20.4 %) in JJA and +3.6 % (+10.4 %) in DJF until the mid (end) of the 21st century. A distinct impact of the Alpine ridge on the spatial distribution of the projected precipitation changes is present especially in MAM and SON, indicating an increase of precipitation north of the Alps, while the southern and western parts show a decrease of the multi-model mean. Furthermore, pronounced increases of precipitation along the Alpine ridge in DJF until the end of the 21st century are obtained.

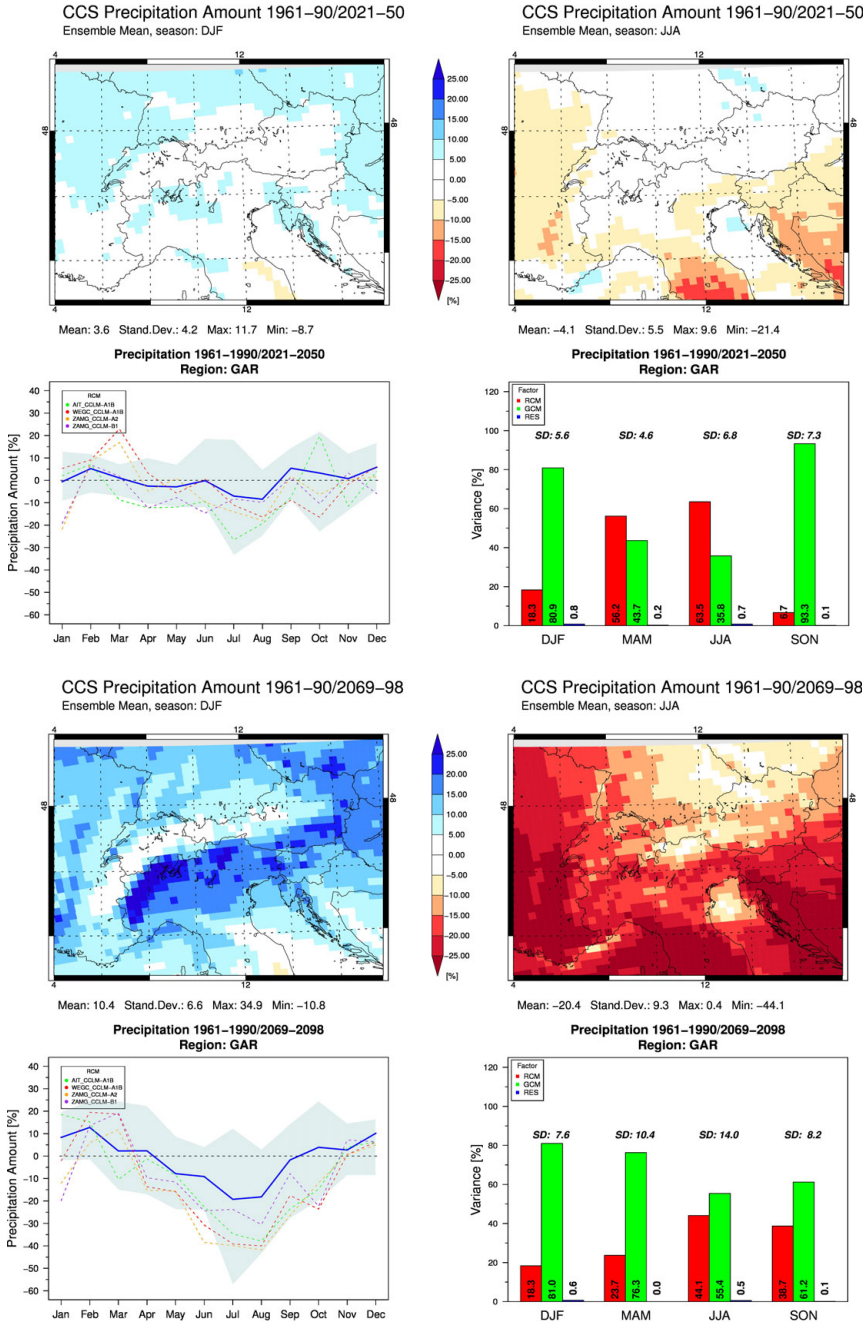

Fig. 4 Same as **Fig. 3** but for precipitation amount.

However, the ensemble accordance indicates here that the sign of the projected changes is highly diverse among the RCMs. The largest accordance is obtained for the decrease in JJA until the end of the 21st century with a spatial mean magnitude of 89.0 %. The annual cycle of the reconstructed CCSs shows an increase in winter and a decrease in summer concerning all sub regions (Fig. 4 and Fig. A 12). The CCSs are generally more pronounced until the end of the 21st century. However, the according uncertainties are rather large, especially for the long-term projections. Fairly similar characteristics are found for the reclip:century simulations. However, especially the expected decrease of summer precipitation and the spread of the ensemble are underestimated by the reclip:century simulations compared to the ENSEMBLES projections, particularly until the end of the 21st century. The ANOVA for the reconstructed ENSEMBLES CCS matrix (Fig. 4 and Fig. A 17) reveals that the choice of the RCM mainly contributes in MAM and JJA to the total variation of the precipitation CCSs. The contribution is generally larger until the mid of the 21st century and shows a maximum of 69.7 % for GAR-Southeast in SON.

I-4.3 Global Radiation

Fig. 5 depicts maps of the multi model mean changes for global radiation in DJF and JJA for the GAR concerning the original CCS matrix, and the annual cycle of the spatial average and the results of the ANOVA concerning the reconstructed CCS matrix until the mid and the end of the 21st century. As it can be seen from Fig. A 3 and Fig. A 5, areas with a global radiation increase (decrease) largely correspond to areas with a decrease (increase) of precipitation amount. This is physically plausible as especially the precipitation producing lower clouds mainly reflect the incoming solar radiation. The spatial multi-model mean in the GAR is seasonally varying between -1.2 W/m^2 (-4.0 W/m^2) in JJA and +0.4 W/m^2 (+3.4 W/m^2) in DJF until the mid (end) of the 21st century (Fig. 5). The spatial pattern reveals a pronounced decrease until the end of the 21st century along the Alpine ridge in MAM. Here, the different RCM projections largely accord in a decrease of global radiation (Fig. A 6). The annual cycle of the reconstructed CCSs indicates a decrease during winter and an increase during summer which is strongly pronounced until the end of the 21st century (Fig. 5 and Fig. A 13). However, the according uncertainties of the projected changes strongly increase until the end of the 21st century. Fairly similar characteristics are found for the reclip:century simulations. However, the expected increase in summer global radiation is overestimated and uncertainty is generally underestimated by the reclip:century simulations compared to the ENSEMBLES projections, particularly until the end of the 21st century. Concerning the results of the ANOVA (Fig. 5 and Fig. A 18), the RCMs generally show a large contribution to the overall variability, particularly until the end of the 21st century (e.g. for the northern HISTALP regions in DJF, MAM, and JJA) with a maximum RCM contribution of 70 % for GAR-Northeast in MAM.

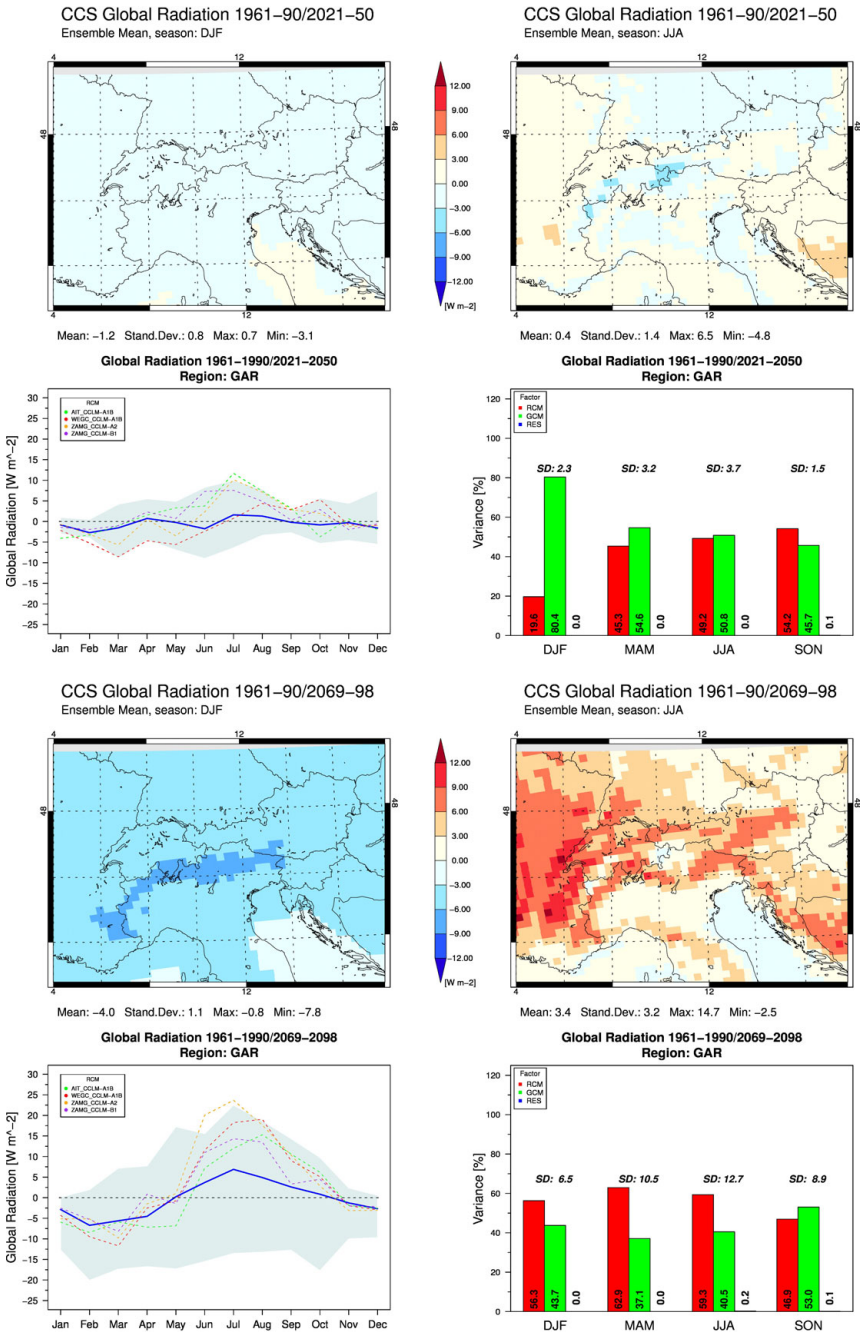

Fig. 5 Same as **Fig. 3** but for global radiation.

I-4.4 Relative Humidity

Fig. 6 depicts maps of the multi model mean changes for relative humidity in DJF and JJA for the GAR concerning the original CCS matrix, and the annual cycle of the spatial average and the results of the ANOVA concerning the reconstructed CCS matrix until the mid and the end of the 21st century. As it can be seen, land areas with an increase (decrease) of relative humidity are related to areas with an increase (decrease) of precipitation amount (Fig. A 3 and Fig. A 7). This is again physically plausible and can be related to the soil moisture-atmosphere feedback. In areas with wet soils, the latent heat

flux due to evapotranspiration dominates and results in enhanced humidity and cloud formation, creating a positive feedback loop . By contrast, dry soils raise the sensible heat flux, resulting in a warmer, drier, and deeper boundary layer which inhibits convection and cloud formation (e.g., Alexander 2011). The spatial multi-model mean in the GAR is seasonal varying between -0.5 % (0.5 %) in DJF and -1.4 % (-3.9 %) in JJA until the mid (end) of the 21st century (Fig. 6). The largest accordance is obtained for the precipitation decrease in JJA until the end of the 21st century with a magnitude of 85.1 % in the spatial mean.

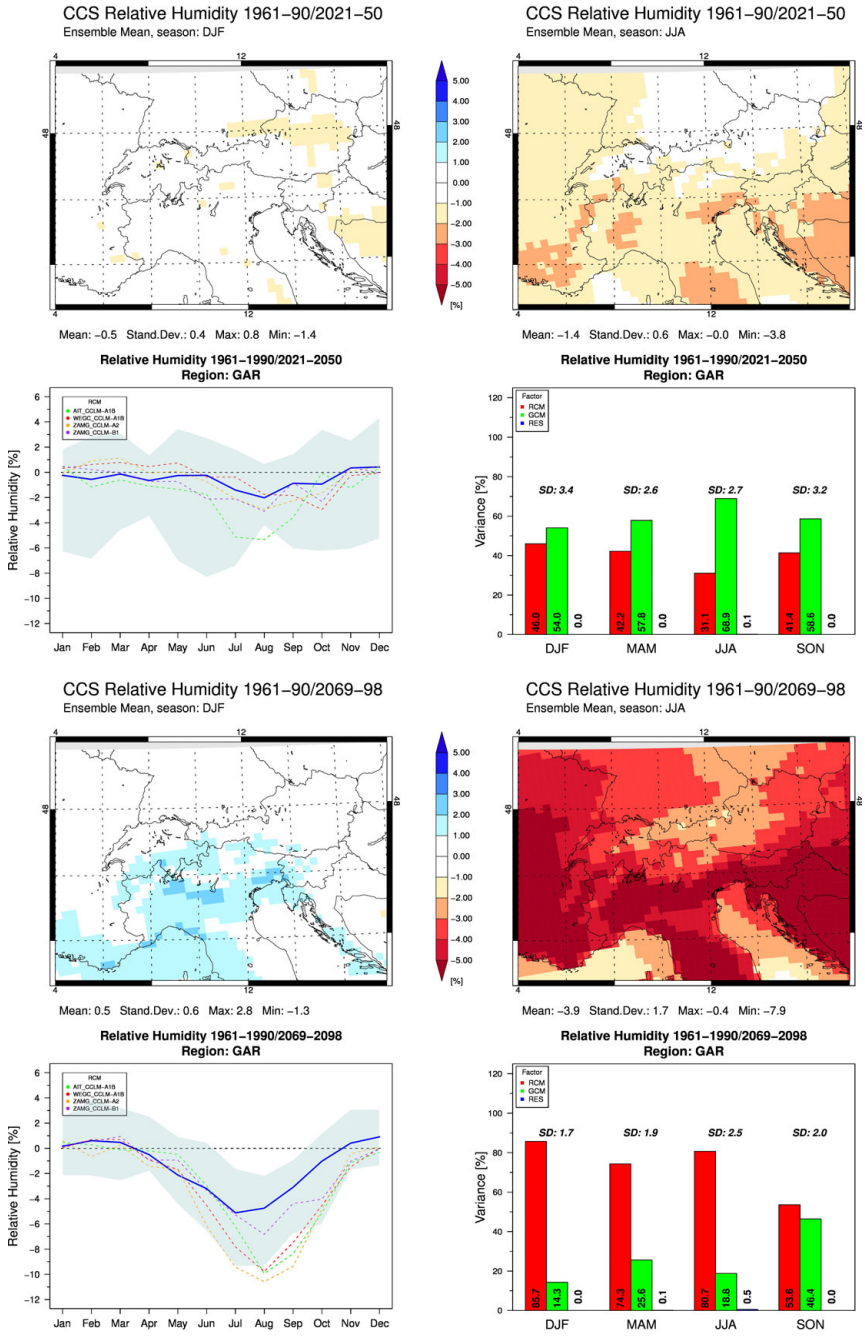

Fig. 6 Same as **Fig. 3** but for relative humidity.

The annual cycle of the reconstructed CCSs (Fig. 6 and Fig. A 14) indicates a decrease during spring and summer which is strongly pronounced until the end of the 21st century. Here, a decrease of relative humidity during the summer months is consistently projected. Fairly similar characteristics are found for the reclip:century simulations. However, especially the expected decrease in summer relative humidity and the spread of the ensemble are underestimated by the reclip:century simulations compared to the ENSEMBLES projections, particularly until the end of the 21st century. The results of the ANOVA (Fig. 6 and Fig. A 19) show that the RCMs largely contribute to the overall variability. The RCM contributions are generally larger until the end of the 21st century for which the choice of the RCM is mostly dominant. The maximum RCM contribution is obtained for GAR-Northwest in DJF with 93.1 %.

I-4.5 Wind Speed

Fig. 7 depicts maps of the multi model mean changes for wind speed in DJF and JJA for the GAR concerning the original CCS matrix, and the annual cycle of the spatial average and the results of the ANOVA concerning the reconstructed CCS matrix until the mid and the end of the 21st century. As it can be seen from Fig. A 9, wind speed shows more pronounced changes over sea areas, especially until the end of the 21st century. Here, mainly a decrease over the European North Atlantic Ocean is obtained which is most pronounced in JJA. The projected changes for the GAR are close to zero in the area mean (Fig. 7 and Fig. A 10). More pronounced decreases are obtained along the Alpine ridge and for the northern parts of the Mediterranean and the Adriatic Sea, particularly in JJA and SON until the end of the 21st century. Especially the decrease in the southern parts until the end of the 21st century in SON shows high accordance between the RCM projections. The annual cycle of the reconstructed CCSs (Fig. 7 and Fig. A 15) indicates a decrease during autumn which is stronger pronounced until the end of the 21st century. However, the according uncertainties increase for the long-term projections. For the reclip:century simulations, the spread of the ensemble is generally underestimated compared to the ENSEMBLES projections, particularly until the end of the 21st century. The results of the ANOVA (Fig. 7 and Fig. A 20) show that the choice of the driving RCM largely contributes to the overall variability, mainly in JJA and SON. The RCM contributions are generally larger until the end of the 21st century. The maximum RCM contribution is obtained for GAR-Northeast in JJA with 38.2 %.

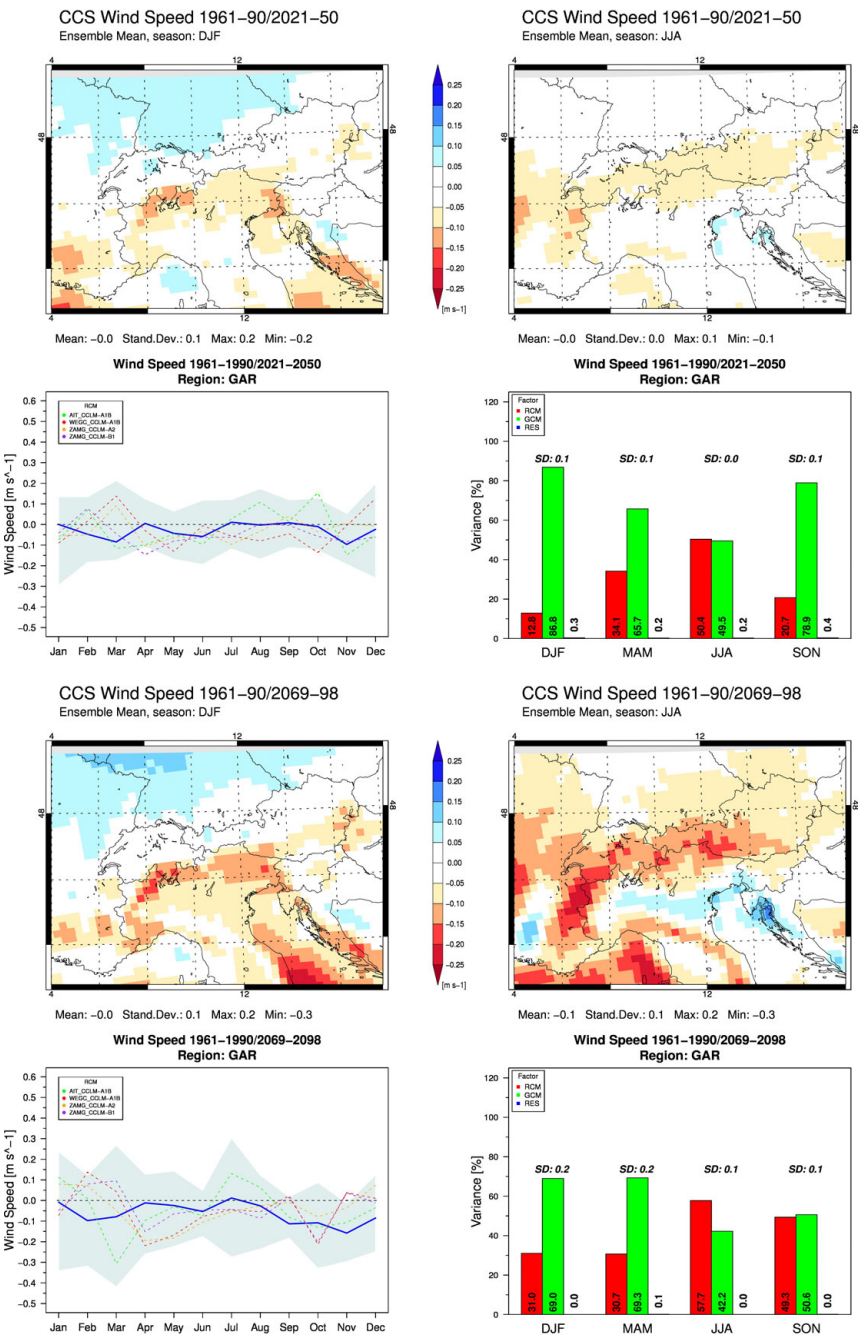

Fig. 7 Same as **Fig. 3** but for wind speed.

I-5 Summary

The RCM ensemble produced in reclip:century is subject to different sources of uncertainty, namely uncertainty due to natural variability, uncertainty due to unknown future GHG emissions scenario, uncertainties due to choice of the driving GCMs. In this report, we updated the uncertainty analysis of the first phase of reclip:century (Heinrich and Gobiet 2011b) by extending the analysis from mid to end of the 21st century. In addition, we extended the uncertainty analysis to the core set of "key climate variables" for climate change impact research: air temperature, precipitation, global radiation,

relative humidity, and wind speed. We analysed the reclip:century simulations in the context of the A1B uncertainty range of the ENSEMBLES simulations which aims at facilitating the interpretation of the reclip:century simulations with respect to their position within the bandwidth of possible future climate under the A1B emission scenario.

The key findings can be summarized as follows:

- The Greater Alpine Region will be considerably affected by global warming in the 21st century. This statement does not only refer to rising temperature, but also to significantly changing precipitation, radiation, and humidity regimes.
- Within 60 years, we expect 1.5°C average warming in the Alpine area (0,25°C per decade in the first half of the 21st century). Until the end of the century (within 110 years), the warming is expected to accelerate and amount 3.3°C (0.36°C per decade in the second half of the 21st century)
- The annual cycle of precipitation is expected to change only slightly in the first half of the 21st century (slight increase in winter and autumn), but considerably until the end of the century: In summer and particularly in the southern regions, precipitation has to be expected de decrease beyond -20%. In turn, the winter is expected to receive more precipitation (about +10%).
- Global radiation until the end of century is expected to decrease in winter and increase in summer.
- Relative humidity until the end of century is expected to strongly decrease in summer.
- Notable changes for mean wind speed are expected along the Alpine main ridge within the 21st century.
- The uncertainty in the climate projections is low for temperature, but considerably higher for the other parameters.
- Qualitatively, the reclip:century simulations fairly well fit into the pattern from the ENSEMBLES simulations
- For air temperature, the choice of the GCM has by far the largest effect on uncertainty, while for all other parameters, the RCMs' contributions are considerably and may even exceed the influence of the GCMs in some regions and seasons.

Appendix I

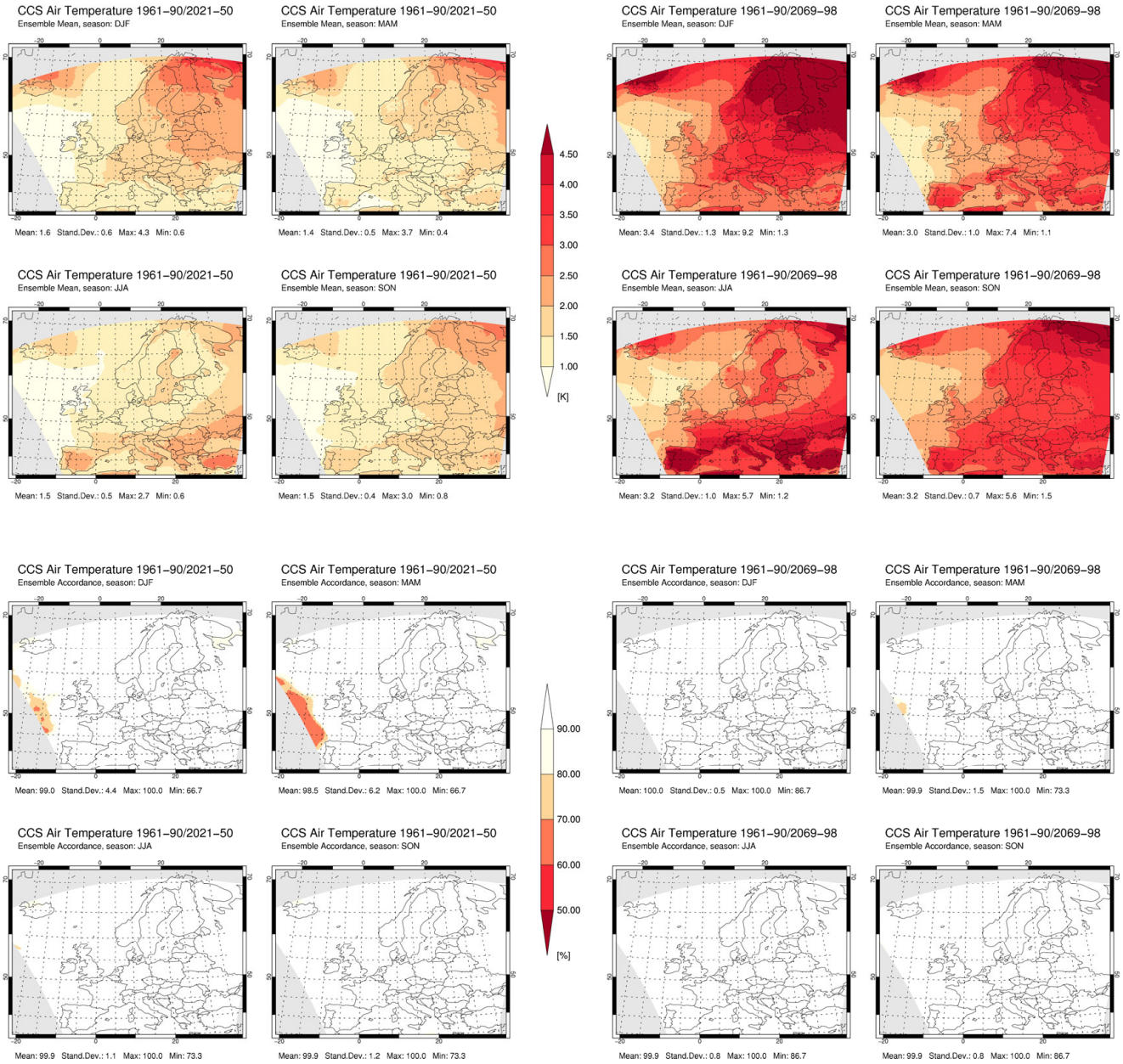

Fig. A 1 Multi-model mean changes (upper four panels) and ensemble accordance (lower four panels) of air temperature for the 15 ENSEMBLES simulations between 2021-2050 (left panels) and 2069-2098 (right panels) with respect to 1961-1990 for Europe.

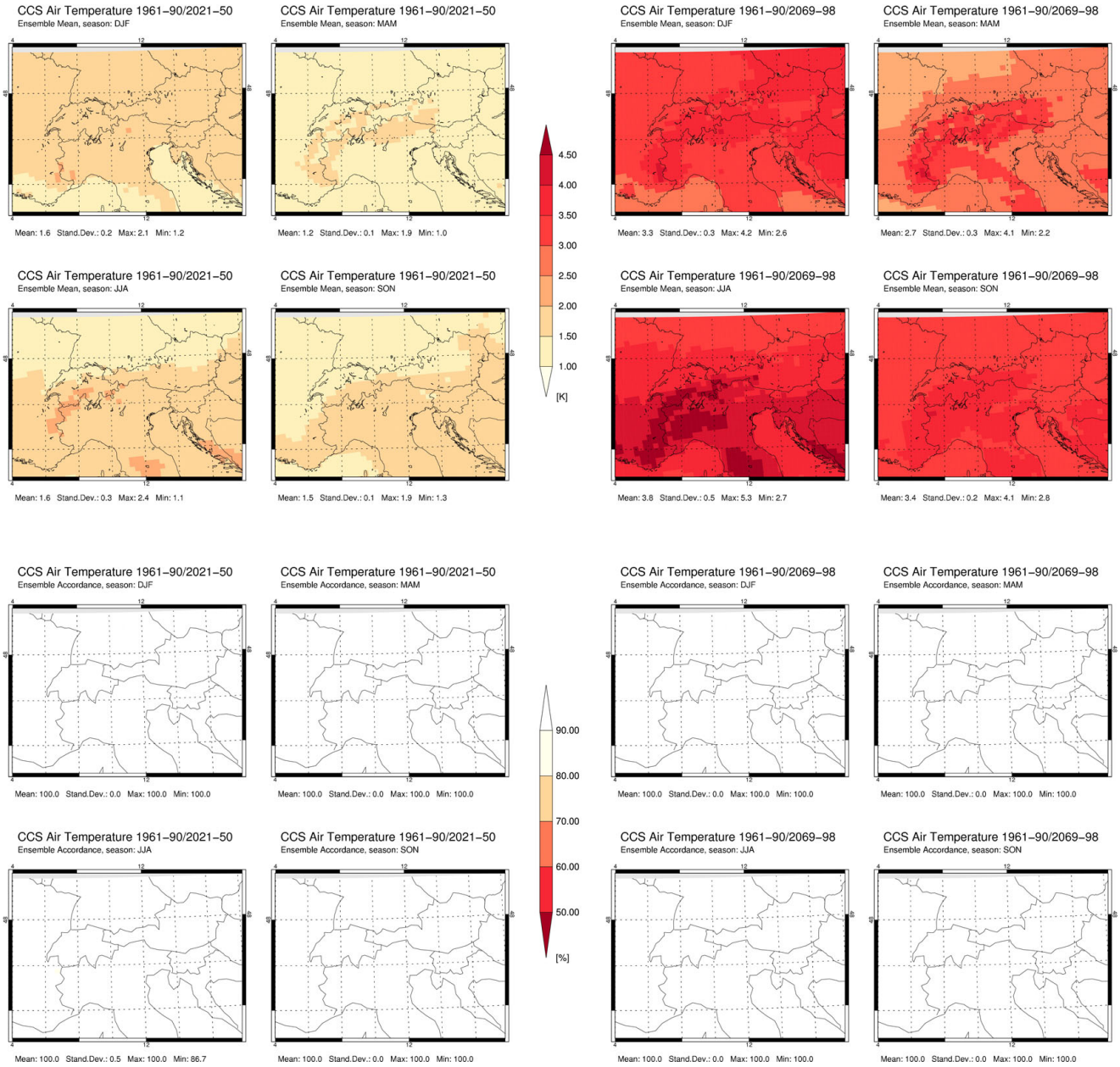

Fig. A 2 Multi-model mean changes (upper four panels) and ensemble accordance (lower four panels) of air temperature for the 15 ENSEMBLES simulations between 2021-2050 (left panels) and 2069-2098 (right panels) with respect to 1961-1990 for the GAR.

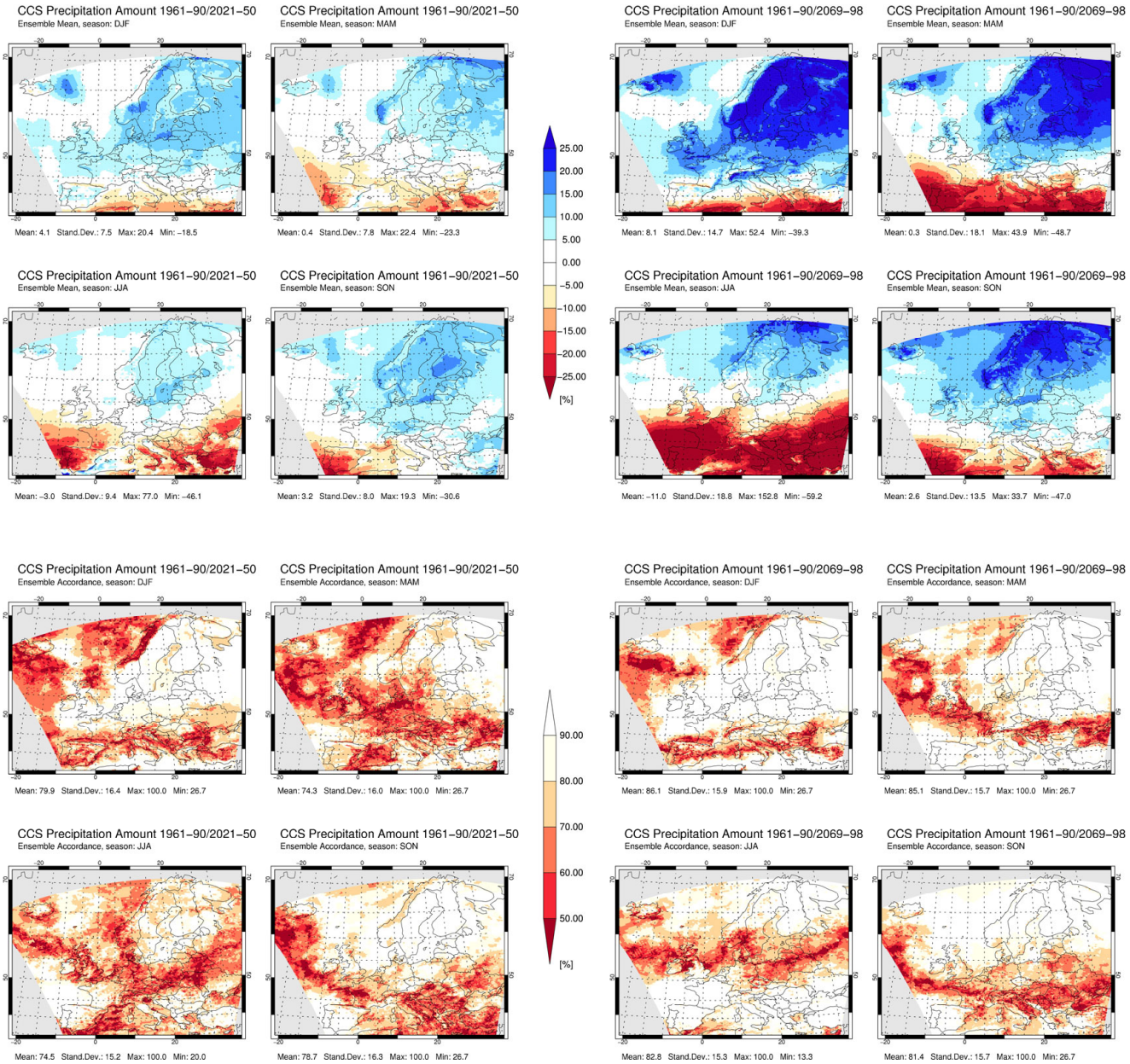

Fig. A 3 Multi-model mean changes (upper four panels) and ensemble accordance (lower four panels) of precipitation for the 15 ENSEMBLES simulations between 2021-2050 (left panels) and 2069-2098 (right panels) with respect to 1961-1990 for Europe. The precipitation changes are calculated relative with respect to 1961-1990.

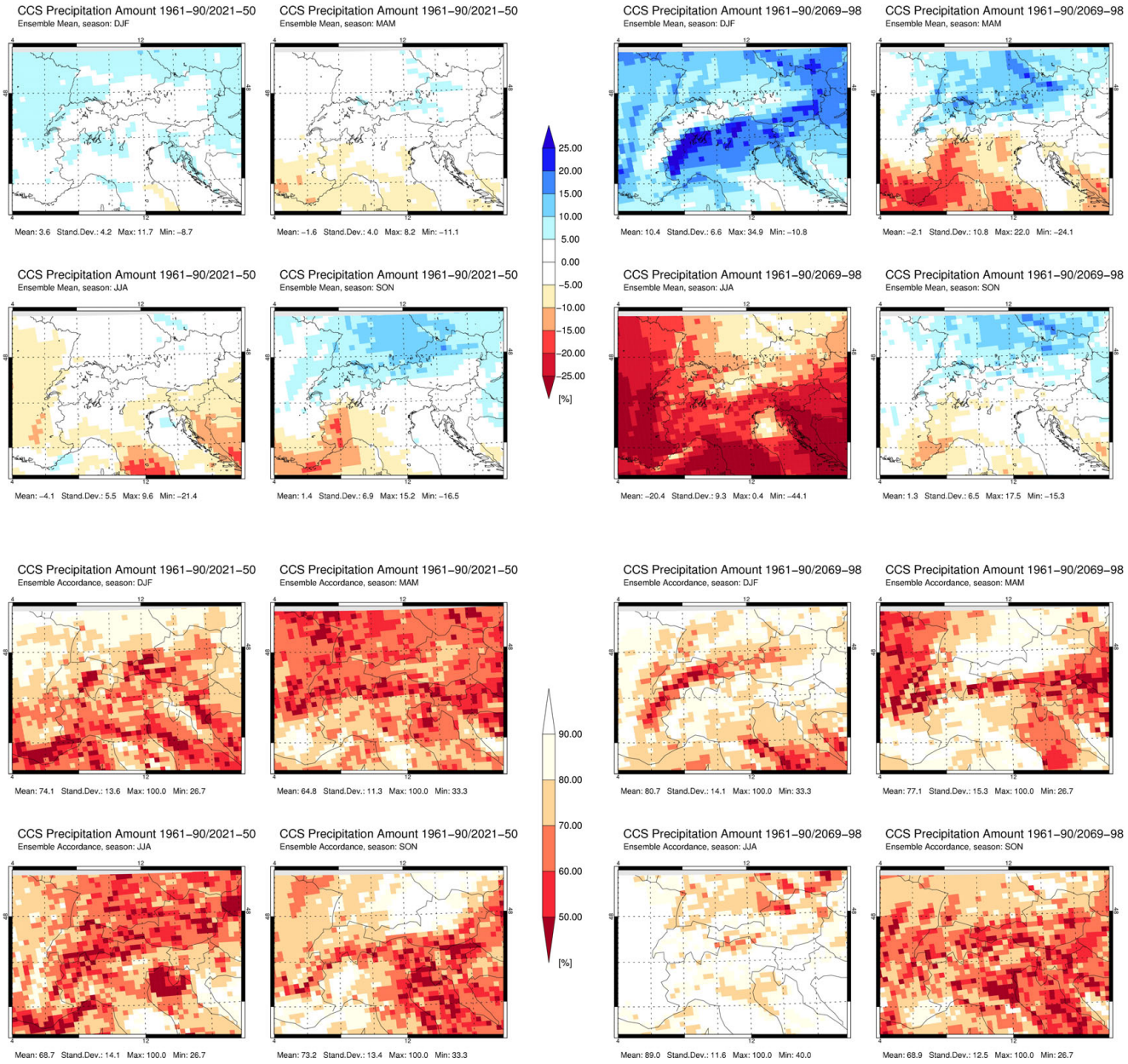

Fig. A 4 Multi-model mean changes (upper four panels) and ensemble accordance (lower four panels) of precipitation for the 15 ENSEMBLES simulations between 2021-2050 (left panels) and 2069-2098 (right panels) with respect to 1961-1990 for the GAR. The precipitation changes are calculated relative with respect to 1961-1990.

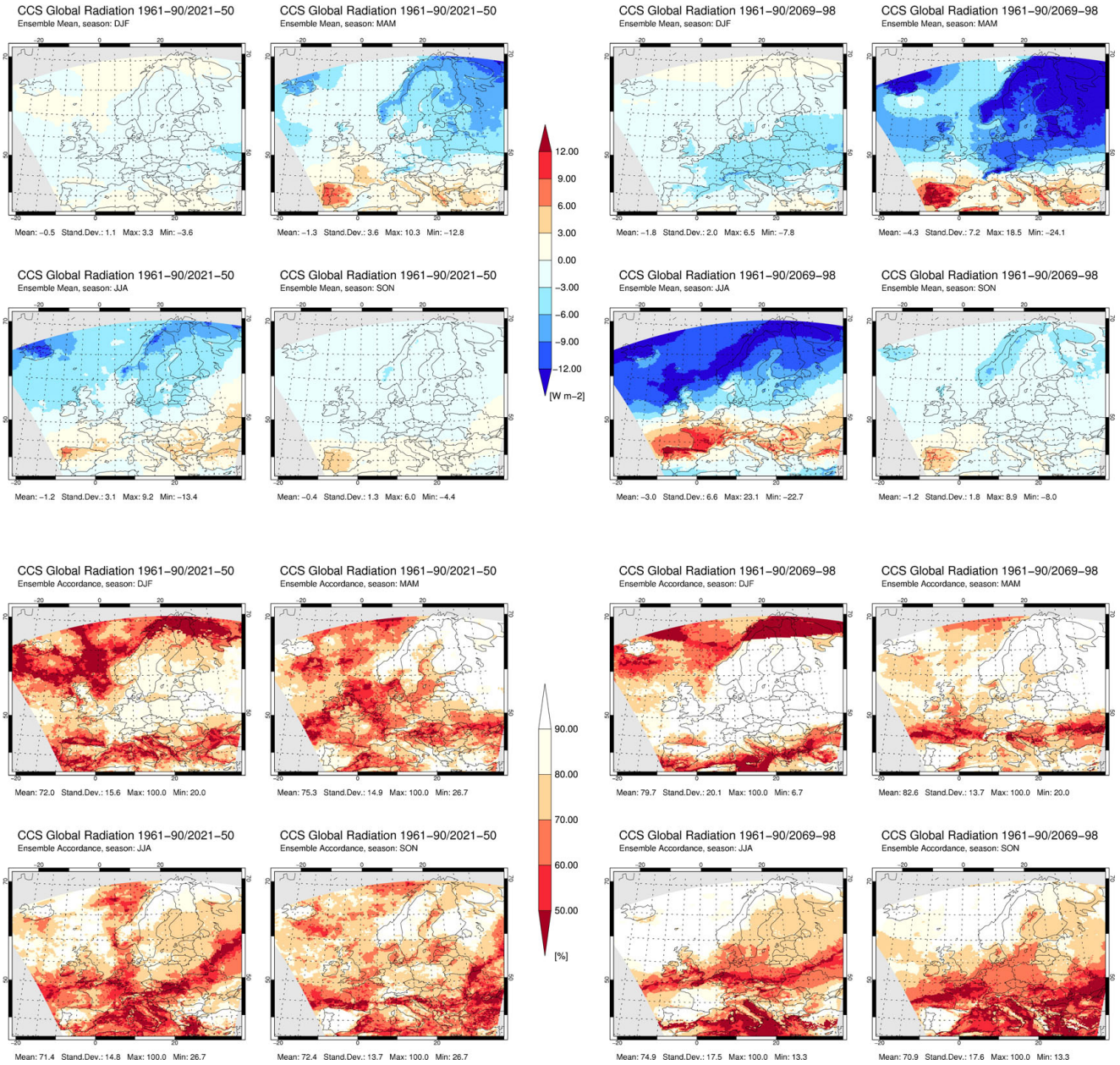

Fig. A 5 Multi-model mean changes (upper four panels) and ensemble accordance (lower four panels) of global radiation for the 15 ENSEMBLES simulations between 2021-2050 (left panels) and 2069-2098 (right panels) with respect to 1961-1990 for Europe.

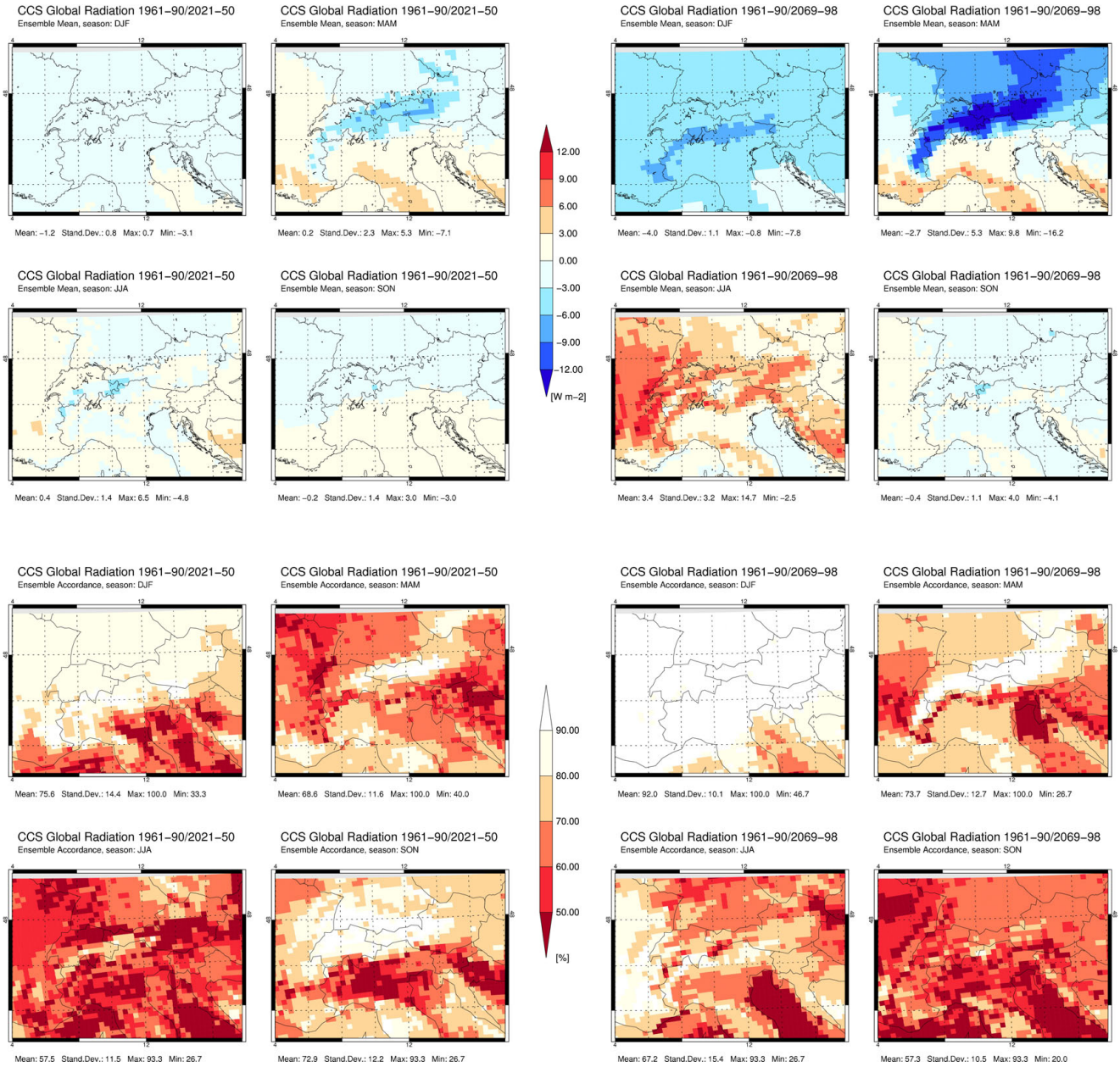

Fig. A 6 Multi-model mean changes (upper four panels) and ensemble accordance (lower four panels) of global radiation for the 15 ENSEMBLES simulations between 2021-2050 (left panels) and 2069-2098 (right panels) with respect to 1961-1990 for the GAR.

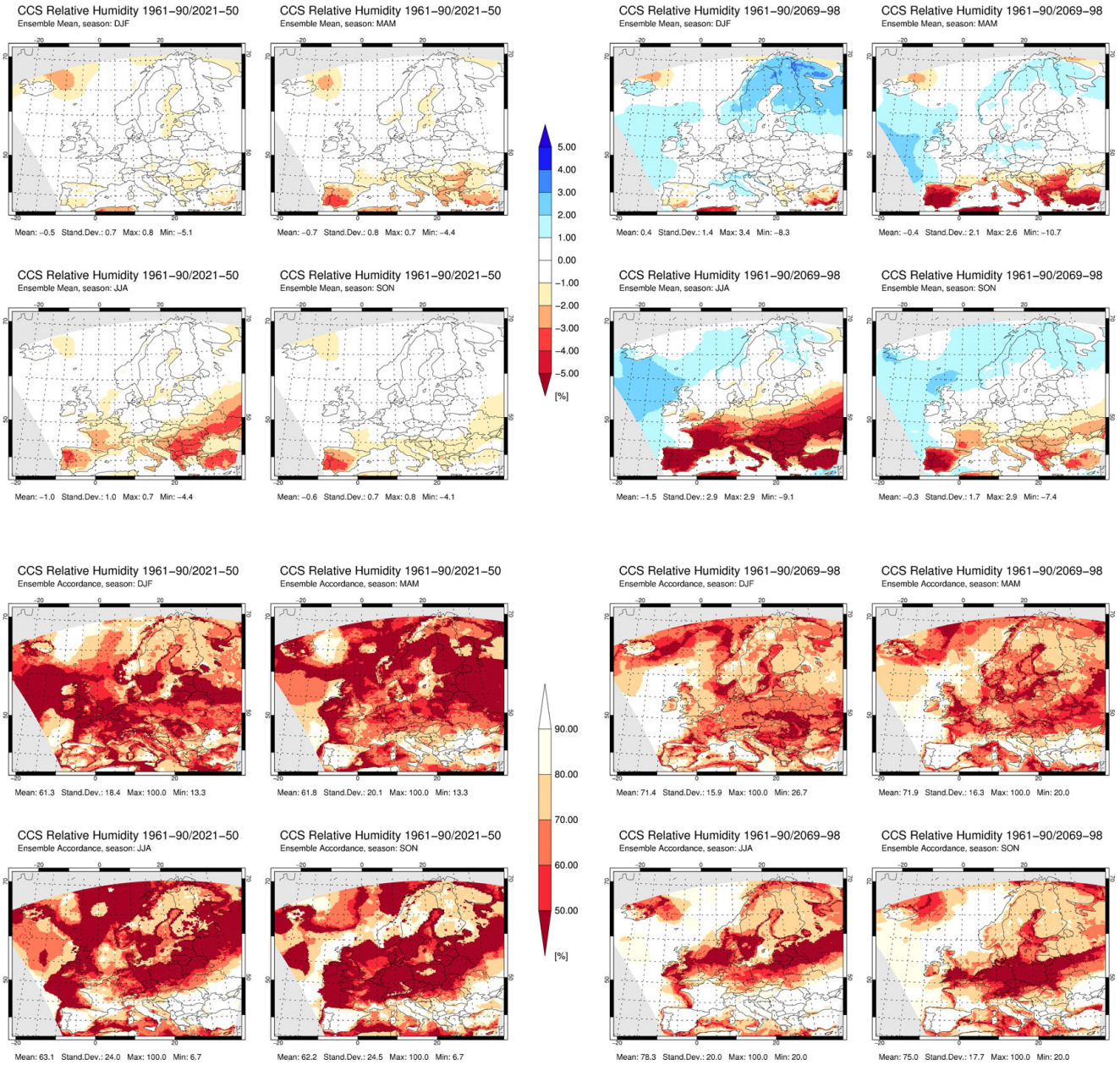

Fig. A 7 Multi-model mean changes (upper four panels) and ensemble accordance (lower four panels) of relative humidity for the 15 ENSEMBLES simulations between 2021-2050 (left panels) and 2069-2098 (right panels) with respect to 1961-1990 for Europe.

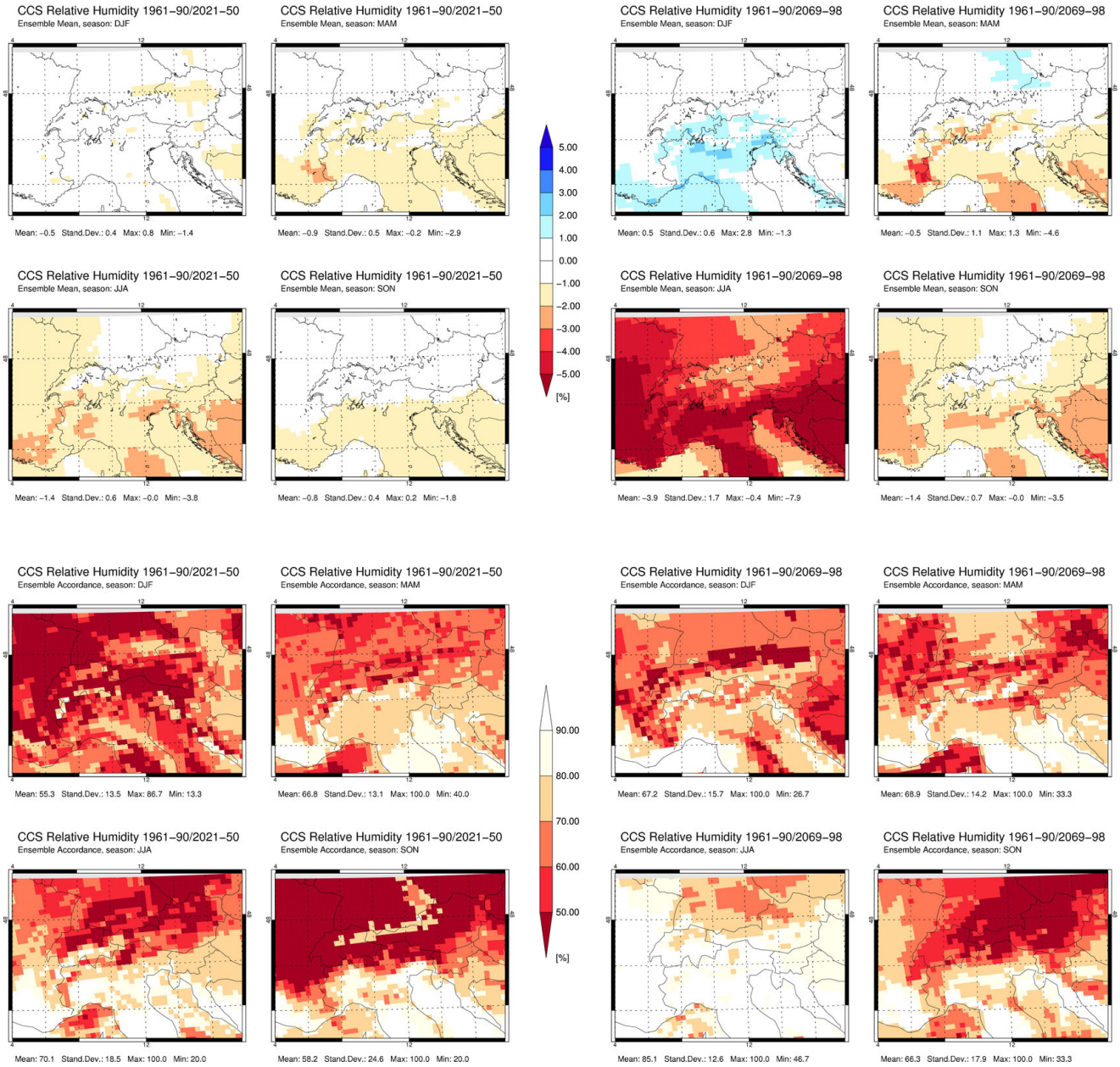

Fig. A 8 Multi-model mean changes (upper four panels) and ensemble accordance (lower four panels) of relative humidity for the 15 ENSEMBLES simulations between 2021-2050 (left panels) and 2069-2098 (right panels) with respect to 1961-1990 for the GAR.

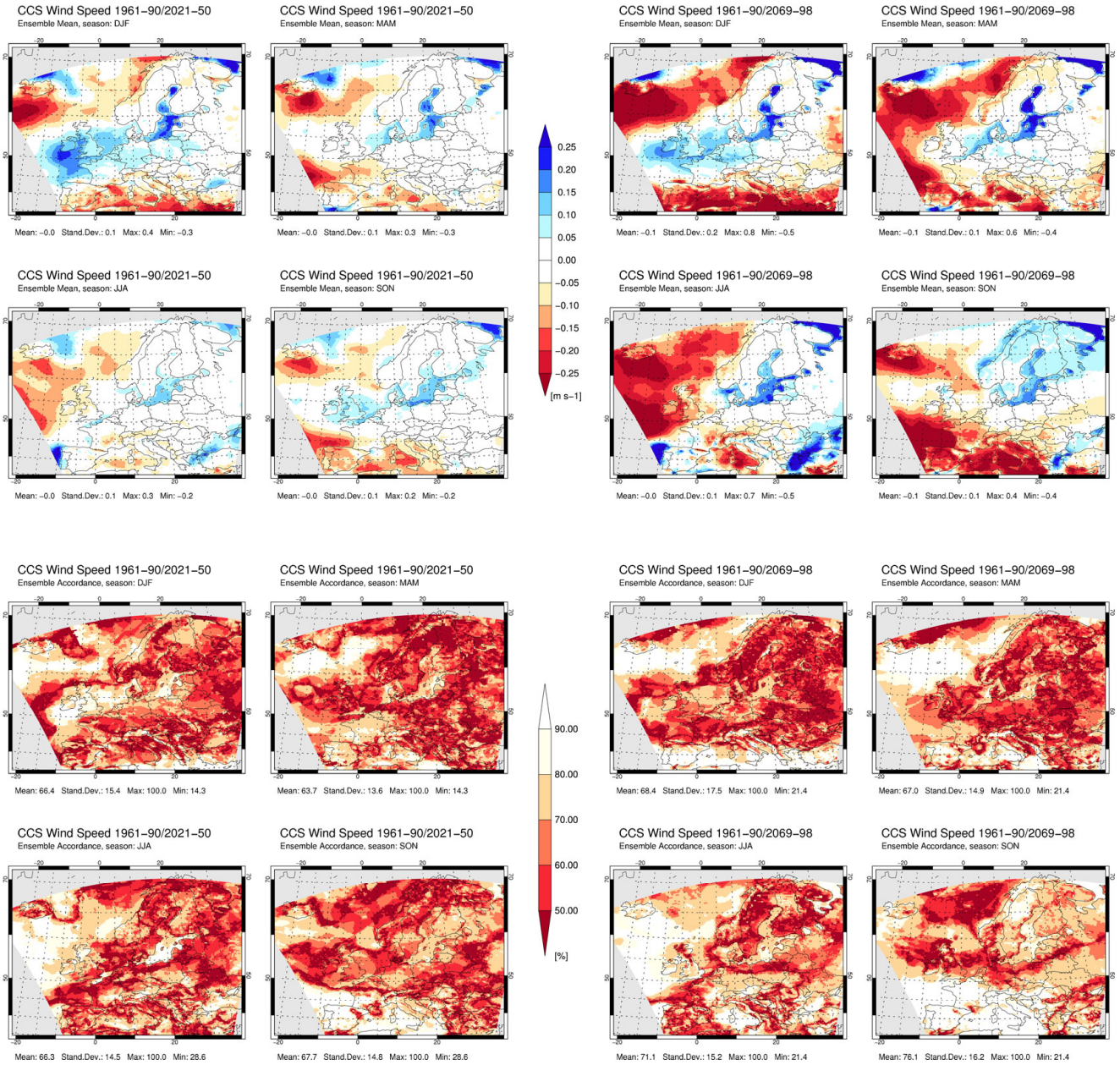

Fig. A 9 Multi-model mean changes (upper four panels) and ensemble accordance (lower four panels) of wind speed for the 15 ENSEMBLES simulations between 2021-2050 (left panels) and 2069-2098 (right panels) with respect to 1961-1990 for Europe.

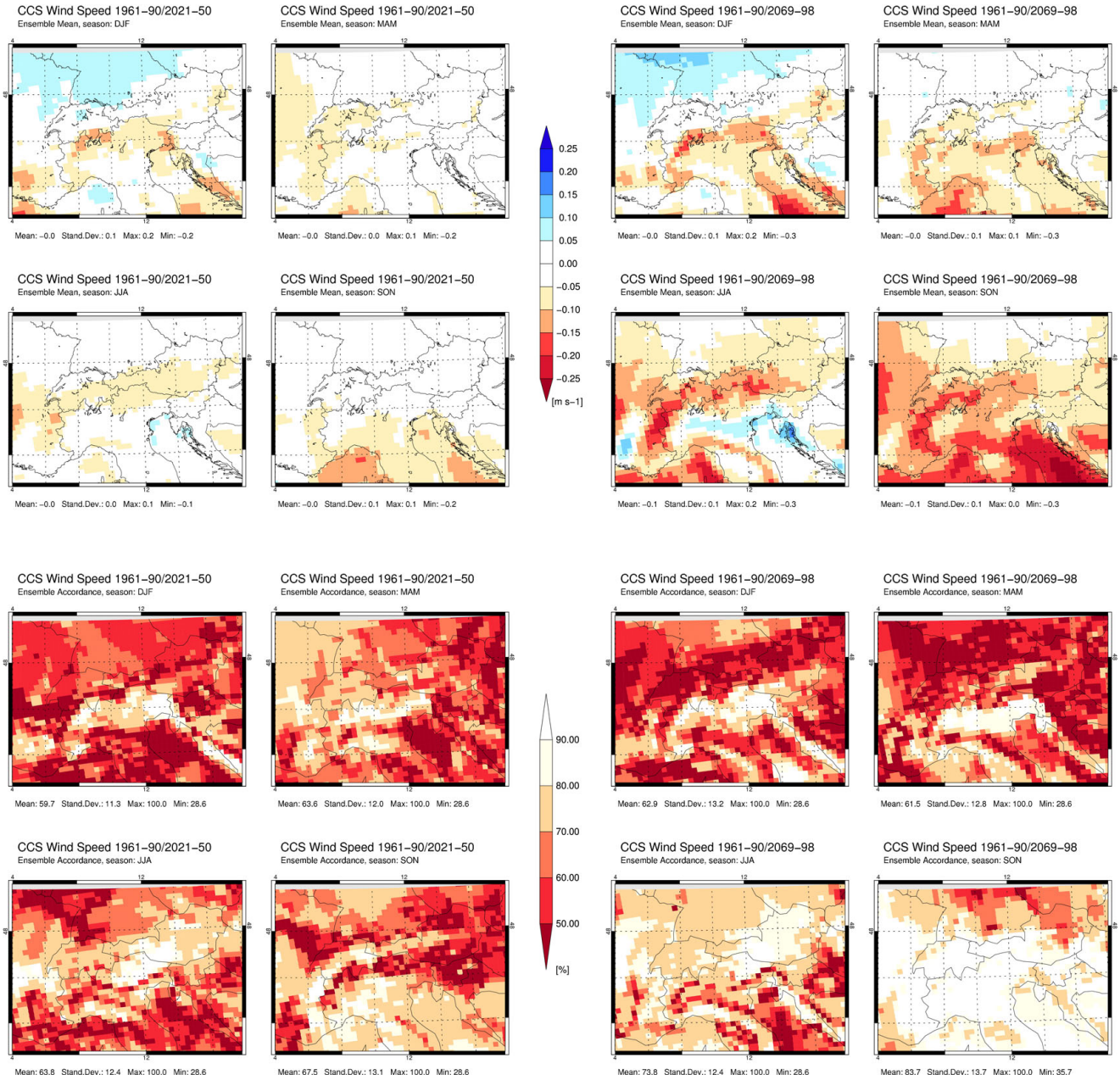

Fig. A 10 Multi-model mean changes (upper four panels) and ensemble accordance (lower four panels) of precipitation for the 15 ENSEMBLES simulations between 2021-2050 (left panels) and 2069-2098 (right panels) with respect to 1961-1990 for Europe.

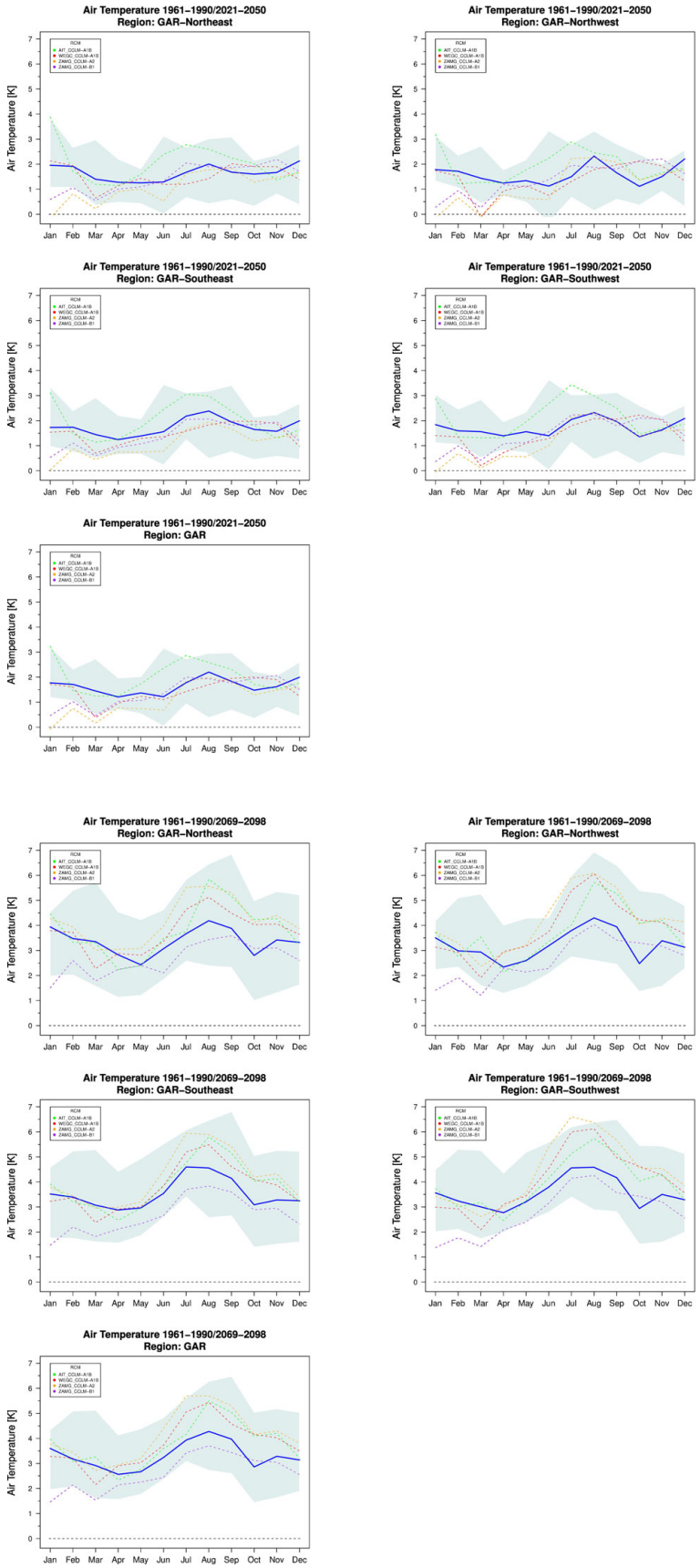

Fig. A 11 Annual cycle of the reconstructed wind speed changes between 2021-2050 (upper five panels) and 2069-2098 (lower five panels) with respect to 1961-1990 for the four HISTALP regions and the GAR. The blue thick line represents the 50th percentile of the reconstructed ENSEMBLES projections and the blue shaded area indicates the 10th and 90th percentile. The colored lines represent the reclip:century simulations.

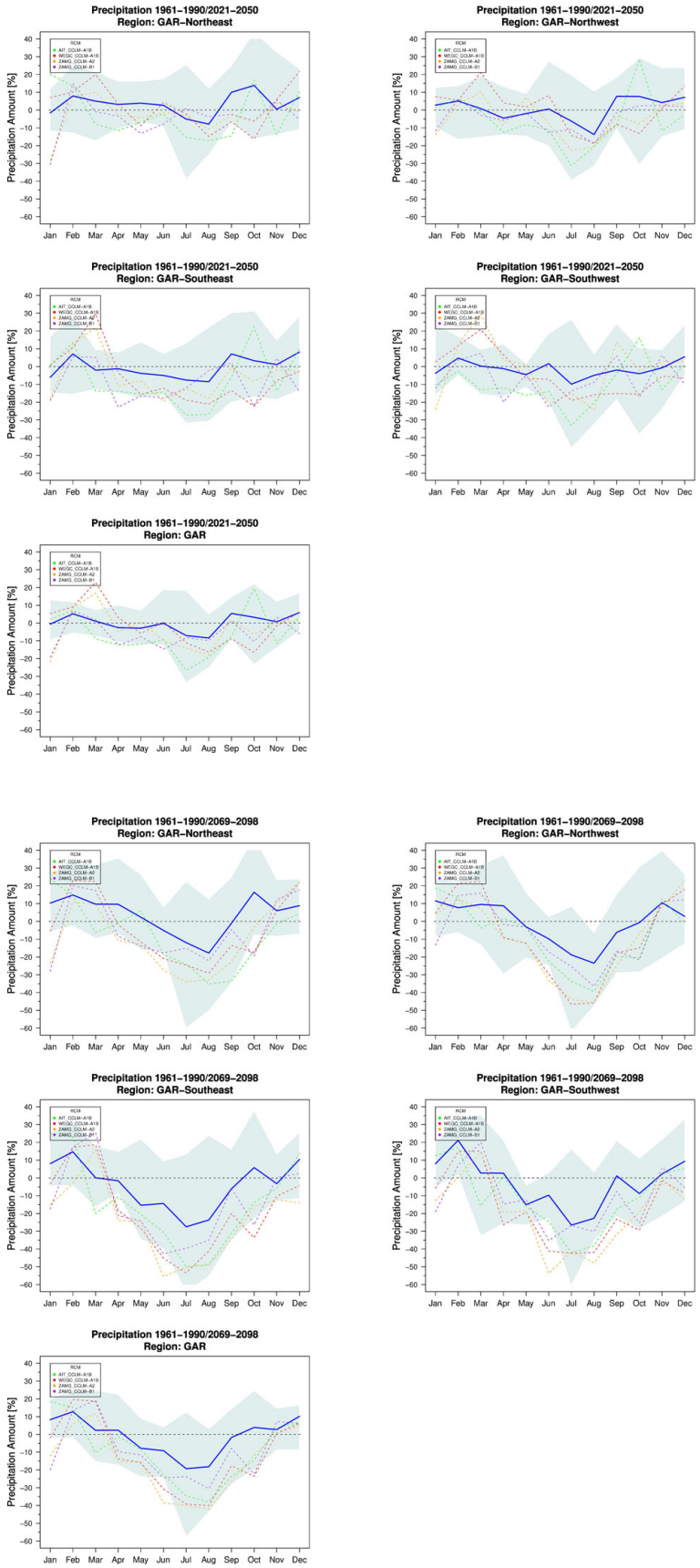

Fig. A 12 Annual cycle of the reconstructed precipitation changes between 2021-2050 (upper five panels) and 2069-2098 (lower five panels) with respect to 1961-1990 for the four HISTALP regions and the GAR. The blue thick line represents the 50th percentile of the reconstructed ENSEMBLES projections and the blue shaded area indicates the 10th and 90th percentile. The colored lines represent the reclip:century simulations.

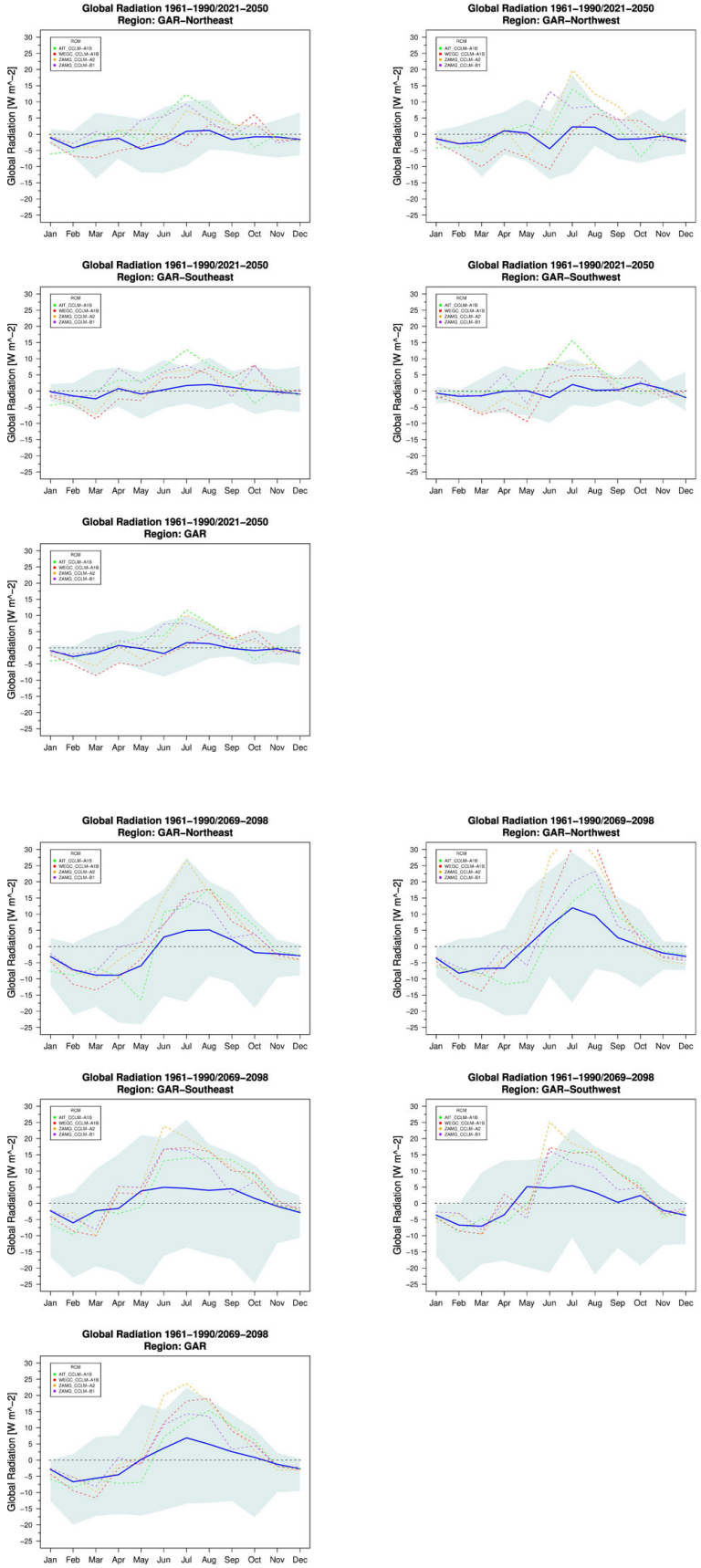

Fig. A 13 Annual cycle of the reconstructed global radiation changes between 2021-2050 (upper five panels) and 2069-2098 (lower five panels) with respect to 1961-1990 for the four HISTALP regions and the GAR. The blue thick line represents the 50th percentile of the reconstructed ENSEMBLES projections and the blue shaded area indicates the 10th and 90th percentile. The colored lines represent the reclip:century simulations.

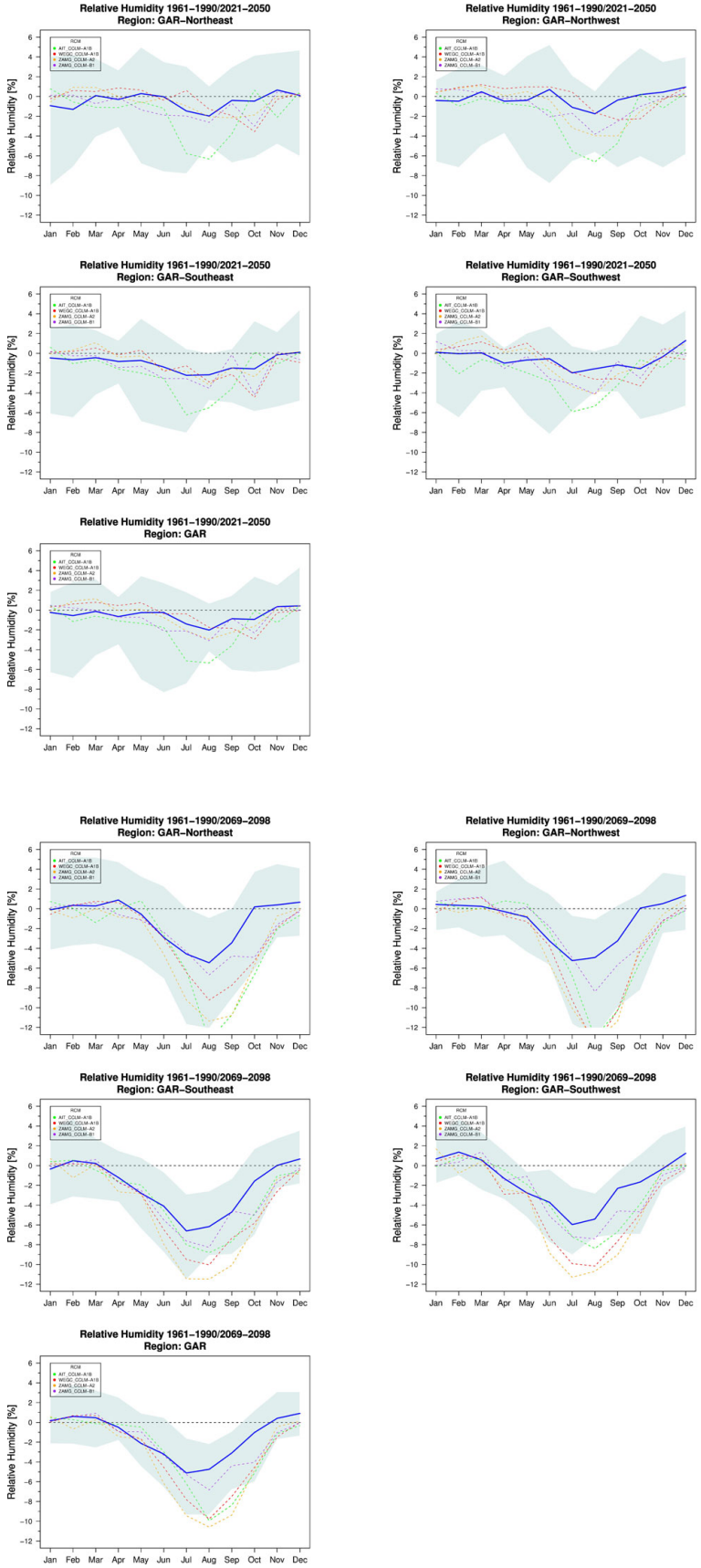

Fig. A 14 Annual cycle of the reconstructed relative humidity changes between 2021-2050 (upper five panels) and 2069-2098 (lower five panels) with respect to 1961-1990 for the four HISTALP regions and the GAR. The blue thick line represents the 50th percentile of the reconstructed ENSEMBLES projections and the blue shaded area indicates the 10th and 90th percentile. The colored lines represent the reclip:century simulations.

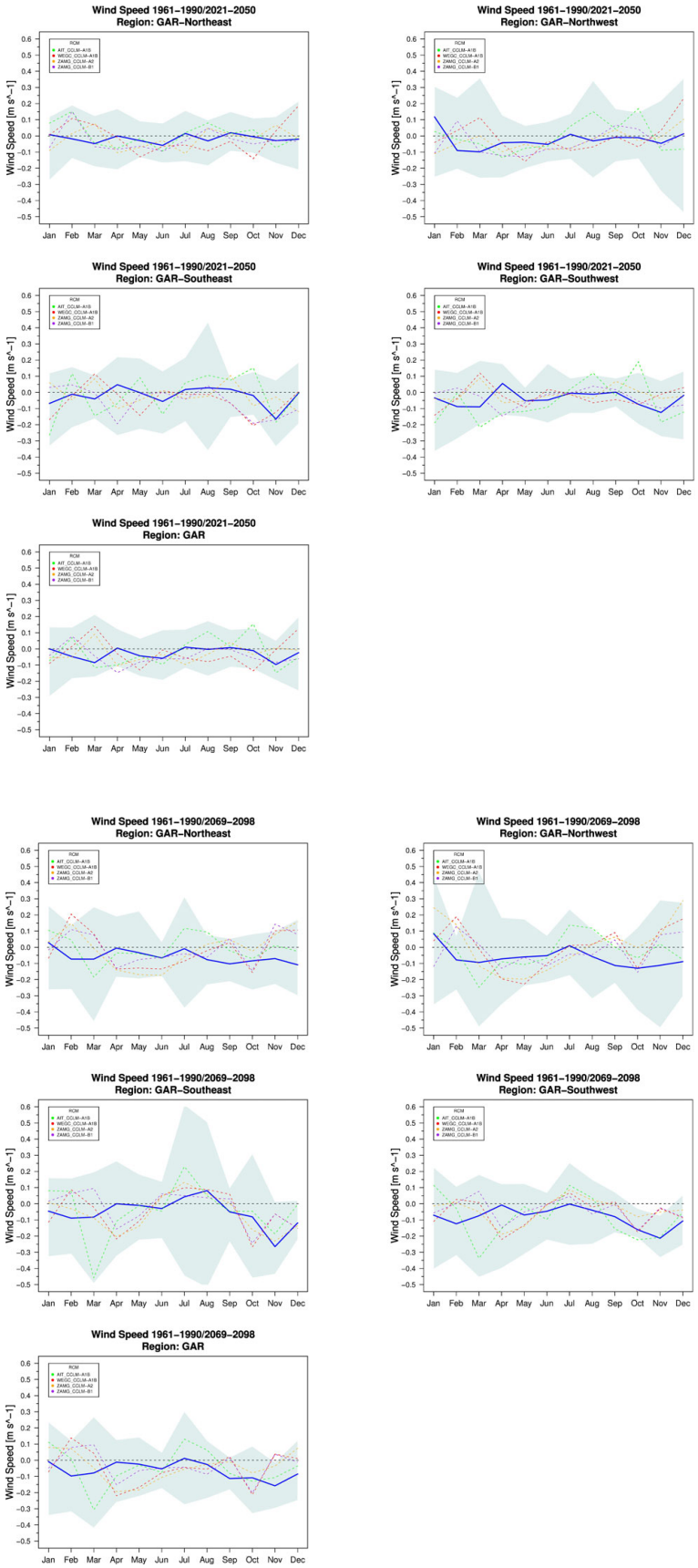

Fig. A 15 Annual cycle of the reconstructed wind speed changes between 2021-2050 (upper five panels) and 2069-2098 (lower five panels) with respect to 1961-1990 for the four HISTALP regions and the GAR. The blue thick line represents the 50th percentile of the reconstructed ENSEMBLES projections and the blue shaded area indicates the 10th and 90th percentile. The colored lines represent the reclip:century simulations.

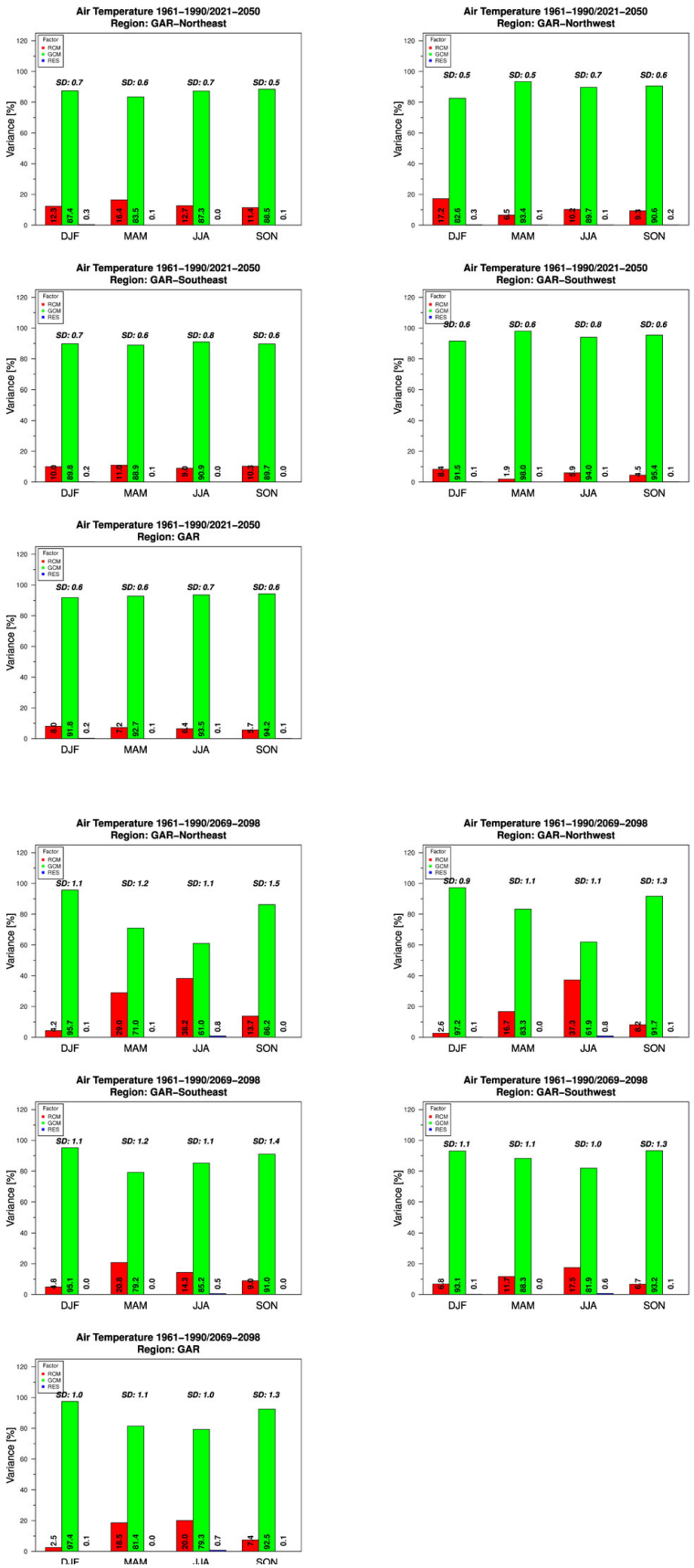

Fig. A 16 Analysis of variance of the reconstructed changes in air temperature between 2021-2050 (upper five panels) and 2069-2098 (lower five panels) with respect to 1961-1990 for the four HISTALP regions and the GAR.

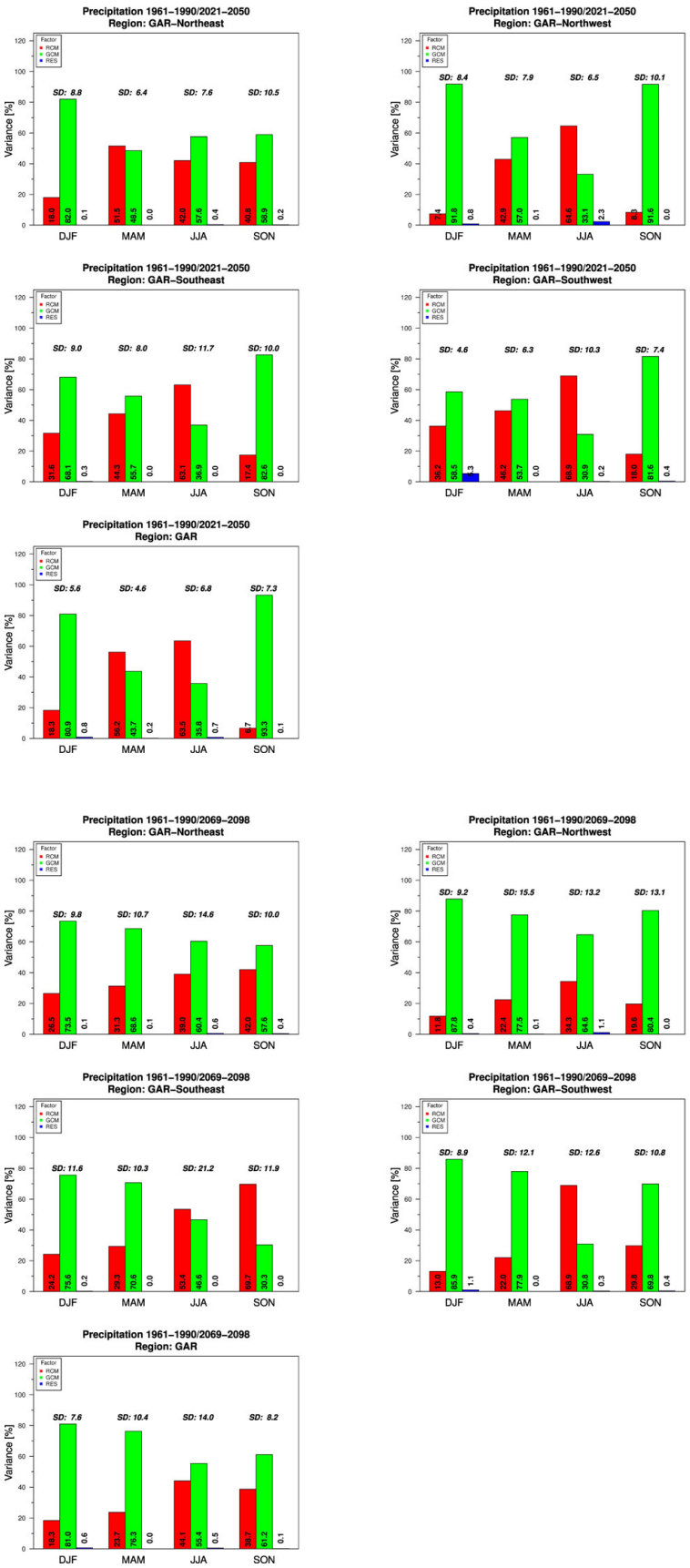

Fig. A 17 Analysis of variance of the reconstructed changes in precipitation between 2021-2050 (upper five panels) and 2069-2098 (lower five panels) with respect to 1961-1990 for the four HISTALP regions and the GAR.

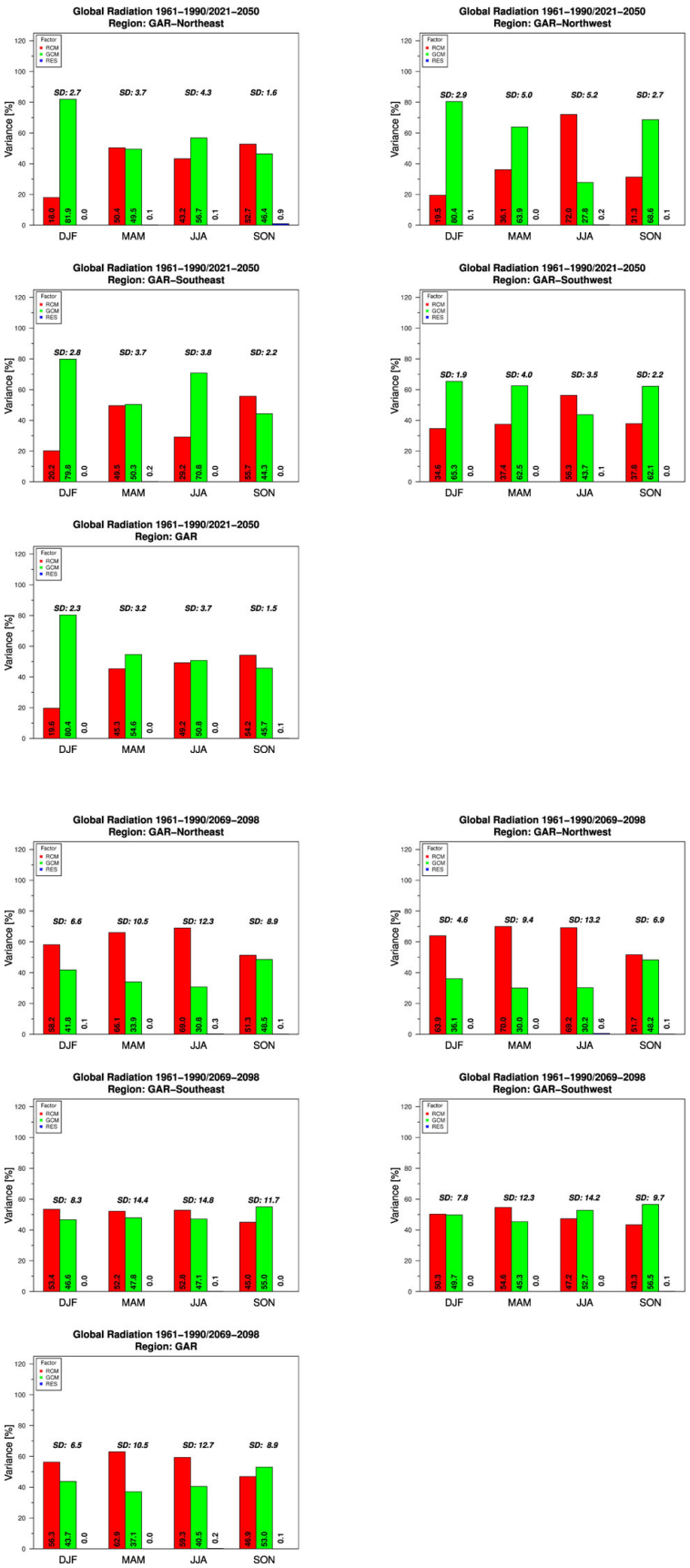

Fig. A 18 Analysis of variance of the reconstructed changes in global radiation between 2021-2050 (upper five panels) and 2069-2098 (lower five panels) with respect to 1961-1990 for the four HISTALP regions and the GAR.

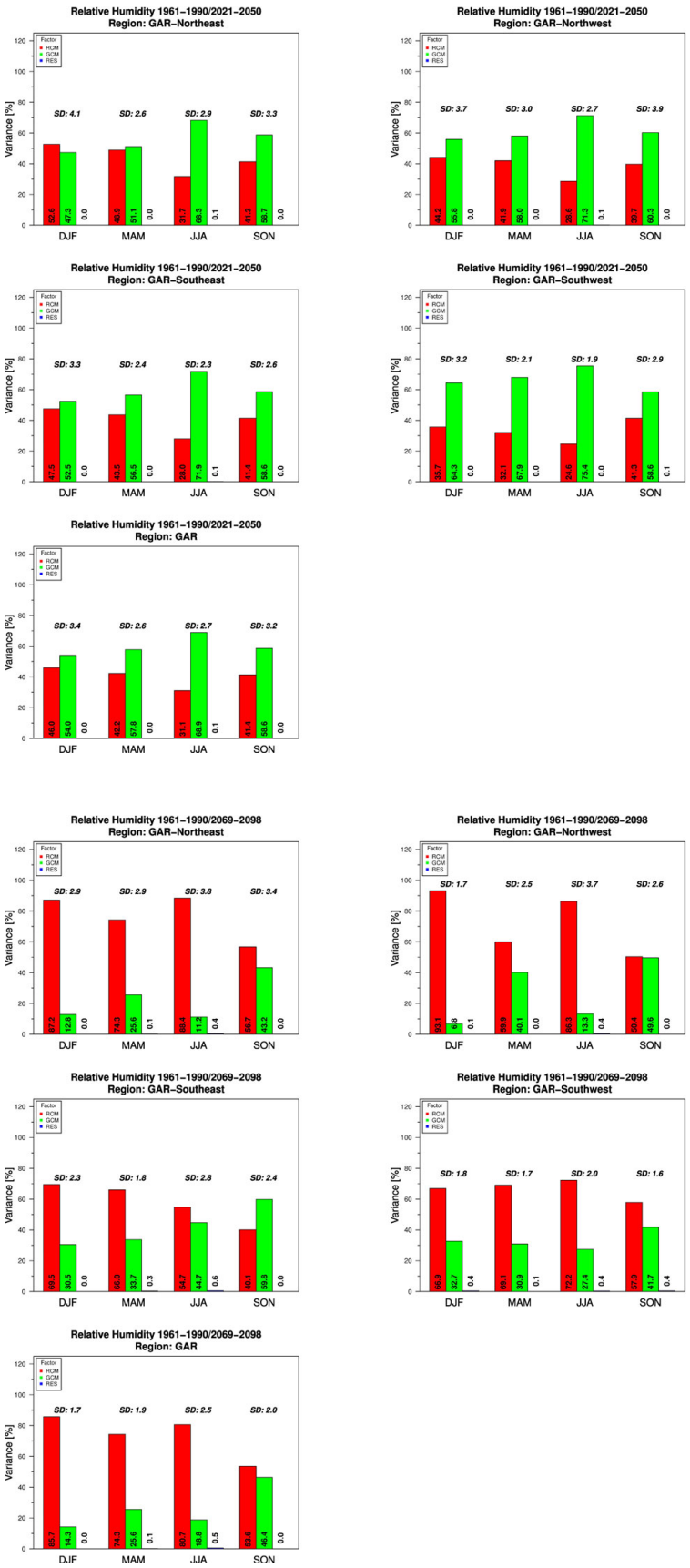

Fig. A 19 Analysis of variance of the reconstructed changes in relative humidity between 2021-2050 (upper five panels) and 2069-2098 (lower five panels) with respect to 1961-1990 for the four HISTALP regions and the GAR.

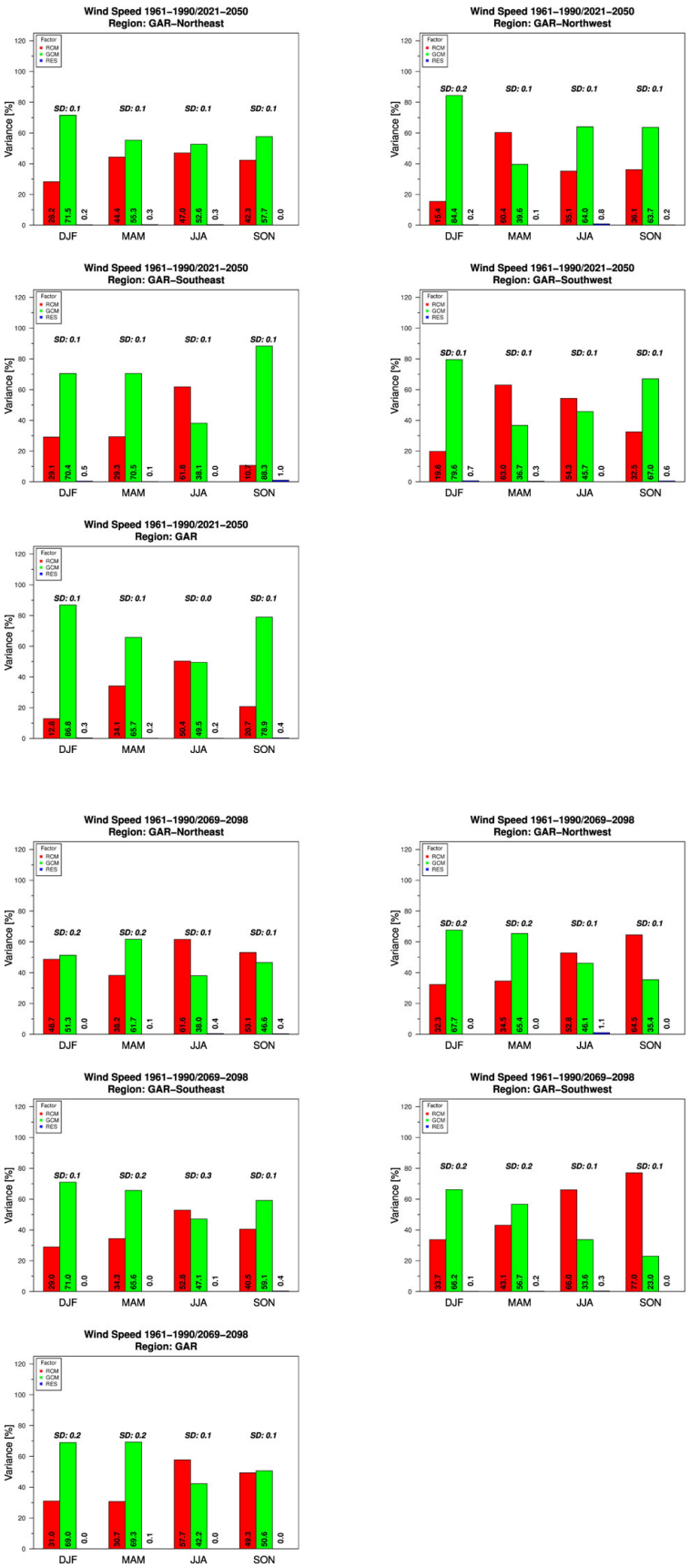

Fig. A 20 Analysis of variance of the reconstructed changes in wind speed between 2021-2050 (upper five panels) and 2069-2098 (lower five panels) with respect to 1961-1990 for the four HISTALP regions and the GAR.

II Extended RCM projections for Europe based on ENSEMBLES and CMIP3

II-1 Introduction

The application of general circulation models (GCMs) driven by prescribed greenhouse gas (GHG) emission scenarios is nowadays the most common way to obtain physically based climate projections. Due to their coarse spatial resolution (typically 100 km to 300 km horizontal grid spacing and an effective resolution of about 1000 km) GCMs currently fail to properly represent many regional and local climate processes, such as, e.g., orographic precipitation (McGregor 1997). In order to generate climate simulations with finer horizontal resolution, regional climate models (RCMs) are nested within the GCM large scale atmospheric circulation over a limited area (Giorgi and Mearns 1991; 1999; McGregor 1997; Wang et al. 2004; Rummukainen 2010). The added value of RCMs in representing regional climate characteristics has been demonstrated in several studies (Jones et al. 1995; Laprise 2003, Castro et al. 2005; Buonomo et al. 2007; Feser et al. 2011).

Regional as well as global climate projections are subject to considerable uncertainties which can be roughly divided into three components: (1) Uncertainty due to natural variability, (2) uncertainty due to unknown future GHG emissions, and (3) uncertainty due to imperfect simulation of the climate system (Collins 2007). In order to analyse these uncertainties in RCM projections, large-scale European projects such as PRUDENCE (http://prudence.dmi.dk/; Christensen and Christensen 2007) and ENSEMBLES (http://ensembles-eu.metoffice.com/; van der Linden and Mitchell 2009) produced coordinated multi-model ensembles, improving rapidly the knowledge about uncertainties in regional climate projections in the last decade. Furthermore, these simulations provided the basis for most investigations of regional climate change impacts over Europe in recent years. Due to computational constraints, only a limited number of RCM simulations can be realised and it is a question of the experimental design which uncertainty components are primarily tackled within the ensemble. Therefore, missing realisations within RCM ensembles are a common problem and even simple ensemble estimates such as mean and variability are potentially biased due to unequal sampling of the uncertainty components. In order to avoid such biases, Déqué et al. (2007) introduced an iterative data reconstruction method which assumes additivity between uncertainty components in order to estimate missing climate change signals (CCSs). This reconstruction method was further applied in several studies in order to obtain a balanced design for the analysis of variance components (Déqué et al. 2007; Heinrich and Gobiet 2011b; Prein et al. 2011; Déqué et al. 2012). However, as the method relies on an implicit formulation of the uncertainty components, it cannot be used to extend the ensemble to experiments outside of the original experimental design (e.g., for GCMs that have not been used as driver for any RCM in the ensemble). For such an extension, scaling techniques are

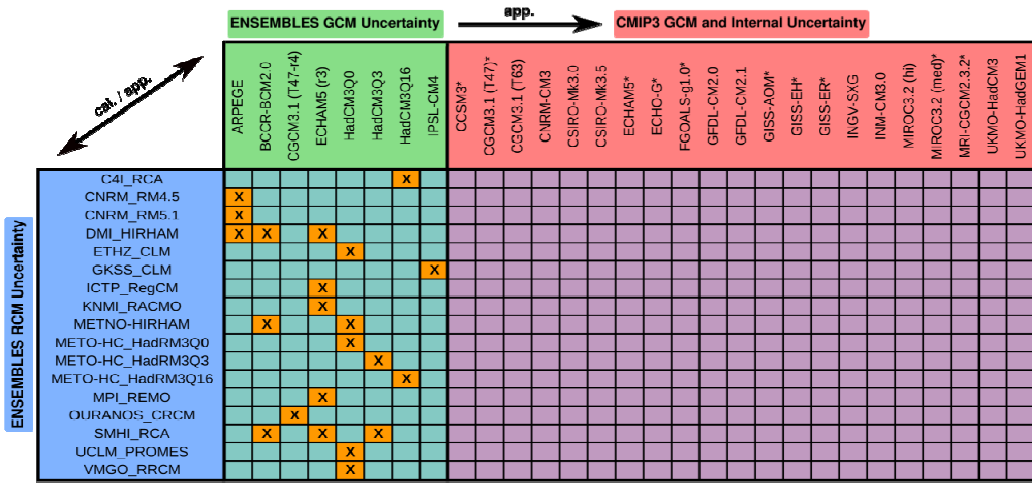

Fig. 8 The ENSEMBLES simulation matrix of the 25 km runs until 2050. The orange coloured cells marked with X's indicate the available simulations and empty cells represent the missing realisations. The models spanning the GCM and RCM uncertainty of ENSEMBLES are highlighted in green and blue, respectively. Additional uncertainty due to the CMIP3 GCMs is displayed in red and GCMs which are driven by multiple initial conditions are marked with an asterisk. The GCMs and RCMs of ENSEMBLES are used for calibrating the statistical reconstruction methods which are then applied to the GCMs of both ENSEMBLES and CMIP3 in order to fill the according missing values.

widely applied (Mitchell et al. 1999; Mitchell 2003; Rummukainen et al. 2003; Harris et al. 2006; Hingray et al. 2007; Ruosteenoja et al. 2007). They have been originally used to derive regional climate projections of time horizons or emission scenarios which have not been GCM simulated, by scaling the global mean temperature change of simple energy balance models with the geographical pattern of the GCM simulations (pattern-scaling). In our case, we aim at predicting the RCM response from the driving GCM response, by applying a scaling relationship between the according regional CCSs. In this respect, it has already been shown that scaling has skill at the GCM grid point scale by Kendon et al. (2010).

The aim of our study is to assess and compensate for the potential GCM sampling bias in expected regional climate change and the associated uncertainty of the ENSEMBLES RCM projections by data reconstruction and combination with the much larger GCM ensemble of the third phase of the Coupled Model Intercomparison Project (CMIP3; Meehl et al. 2007). For this purpose, we first assess the skill of different statistical additive and scaling reconstruction methods in reproducing ensemble mean and standard deviation. We then apply the most appropriate reconstruction method to the sparsely filled ENSEMBLES simulation matrix and further extend the matrix to all available GCM simulations of the CMIP3 ensemble forced by the A1B emission scenario (Nakicenovic et al. 2000). As final result, we present an update of expected regional climate change for air temperature and precipitation amount in eight European subregions until the mid-21st century and reassess its uncertainty under the light of the extended ensemble.

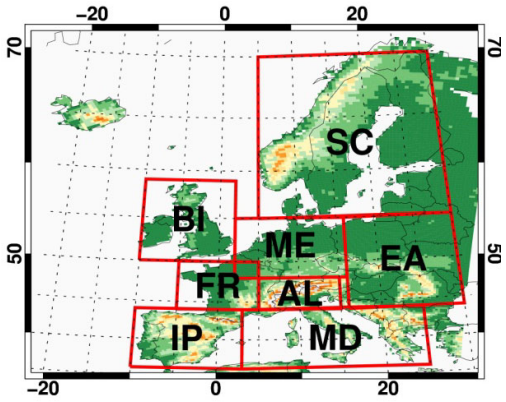

Fig. 9 The eight subregions investigated: Iberian Peninsula (IP), Mediterranean (MD), France (FR), Middle Europe (ME), Alps (AL), Eastern Europe (EA), British Isles (BI), and Scandinavia (SC).

The study is structured as follows. Section 2 introduces the data and study regions. In Section 3 we describe the reconstruction methods. In Section 4 we explain the setup of the cross-validation and the statistical analysis. In Section 5 we present the cross-validation results. Section 6 provides a revision of expected regional climate change and its uncertainty over Europe, followed by Section 7 which sums up the key findings of this study.

II-2 Climate Model Data and Study Regions

For an extended analysis of RCM projections over Europe and the Alpine Region, we use the most recent RCM simulations from the ENSEMBLES project which produced a set of 22 high resolution RCM runs with a horizontal grid spacing of about 25 km (Fig. 8). The ensemble consists of 8 GCMs and 17 RCMs, but due to limited computational resources, only a small fraction (16.2 %) of the possible GCM-RCM combinations could be realised. Subsampling mainly addressed uncertainty in boundary conditions (choice of the driving GCM) and RCM model formulation (Christensen et al., 2010). Since the choice of the GHG emission scenario is less important until the mid-21st century (Hawkins and Sutton 2009; 2011; Prein et al. 2011), only the A1B emission scenario was used to force the climate simulations. As suggested by Christensen et al. (2010), we consider the three sensitivity experiments of HadCM3-HadRM3 as different model combinations, as their climate response is highly variable (Collins et al. 2006). For the same reason, we take into account both model versions of CNRM driven by ARPEGE.

Many of the RCM simulations (10 out of 22) were driven by only two GCMs, namely ECHAM5 and HadCM3Q0. All GCMs, except CGCM3.1 and IPSL-CM4, drive at least two RCMs. Three RCMs were forced by multiple GCMs, namely DMI-HIRHAM, METNO-HIRHAM, and SMHI-RCA. The driving GCM data of ENSEMBLES was either obtained by the ENSEMBLES or CMIP3 database (https://esg.llnl.gov:8443/). As we aim at extending the uncertainty analysis to unknown GCMs, we

also take into account all additional available GCM simulations of CMIP3 forced by the A1B emission scenario. Altogether, we have 53 GCM simulations for air temperature and 50 for precipitation amount from a set of 27 GCMs (10 GCMs were started with different perturbed initial conditions and therefore cover uncertainty due to natural variability, see Fig. 8).

In order to be comparable to previous studies conducted within PRUDENCE and ENSEMBLES, we focus on the land grid points of eight European subregions (Fig. 9) according to Christensen and Christensen (2007): Iberian Peninsula (IP), Mediterranean (MD), France (FR), Middle Europe (ME), Alps (AL), Eastern Europe (EA), British Isles (BI), and Scandinavia (SC). In addition, we also provide information concerning entire Europe (EU). The selected subregions cover the diversity of main climate characteristics in Europe, ranging from arid climate conditions during summer in the southern European regions IP and MD to humid maritime climate characteristics in BI and SC (Heinrich and Gobiet, 2011a). The focus is on seasonal mean CCSs, calculated as the difference between the two periods of 2021-2050 (future period) and 1961-1990 (baseline period). The precipitation CCSs are calculated relatively with respect to the baseline period.

II-3 Missing Data Reconstruction Methods

II-3.1 Additive Methods

First, we consider the additive reconstruction method introduced by Déqué et al. 2007 (D07). The reconstruction method is embedded in the framework of an analysis of variance (ANOVA), neglecting the highest interaction term in order to reconstruct the actual missing value. The reconstruction algorithm writes in case of the ENSEMBLES simulation matrix as follows:

$$\Delta X_{ij} = \Delta X_{i\bullet} + \Delta X_{\bullet j} - \Delta X_{\bullet\bullet} = \Delta X_{\bullet\bullet} + (\Delta X_{i\bullet} - \Delta X_{\bullet\bullet}) + (\Delta X_{\bullet j} - \Delta X_{\bullet\bullet}) \qquad (2)$$

where ΔX denotes the CCS of a RCM for a specific subregion, i is the index of the RCM ($i = 1,\ldots,17$), and j the index of the driving GCM ($j = 1,\ldots,8$). The dot operator denotes averaging across the according indices. The reconstruction algorithm can be understood intuitively: consider RCM1 driven by a set of GCMs and RCM2 driven by the same GCMs except one. This missing value is then reconstructed by adding the mean difference between RCM2 and RCM1 to RCM1. Since the reconstruction of the missing values depends on the grand mean of the entire GCM-RCM matrix, 30 iterations are performed (Déqué et al., 2007).

D07 cannot be used for an extension to unknown GCMs, as there is no explicit formulation between the CCSs of RCMs and according driving GCMs. We therefore extend the concept of additivity to unknown GCMs and write the following model:

$$\Delta X_{ij} = \Delta Y_j + \overline{DE} + \delta_{ij} \qquad (3)$$

where ΔY denotes the CCS of the driving GCM and $\overline{DE}$ denotes the mean downscaling effect which is calculated from the available GCM-RCM combinations with index k for the RCMs and l for the GCMs as follows:

$$\overline{DE} = \sum_{k=1}^{n}\sum_{l=1}^{m} I_{kl} \cdot (\Delta Y_l - \Delta X_{kl}) / \sum_{k=1}^{n}\sum_{l=1}^{m} I_{kl} \quad (4)$$

$$I_{kl} = \begin{cases} 1 : \Delta X_{kl}\ exists \\ 0 : \Delta X_{kl}\ does\ not\ exist \end{cases} \quad (5)$$

In order to account for the effect which is specific for a particular RCM, we introduced the additive term δ_{ij}. In our study, three different formulations of the RCM specific downscaling effect are used: (1) there exists no RCM specific effect with $\delta_{ij} = 0$ (ADD1), (2) the RCM specific effect is the mean RCM specific difference to $\overline{DE}$ (ADD2), (3) the RCM specific effect is randomly sampled from a normal distribution with zero mean and standard deviation estimated from the anomalies of all RCMs relative to $\overline{DE}$ (ADD3).

II-3.2 Scaling Methods

As second class of reconstruction methods, we assess the capability of different scaling methods in reconstructing the RCM projections, which can be formulated as follows:

$$\Delta X_{ij} = \Delta Y_j \cdot \tilde{k} + \tilde{d} + \varepsilon_{ij} \qquad (6)$$

where $\tilde{k}$ and $\tilde{d}$ are the linear regression coefficients of a least-square-fit to the data. In order to account for a RCM specific downscaling effect, we again introduced the additive term ε_{ij}. Similar to the additive methods, we assess three different cases for ε_{ij}: (1) there exists no RCM specific effect with $\varepsilon_{ij} = 0$ (SCA1), (2) the RCM specific effect is the mean RCM specific residual of the least-square-fit (SCA2), (3) the RCM specific effect is randomly sampled from a normal distribution with zero mean and standard deviation estimated from the regression residuals of all RCMs (SCA3).

Forcing the regression line to cross the abscissa at zero (intercept $\tilde{d} = 0$ in Eq. 6) is reasonable if global mean temperature change is used as predictor for the regional climate response (e.g., Hingray et al. 2007; Ruosteenoja et al. 2007). However, as the relevance of this assumption has not been assessed so far for a scaling relationship at the GCM scale, we also consider scaling without intercept (SCA0). The additive methods (Eq. 5) can be regarded as degenerated linear regression with slope 1 and intercept $\overline{DE}$, while scaling (Eq. 7) is a full linear regression with varying intercept and slope

(except SCA0 where the intercept is forced to zero). We also note that RCM specific sampling is not feasible as the majority of RCMs is only driven by a single GCM (see Fig. 8). In addition, the insufficient sample size at the RCM specific level does not allow for applying a hierarchical linear model in order to estimate RCM specific regression lines (Gelman and Hill, 2009). Furthermore, we note that the random sampling approaches ADD3 and SCA3 are embedded in the framework of multiple imputation (MI; Rubin 1987; Little and Rubin, 2002). MI aims at generating a set of multiple plausibly reconstructed data sets and common statistical analysis is applied to each individual data set, generating a set of parameter estimates of interest. As we are dealing with a large fraction of missing values, we generate 1000 reconstructed data sets throughout the study in order to ensure convergence of random sampling. The final parameter estimate is then achieved by simply taking the average of the 1000 realizations (Rubin, 1987).

II-4 Design of the Cross-Validation and Statistical Analysis

II-4.1 Cross-Validation

In order to compare the skill of the different reconstruction methods, we follow a cross-validation (CV) strategy. CV is often used to estimate the predictive skill of statistical models in application and has the advantage that it can be applied to small sample sizes as it does not rely on asymptotic theory. In this study, we apply a leave-one-out cross-validation (LOOCV) method by fitting the statistical model to a training data set which consists of leaving out a data point from the original sample. This data point is then predicted by the statistical model and the procedure is repeated for each single data point in the sample, generating a completely reconstructed data set. Concerning the LOOCV, we follow two strategies. First, we compute a LOOCV which is based on leaving out the CCS of a single RCM (LOOCV-RCM). As most of the GCMs are used as driving data for at least two RCMs, the entire GCM information is available for predicting the RCM change in most cases. Therefore, this strategy can be regarded as measuring the performance of deriving the missing CCSs of the ENSEMBLES simulation matrix (Fig. 8). However, as we aim at extending the ENSEMBLES simulation matrix to unknown GCMs, we also apply a more stringent cross-validation which is achieved by leaving out the CCSs of a GCM and all RCMs driven by this GCM as second LOOCV strategy (LOOCV-GCM).

Furthermore, CV of methods based on RCM specific information (D07, ADD2, and SCA2) requires RCMs which are driven by more than one GCM. Unfortunately, only eight simulations of three RCMs were forced by multiple GCMs in ENSEMBLES (see Fig. 8). Although the according LOOCV results are only a rough estimate of the skill due to the rather small sample size, it is the only possibility for comparing the skill of all implemented reconstruction methods. All other reconstruction methods allow for a LOOCV based on the full sample of 22 simulations.

As the focus of our study is on estimating expected climate change and its uncertainty, we use the LOOCV in order to assess the skill of the reconstruction methods in reproducing ensemble mean and standard deviation. However, it can be easily shown that the LOOCV ensemble mean of the additive reconstruction methods reduces to the ensemble mean of the real data. In particular, this is the case for all additive methods concerning LOOCV-RCM. For LOOCV-GCM, this is only the case for ADD2 since the number of RCMs and GCMs for deriving the mean downscaling effect of Eq. 5 varies for ADD1 and ADD3. In these cases, the bias of the CV evaluation cannot be interpreted. Therefore, although the performance in reconstructing single RCMs is not the focus here, we also report the mean square deviations (MSD) between reconstructed and real CCSs as background information and for comparative purposes.

II-4.2 Statistical Analysis

II-4.2.1 Statistical Significance

After reconstructing the missing values of the simulation matrix, we assess the statistical significance of the differences in expected climate change and uncertainty between original and reconstructed ensemble. Statistical tests for differences in the mean generally require equal variances (Behrens-Fisher problem). However, this cannot be assumed here, as the reconstruction of the missing values potentially changes the spread of the ensemble. Therefore, we apply a t-test for unequal variances (Welch-test) under the null hypothesis that the ensemble mean of original and reconstructed ensemble are equal. The application of the t-test requires independently and normally distributed samples. As we are dealing with rather small sample sizes, it is difficult to assess the normality of the data. However, the assumption of normality in our study is supported by the central limit theorem since multiple averaged quantities are applied. The statistical significance of the differences in the ensemble spread is assessed by applying the robust Fligner-Killeen test under the null hypothesis that the ensemble variances of original and reconstructed ensemble are equal (Conover et al. 1981).

In order to eliminate possible dependencies among the RCM simulations due to their driving GCMs, we average across the RCMs according to their driving GCMs. For the same reason, we average across the different GCM runs of the CMIP3 database after reconstructing the RCM changes. Therefore, the sample sizes of original and reconstructed simulation matrices reduce to the number of GCMs indicated in Fig. 8 (8 for the ENSEMBLES simulation matrix and 27 for the extended matrix). Significance levels lower than 5 %, 5 % to 10 %, 10 % to 20 %, and greater 20 % are termed as strongly significant, significant, weakly significant, and insignificant, respectively.

II-4.2.2 Quantification of Uncertainty

The uncertainties of the projected changes are quantified by two measures. First, we calculate the ensemble standard deviation. As its calculation is based on rather small sample sizes in this study, we apply a minor bias correction of the standard deviation (Johnson et al. 1994) as proposed in Knutti et al. (2010). Second, we calculate the percentage of models which coincide in the sign of change as a non-parametric uncertainty measure. Applying the confidence terminology of the fifth assessment report of the intergovernmental panel on climate change (Mastrandrea et al. 2010), very high confidence, high confidence, and medium confidence is obtained if at least 90 %, at least 80 %, and at least 50 % agree in the sign of the multi-model mean change, respectively.

II-5 Results of the Cross-Validation

Fig. 10 and Fig. 11 depict the results of the LOOCV for air temperature and precipitation amount, respectively. The spread of the box-whisker plots displays variability among subregions. For comparative purposes, we only show the results of LOOCV-RCM based on the subset of RCM simulations driven by multiple GCMs including all reconstruction methods. All additional LOOCV results based on LOOCV-GCM and the full sample are provided in Appendix II, Fig. A 21 to Fig. A 26.

For air temperature, the largest differences between reconstructed and original ensemble mean are obtained for D07 concerning all seasons. However, the bias is rather small, showing mostly an underestimation of the ensemble mean. The largest bias of D07 is obtained in DJF with -0.06 K in the median and ranging from -0.13 K to -0.04 K. SCA0 shares this negative bias in DJF, but with a lower magnitude of -0.01 K in the median. For all other methods, biases in both directions are obtained with magnitudes lower than ±0.02 K in the median. The ensemble averages of the additive reconstruction methods reduce per definition to that of the original ensemble which trivially results in a zero bias. The small differences between ADD1 and ADD3 (SCA1 and SCA3) can be related to finite sampling of the anomalies (residuals) which converges to zero as the number of random draws increases. For the ensemble standard deviation, D07 shows an underestimation which is largest in DJF with -0.23 K in the median. All other additive methods overestimate the ensemble spread with the largest difference of +0.50 K in the median for ADD2 in JJA. The scaling methods generally perform better in reconstructing the ensemble standard deviation. Especially SCA3 compensates for the underestimated standard deviation obtained by the other scaling methods due to random sampling of the residuals, resulting in differences close to zero. The MSD is generally lower for the scaling methods. The difference between ADD1 and ADD3 (SCA1 and SCA3) can be related to the additional variability due to sampling of the anomalies (residuals). This effect is highly pronounced in JJA, indicating large variability of the CCSs among RCMs.

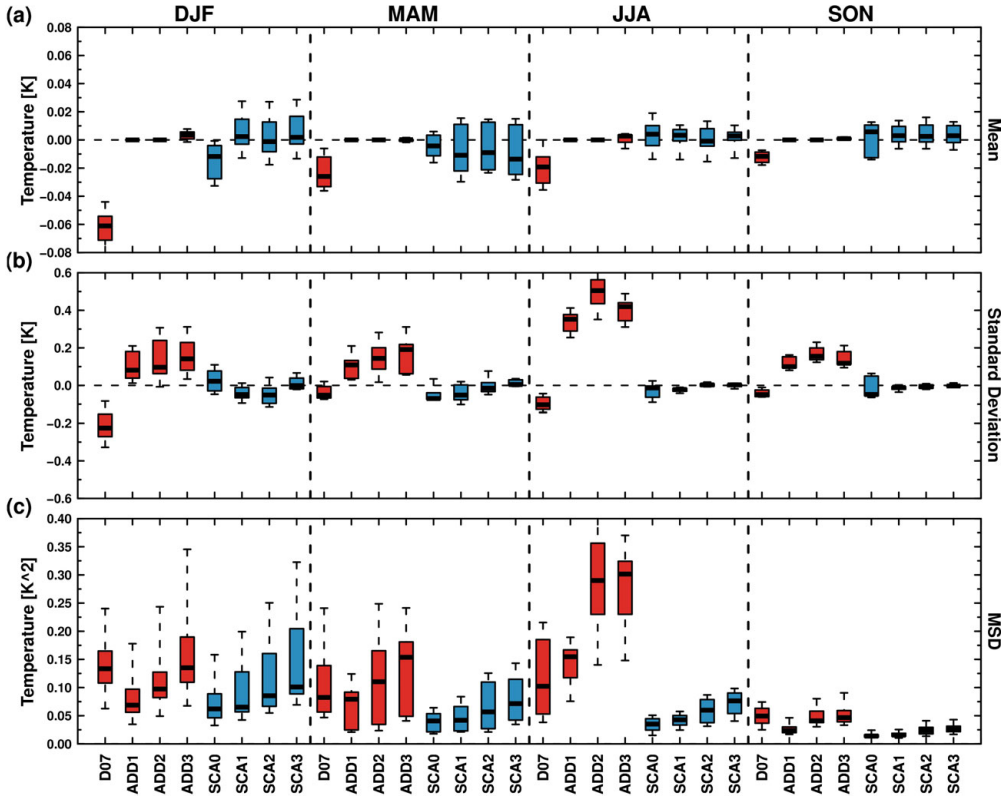

Fig. 10 Results of the LOOCV-RCM for air temperature based on the subset of RCMs which are driven by multiple GCMs. Red and blue colours indicate the additive and scaling reconstruction methods, respectively. Displayed are the differences between reconstructed and original ensemble mean (panel a) and standard deviation (panel b), and the MSD (panel c). The spread of the box-whisker plots shows variability among subregions and displayed are the 10th, 25th , 50th, 75th, and 90th percentile.

For precipitation amount, D07 tends to overestimate (underestimate) the ensemble mean in DJF and JJA (MAM and SON). The biases are rather small with a peak magnitude in SON with -0.3 % in the median. For the scaling methods, an underestimation of the ensemble mean is obtained in MAM and SON. SCA0 generally shows large biases in combination with rather large ranges. The largest bias of SCA0 is found in SON with a median difference of -0.7 % and ranging from -3.0 % to +1.0 %. For the ensemble standard deviation, D07 tends to underestimate the ensemble spread while the other additive reconstruction methods tend to overestimate variability. The largest difference is obtained for ADD2 in MAM with a difference of +3.2 % in the median and ranging from -1.2 % to +5.8 %. The scaling methods generally perform better than the additive methods, especially in DJF and MAM. While SCA0, SCA1, and SCA2 tend to underestimate variability, random sampling of the residuals increases variability and SCA3 again shows the overall best performance in reproducing the ensemble standard deviation. The largest underestimation is obtained for SCA0 in JJA with a difference of -3.3 % in the median and ranging from -4.2 % to +1.4 %. For the MSD, all methods consistently reveal lower deviations in DJF and SON than in MAM and JJA. The methods assuming RCM specific downscaling effects generally show the largest MSD. As expected, large additional variability due to sampling is introduced mainly in JJA, indicating again large variability of the CCSs among RCMs. The results of the

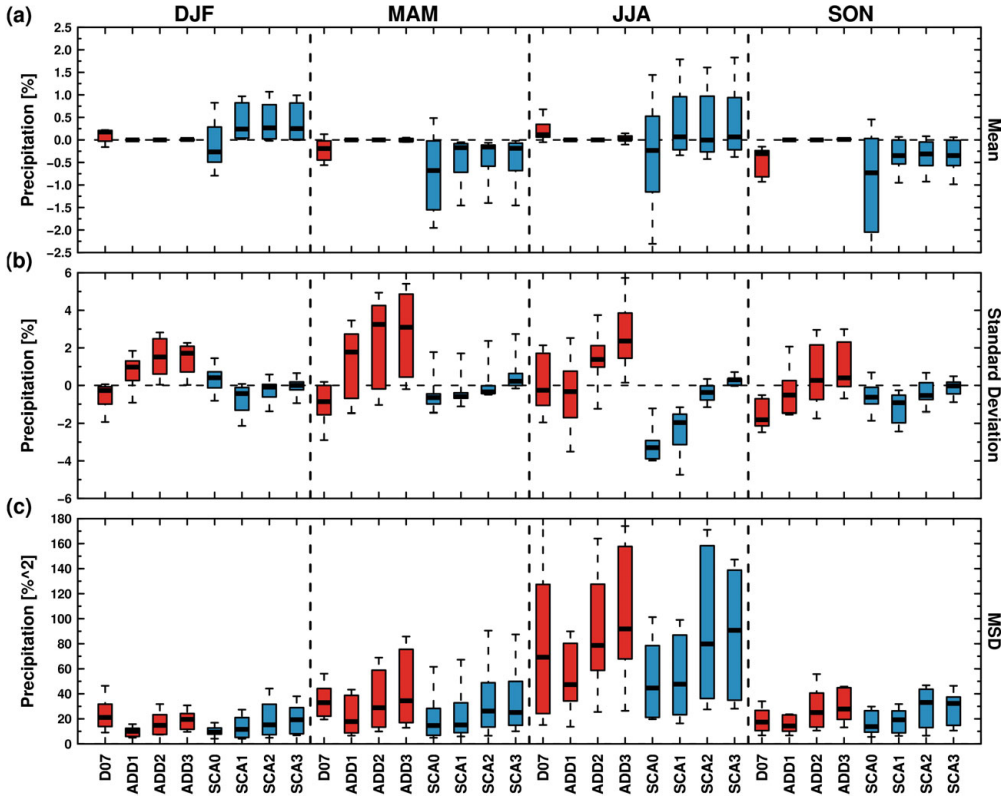

Fig. 11 Same as Fig. 3 but for precipitation amount.

second cross-validation strategy (LOOCV-GCM) based on the same subset are in line with the results reported above. Extending the LOOCV to the entire sample, rather large negative precipitation biases are obtained for SCA0 in all seasons. Concerning the ensemble spread, ADD1 and ADD3 (SCA0 and SCA1) mostly overestimate (underestimate) variability and the superiority of SCA3 in reconstructing the ensemble standard deviation is further underpinned (see Appendix II, Fig. A 21 to Fig. A 26).

Since a specific focus of our study is on uncertainty estimation, we choose SCA3 as preferred reconstruction method based on the results of the LOOCV. Tab. A 1 in Appendix II summarises the results of the two LOOCV strategies for SCA3 based on the entire sample. As expected, the results of the less stringent LOOCV-RCM indicate better performance than LOOCV-GCM due to the larger sample size. Differences in the ensemble mean and spread are mostly clearly below ±0.1 K and ±1 % for air temperature and precipitation amount, respectively. The coefficient of determination (R2) is generally lager for air temperature than for precipitation amount, ranging from 0.09 for precipitation amount for MD in JJA to 0.96 for air temperature for BI in DJF. However, small R2 values are in general not accompanied by large biases and/or differences in the ensemble spread, reflecting a potential instability of the R2 due to a rather small sample size. Fig. 12 displays the linear fits between the CCSs of RCMs and according GCMs as further applied in the study. As it can be seen, intercept and slope are both varying across subregions and seasons, suggesting that the formulation

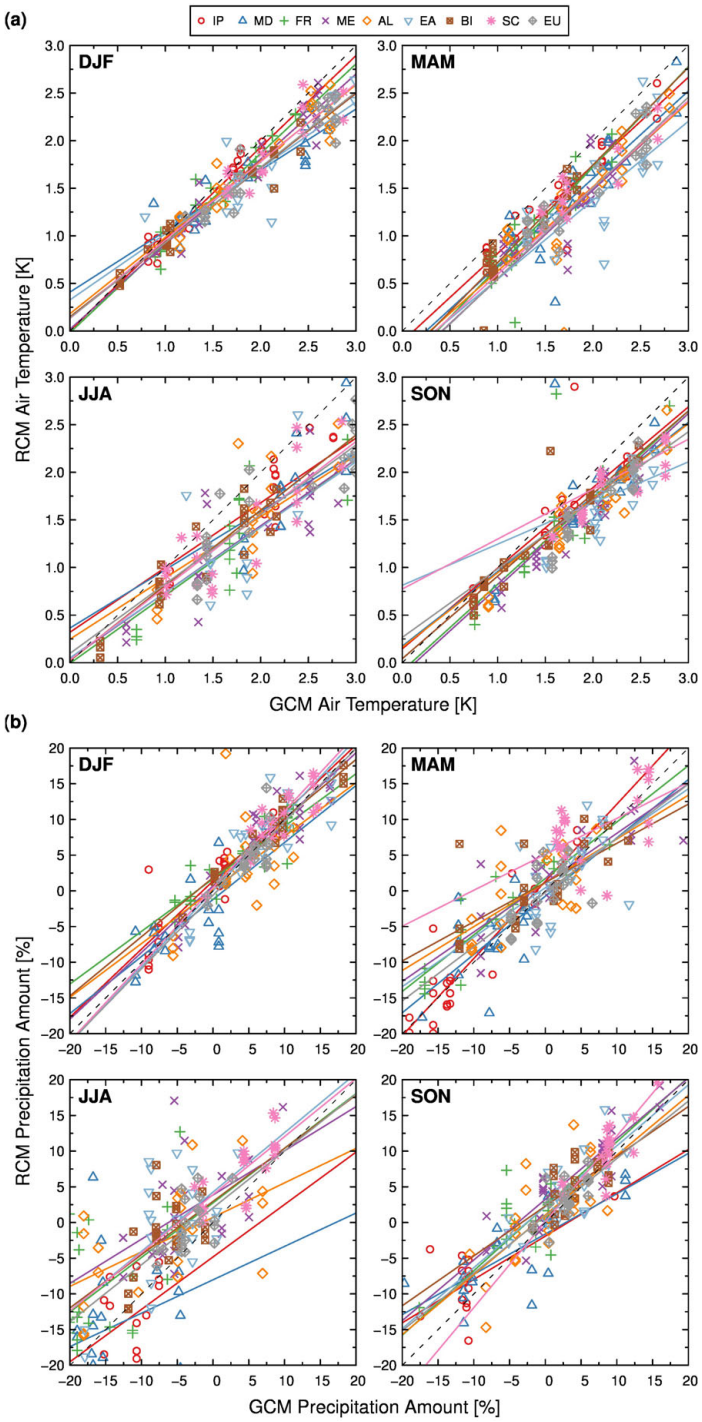

Fig. 12 Linear least-square fits between the seasonal CCSs of RCMs and according GCMs for air temperature (panel a) and precipitation amount (panel b). In each panel, top-left is DJF, top-right is MAM, bottom-left is JJA, and bottom-right is SON.

of the fixed slope models (ADD1, ADD2, and ADD3) as well as the zero intercept model (SCA0) may not be appropriate. This is generally in agreement with the results of the LOOCV. For example, air temperature reveals a distinct non-zero intercept in MAM for all subregions, resulting in poor performance of SCA0 concerning both LOOCV strategies (see Appendix II, Fig. A 23 and Fig. A 25). Fur-

thermore, as ADD1 and ADD3 rely on fixed slopes of 1, the poor skill for air temperature in JJA can be related to the linear fits which consistently show smaller slopes.

II-6 Revision of expected regional climate change and its uncertainty over Europe

Fig. 13a and Fig. 13b show the differences in the ensemble mean and standard deviation between original and filled ENSEMBLES simulation matrix for air temperature and precipitation amount, respectively. The left and right values in each box indicate the estimates of original and filled ensemble, respectively. The brightness of the colours represents the level of significance of the according differences. Blue and red colours indicate a shift towards lower and larger estimates, respectively. For air temperature, the differences in the ensemble mean are mostly negative in DJF, JJA, and SON indicating slightly larger CCSs of the original ensemble, while in MAM larger mean values of the filled ensemble are obtained for all subregions. However, the differences are rather small and insignificant, with a maximum of ±0.2 K. For the standard deviation, mostly lower values for the filled ensemble are obtained. Exceptions are EA and SC in JJA, and BI in DJF and the differences are again small and insignificant, peaking up to -0.5 K for SC in MAM. For precipitation amount, the differences vary across seasons and subregions. As for air temperature, the differences are again small and insignificant, with a maximum of -1.0 % for EA in DJF. Concerning the ensemble spread, mostly lower standard deviations for the filled ensemble are obtained. Exceptions are IP and SC in DJF, and FR and ME in MAM. The differences are again rather small and insignificant, peaking up to -4.2 % for FR in MAM.

Fig. 13c and Fig. 13d show the differences in the ensemble mean and standard deviation between original and extended ensemble concerning all available GCM simulations of CMIP3 forced by the A1B emission scenario. For air temperature, the ensemble mean of the extended matrix mostly shows lower values. The largest differences are -0.3 K for EA in DJF, -0.2 K for MD in MAM, -0.4 K for EA in JJA, and -0.3 K in SON. The changes of MD in DJF and EA in JJA are weakly significant. Concerning the ensemble spread, the extended matrix shows a reduction, except for BI in DJF. The largest changes are -0.4 K for SC in DJF, -0.5 K for EA and SC in MAM, -0.2 K in JJA, and -0.5 K for EA in SON. Strongly significant and significant changes are found for MD, EA, SC, and EU in DJF and for EA in MAM. For precipitation amount, the sign of the difference in the ensemble mean is varying among subregions and seasons. Only in SON, mostly lower CCSs of the extended matrix are obtained. The largest differences are -4.3 % for IP in DJF, -3.7 % for IP in MAM, +1.6 % for EA in JJA, and -2.5 % for SC in SON. Only IP in DJF shows a significant change. Concerning the ensemble spread, mostly lower ensemble standard deviations of the extended matrix are obtained. The largest changes are -2.9 % for BI in DJF, -2.5 % for ME in MAM, -3.3 % for AL in JJA, and -2.2 % for IP and ME in SON. Significant changes are found for EA and BI in MAM, for AL in JJA, and for MD in SON.

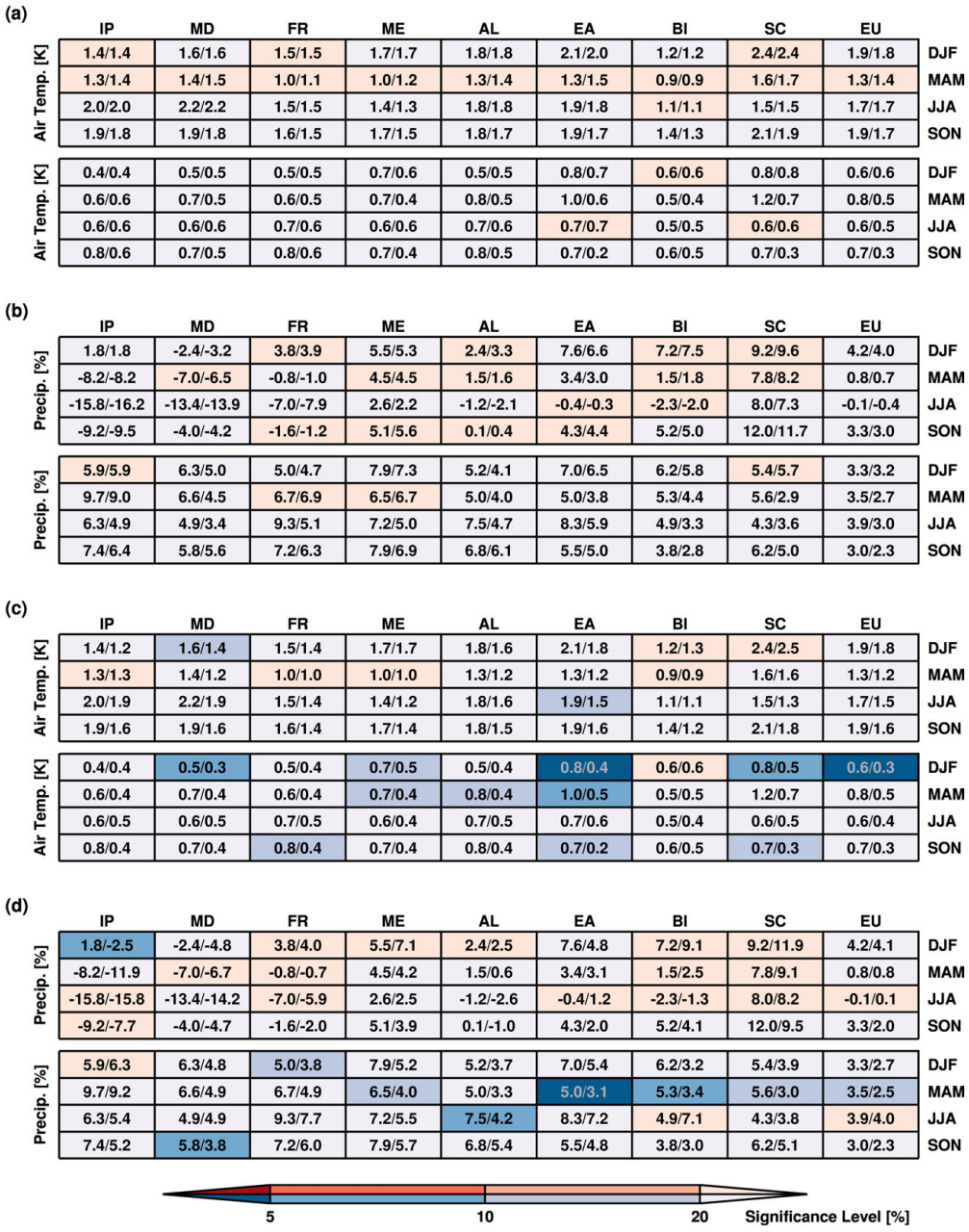

Fig. 13 Ensemble seasonal mean changes (upper rows of each panel) and standard deviations (lower rows of each panel) between 2021–2050 and 1961–1990 of original and filled ENSEMBLES simulation matrix (panel a and b, respectively) and of original and extended ENSEMBLES simulation matrix (panel c and d, respectively). The left and right values in each box indicate the estimates of original and reconstructed ensemble respectively. The brightness of the colours represents the level of significance of the according differences. Blue and red colours indicate a shift towards lower and larger estimates of the reconstructed ensemble, respectively. *** warum zeigen a und c nicht dasselbe? ***

We note that the main characteristics of the geographical pattern of the CCSs are not altered through statistical reconstruction (also see Appendix II, Fig. A 27 and Fig. A 28). These patterns include large spatial differences of winter air temperature change, which are explained by moderate warming of the ocean influencing the maritime climate of western Europe in combination with altered snow-albedo feedback mechanisms in northern and eastern Europe (Rowell 2005), high summer air temperatures in the south, which are related to an earlier and more rapid reduction of

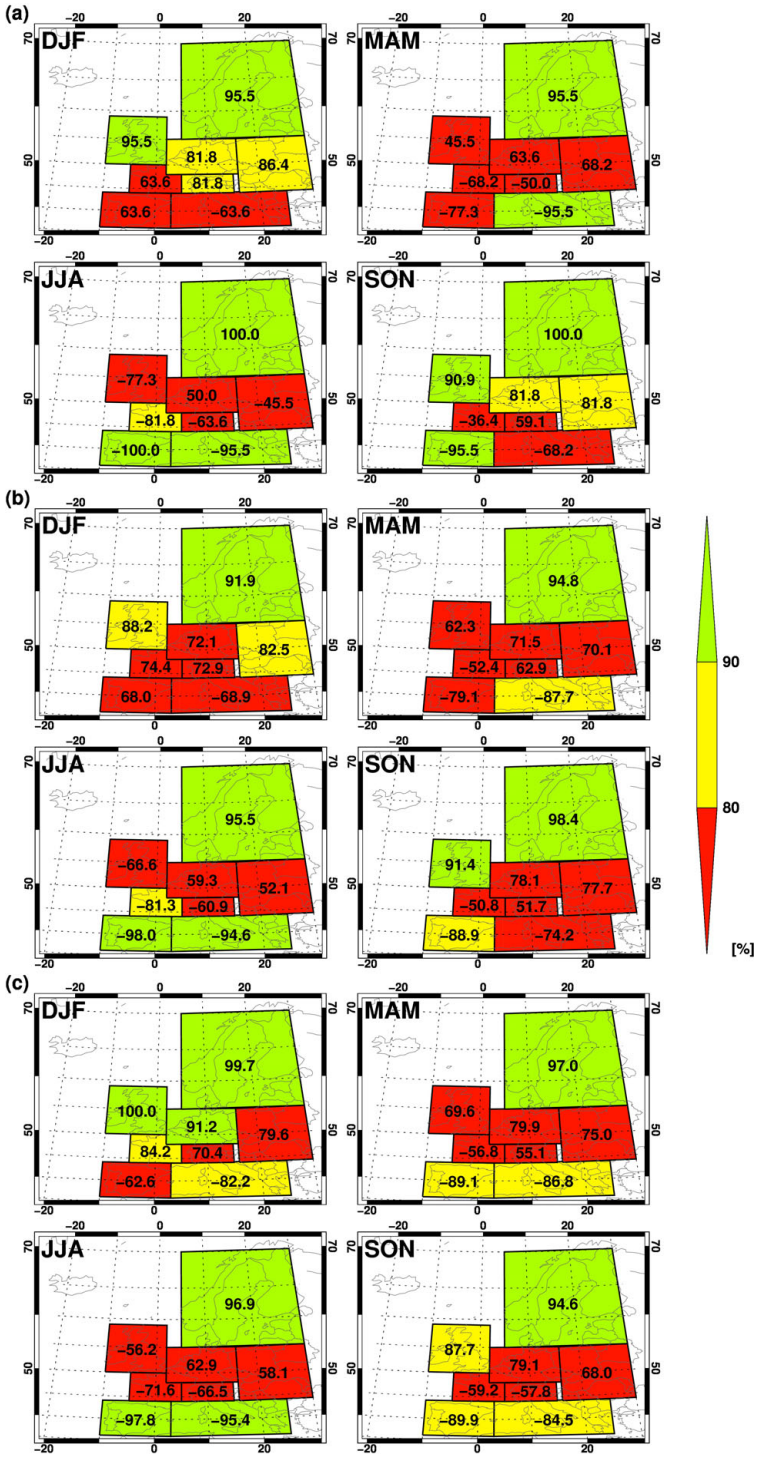

Fig. 14 Confidence of the projected precipitation changes for the original (panel a), filled (panel b), and extended (panel c) ENSEMBLES simulation matrix. Green, yellow, and red colours display very high confidence, high confidence, and medium or no confidence, respectively. The numbers indicate the percentage of models which agree in the sign of the ensemble mean. In each panel, top-left is DJF, top-right is MAM, bottom-left is JJA, and bottom-right is SON.

soil moisture in spring (e.g., Wetherald and Manabe 1995; Gregory et al. 1997), and a dipolar pattern of the precipitation change (decrease in the south and increase in the north), which can be related to

a seasonal dependent northward shift of the mid-latitude storm track which is identified as the European Climate change Oscillation (ECO) (Giorgi and Coppola 2007).

Fig. 14 depicts the confidence levels of the precipitation changes for the original (a), filled (b), and extended (c) ENSEMBLES simulation matrix. Green, yellow, and red colours display very high confidence, high confidence, and medium or no confidence, respectively. The numbers indicate the percentage of models which agree in the sign of the ensemble mean change. Percentages lower than 50 % indicate skewed distributions. Air temperature is not shown, since very high confidence of warming is achieved in all subregions with and without reconstruction (Appendix II, Fig. A 13). The filled ENSEMBLES simulation matrix shows lower confidence levels for AL, BI, and ME in DJF compared to the original ensemble. In MAM, a change from very high confidence to high confidence is obtained for MD. In JJA, the pattern remains unchanged while EA, IP, and ME reveal lower confidence levels in SON. Concerning the extended ENSEMBLES simulation matrix, AL and EA (FR, MD, and ME) reveal changes towards lower (larger) confidence levels in the extended ensemble in DJF. In MAM, the confidence of the southernmost subregions IP and MD changes from medium and very high confidence to high confidence. In JJA, only FR shows a change from high to medium confidence. In SON, larger confidence levels are obtained for the changes in MD, while BI, EA, IP, and ME feature lower confidence. Generally, the differences between original, filled, and extended ENSEMBLES ensemble are small and the overall picture (high confidence in northern and partly in southern Europe, low confidence in-between) remains the same.

II-7 Summary and Conclusions

This study assesses and compensates the GCM sampling bias in expected regional climate change and the associated uncertainty of the ENSEMBLES RCM projections by combining them with the full set of the CMIP3 GCM ensemble. The focus was on eight European subregions and the changes of the two key climate variables air temperature and precipitation amount until the mid-21st century were assessed.

In order to underpin the importance of reconstructing RCM responses, we first highlighted the impact of RCMs on the climate change signals of their driving GCMs and showed that downscaling generally leads to less warming (up to a reduction of 30 % of the GCM CCS) and partly to more precipitation over Europe than projected by GCMs. We introduced and evaluated statistical data reconstruction methods which mimic these effects and allow for an extension of the RCM ensemble to additional driving GCMs. The most appropriate reconstruction method, a randomized scaling approach with errors in ensemble mean and standard deviation mostly below ±0.1 K and ±1 % for air temperature and precipitation amount, respectively, was applied to fill the missing values of the ENSEMBLES

simulation matrix and to further extend the matrix by all available CMIP3 GCM simulations forced by the A1B emission scenario.

Differences between original, filled, and extended ENSEMBLES simulation matrix were assessed in order to identify potential ensemble biases and improperly estimated uncertainty ranges due to the GCM sampling strategy of ENSEMBLES. The key findings of the intercomparison can be summarised as follows: (1) The estimated mean climate change signals of air temperature and precipitation amount over Europe are not altered significantly due to reconstruction in almost all seasons and subregions. (2) The estimated uncertainty is generally not increased by extension of the ENSEMBLES simulation matrix to the entire CMIP3 ensemble. In some seasons and subregions it is even significantly reduced.

We note that no weighting regarding model performance was applied in our study. Although our framework would allow for the incorporation of such weights, the benefits of performance weighting in constraining uncertainty of future projections could yet not be sufficiently demonstrated (e.g., Knutti 2010; Déqué 2012).

From the results of our analysis we conclude that expected climate change and the according uncertainty of the ENSEMBLES RCM projections are both not underestimated using only few driving GCMs. In contrast, the ensemble spread of the extended ensemble is partly significantly lower than that of the original ensemble. Therefore, this study substantially adds to the reliability of numerous recent climate change impact studies over Europe which use the full range or a carefully selected subset of the ENSEMBLES projections (e.g., Heinrich and Gobiet 2011a; Finger et al. 2012), since it confirms that the ensemble is not significantly biased and the uncertainty is not underestimated due to GCM sub-sampling.

Appendix II

		Air Temperature				Precipitation Amount			
		DJF	MAM	JJA	SON	DJF	MAM	JJA	SON
IP	*MEAN*	0.0/0.1	-0.2/-3.7	0.6/3.3	0.7/3.0	0.2/3.8	-3.7/-8.1	1.0/42.0	6.9/-6.8
	STDV	0.0/-0.2	-0.3/1.3	-0.1/-3.0	-0.4/-0.7	-2.5/-9.3	-1.3/-0.1	1.0/-29.8	1.5/25.2
	R^2	0.9/0.9	0.9/0.9	0.8/0.8	0.8/0.8	0.8/0.8	0.8/0.8	0.3/0.3	0.5/0.6
MD	*MEAN*	-0.4/2.7	-0.7/-8.2	0.5/5.7	0.7/8.1	-0.3/3.1	7.4/-14.9	-8.6/19.0	-4.0/-6.0
	STDV	0.0/1.3	-0.2/7.1	-0.2/1.5	-1.2/-6.9	-5.7/0.3	-10.2/9.6	6.8/1.0	3.4/-31.2
	R^2	0.8/0.8	0.7/0.7	0.7/0.7	0.5/0.5	0.6/0.6	0.4/0.5	0.1/0.1	0.6/0.6
FR	*MEAN*	0.0/1.0	0.1/-2.8	0.6/3.3	0.2/2.5	1.2/1.1	5.2/40.0	-12.1/-15.7	22.4/79.1
	STDV	-0.2/-1.0	0.1/1.5	-0.8/-3.8	-0.4/-0.5	-4.4/8.3	0.3/-38.9	-10.0/21.8	-29.5/-114.6
	R^2	0.9/0.9	0.8/0.8	0.8/0.8	0.7/0.7	0.8/0.8	0.8/0.8	0.2/0.2	0.6/0.6
ME	*MEAN*	0.0/2.9	-0.4/-10.7	0.0/2.3	0.4/4.1	9.9/58.6	8.9/18.6	-5.8/27.5	-3.4/-18.6
	STDV	0.2/1.5	0.4/6.5	-0.1/-3.0	-0.7/0.2	-8.5/-24.2	14.1/-1.5	-6.0/8.1	5.6/23.0
	R^2	0.9/0.9	0.5/0.5	0.7/0.7	0.5/0.5	0.8/0.8	0.7/0.6	0.3/0.3	0.8/0.8
AL	*MEAN*	0.2/5.0	-1.0/-12.2	0.6/3.4	0.1/6.1	15.3/88.1	8.9/64.0	10.0/81.3	2.3/2.5
	STDV	0.0/3.6	-0.1/12.1	-0.6/-3.9	-1.4/-2.9	-8.0/-46.6	-5.9/-44.0	9.8/47.2	3.4/-10.8
	R^2	0.9/0.9	0.6/0.6	0.7/0.7	0.5/0.4	0.4/0.4	0.5/0.4	0.3/0.3	0.5/0.5
EA	*MEAN*	-0.6/3.2	-0.3/-11.3	-0.5/2.6	-1.1/5.4	7.9/104.6	6.4/41.6	12.6/85.8	-0.8/-13.2
	STDV	0.2/3.5	0.1/8.7	0.5/-2.6	1.0/3.0	-6.2/-2.6	21.9/-2.5	-25.4/-30.1	1.3/14.5
	R^2	0.8/0.8	0.5/0.5	0.7/0.6	0.1/0.1	0.7/0.7	0.3/0.2	0.3/0.4	0.6/0.6
BI	*MEAN*	0.3/1.3	0.3/-1.5	0.6/1.4	0.2/1.3	6.0/9.6	1.1/-60.9	13.2/63.7	1.4/31.2
	STDV	0.1/-0.5	-0.2/0.4	-0.1/-2.0	-0.1/1.7	-1.5/22.2	5.4/50.5	2.9/38.0	0.2/29.3
	R^2	1.0/1.0	0.8/0.8	0.9/0.8	0.8/0.8	0.9/0.9	0.5/0.5	0.3/0.3	0.4/0.5
SC	*MEAN*	-0.1/-0.3	-0.1/1.3	-0.4/-2.5	-0.8/4.2	-0.3/-21.8	-5.7/-67.7	-1.7/26.2	-8.6/-50.8
	STDV	-0.3/2.0	0.1/10.6	0.2/0.6	-0.2/1.0	1.5/-36.2	-0.4/-14.0	1.2/-24.7	1.7/67.4
	R^2	0.9/0.9	0.7/0.6	0.8/0.7	0.2/0.2	0.7/0.7	0.3/0.2	0.6/0.5	0.7/0.7
EU	*MEAN*	-0.1/2.0	-0.3/-5.8	0.3/0.9	-0.1/3.8	0.2/13.2	10.7/72.9	4.5/22.0	0.9/11.2
	STDV	-0.2/1.0	0.2/5.4	-0.4/-0.9	0.0/1.7	-0.1/-12.3	11.8/-33.7	-4.9/14.3	0.7/-3.3
	R^2	0.9/0.9	0.7/0.6	0.8/0.8	0.3/0.3	0.6/0.7	0.4/0.4	0.3/0.4	0.5/0.5

Tab. A 1 Results of the cross-validation for SCA3. The left and right values indicate the estimates of LOOCV-RCM and LOOCV-GCM, respectively. Differences in the ensemble mean (MEAN) and standard deviation (STDV) between reconstructed and original ensemble are multiplied by a factor of 100 and the units are [K] and [%] for air temperature and precipitation amount, respectively. R^2 represents the coefficient of determination between the CCSs of RCMs and according GCMs.

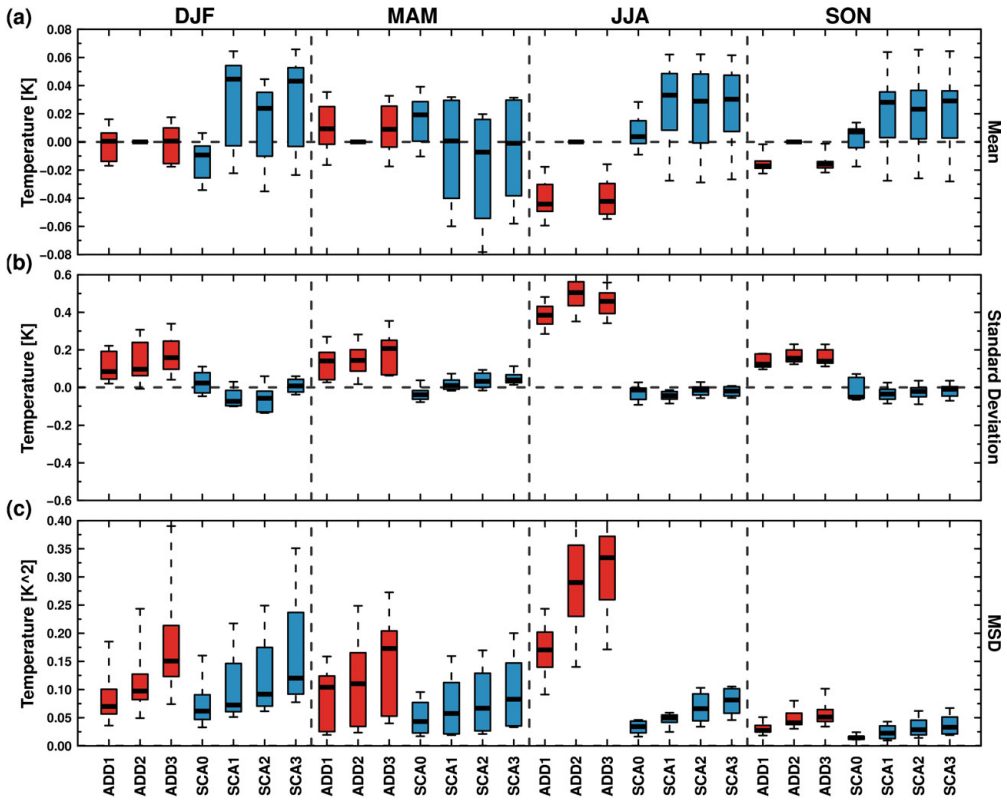

Fig. A 21 Results of the LOOCV-GCM for air temperature based on the subset of RCMs which are driven by multiple GCMs. Red and blue colours indicate the additive and scaling reconstruction methods, respectively. Displayed are the differences between reconstructed and original ensemble mean (panel a) and standard deviation (panel b), and the MSD (panel c). The spread of the box-whisker plots shows variability among subregions and displayed are the 10^{th}, 25^{th} , 50^{th}, 75^{th}, and 90^{th} percentile.

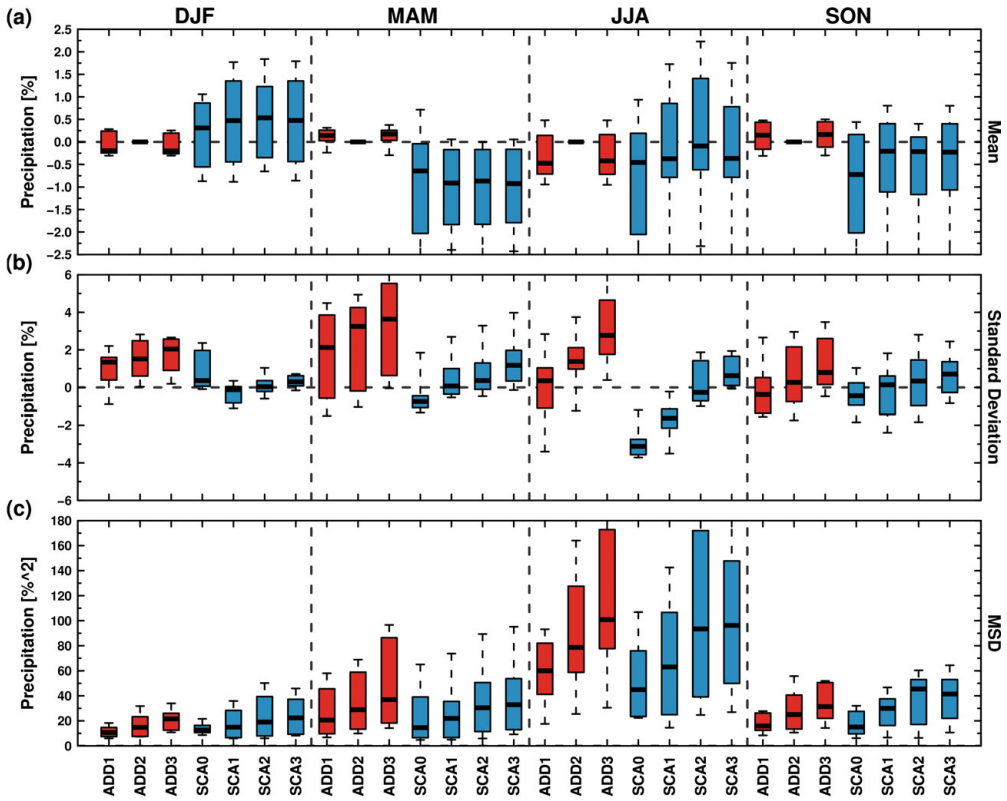

Fig. A 22 Same as Fig. A 21 but for precipitation amount.

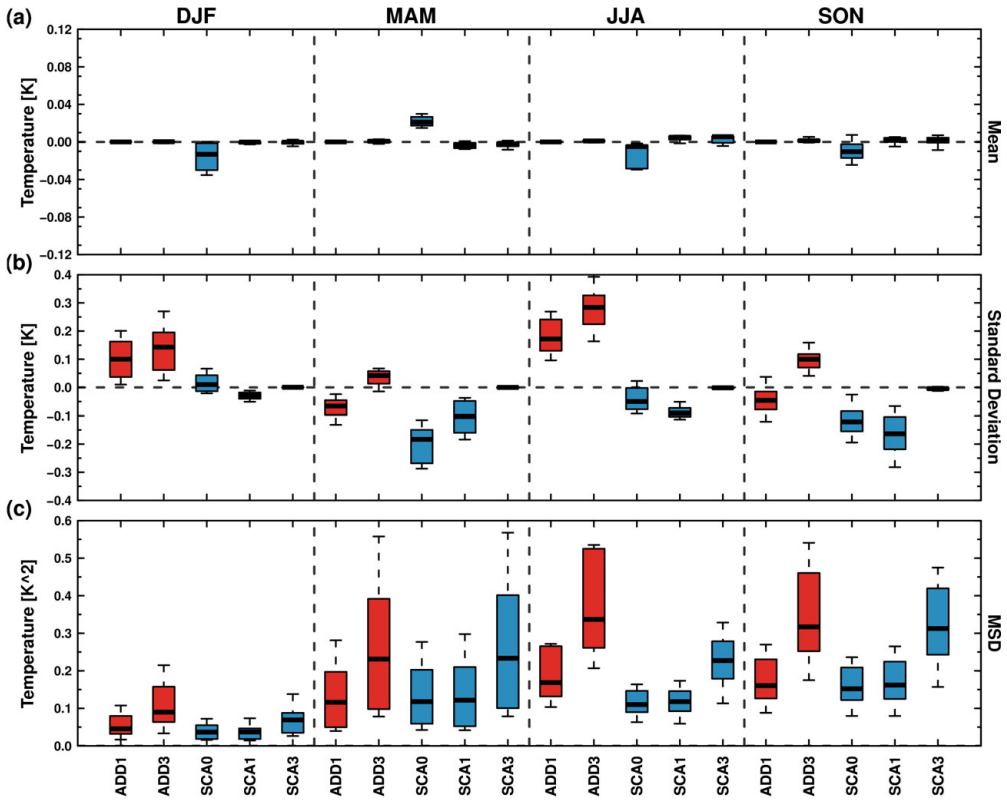

Fig. A 23 Same as Fig. A 21 but for LOOCV-RCM based on the entire sample of RCM simulations.

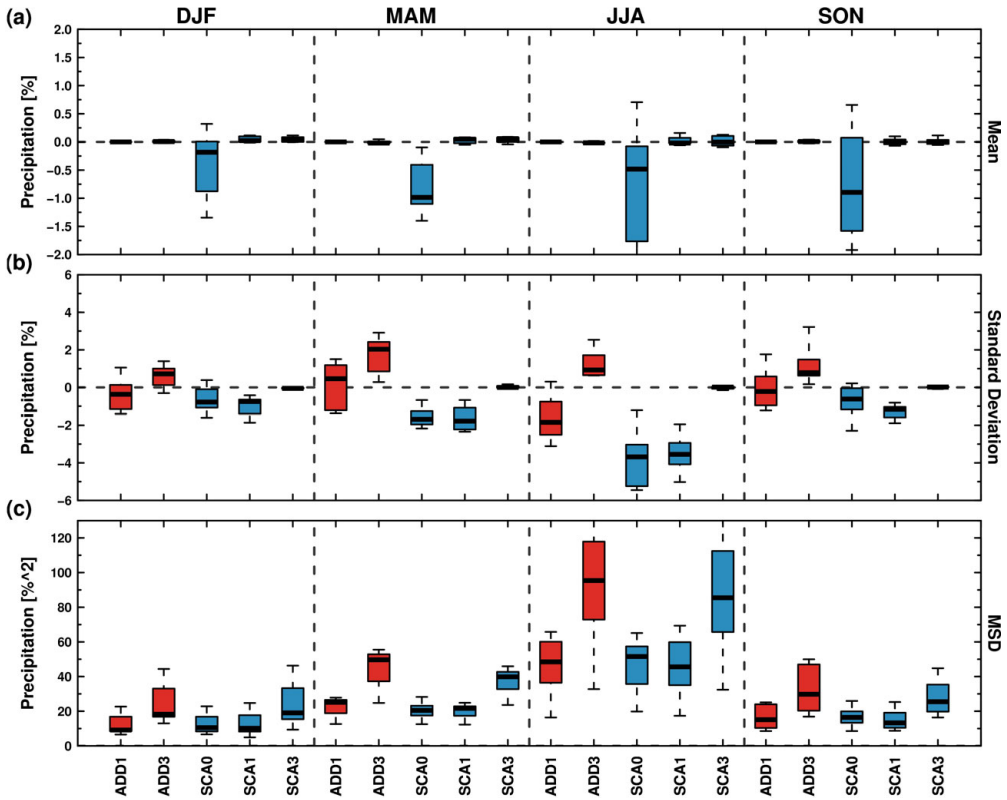

Fig. A 24 Same as Fig. A 23 but for precipitation amount.

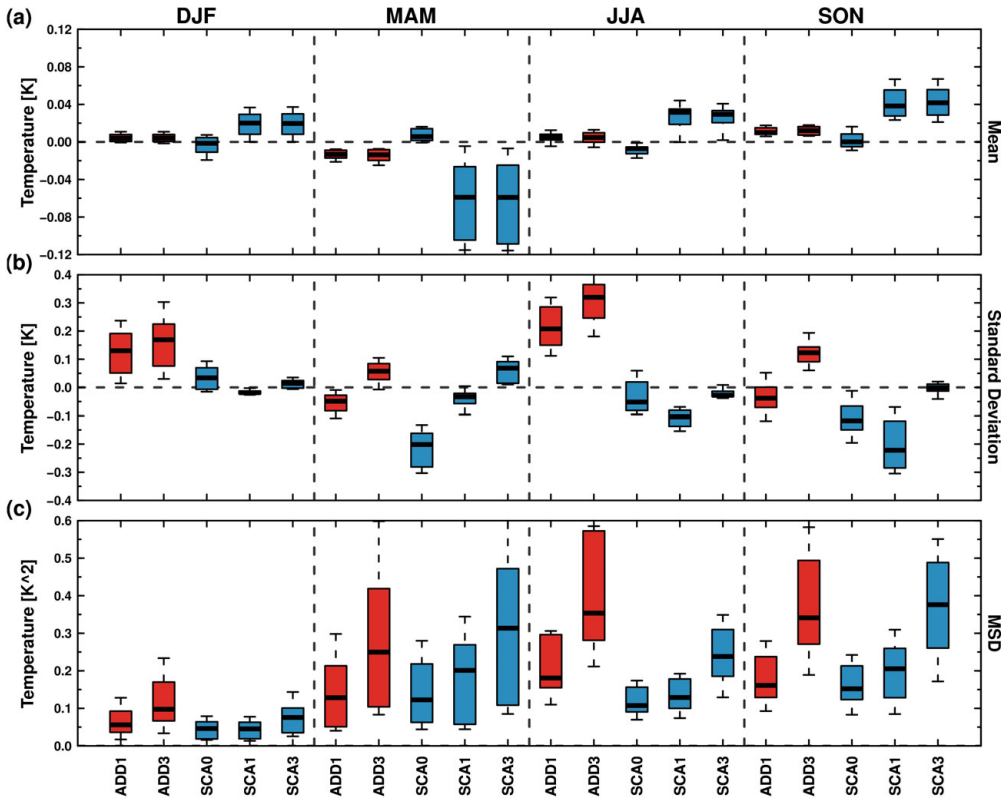

Fig. A 25 Same as Fig. A 21 but for LOOCV-GCM based on the entire sample of RCM simulations.

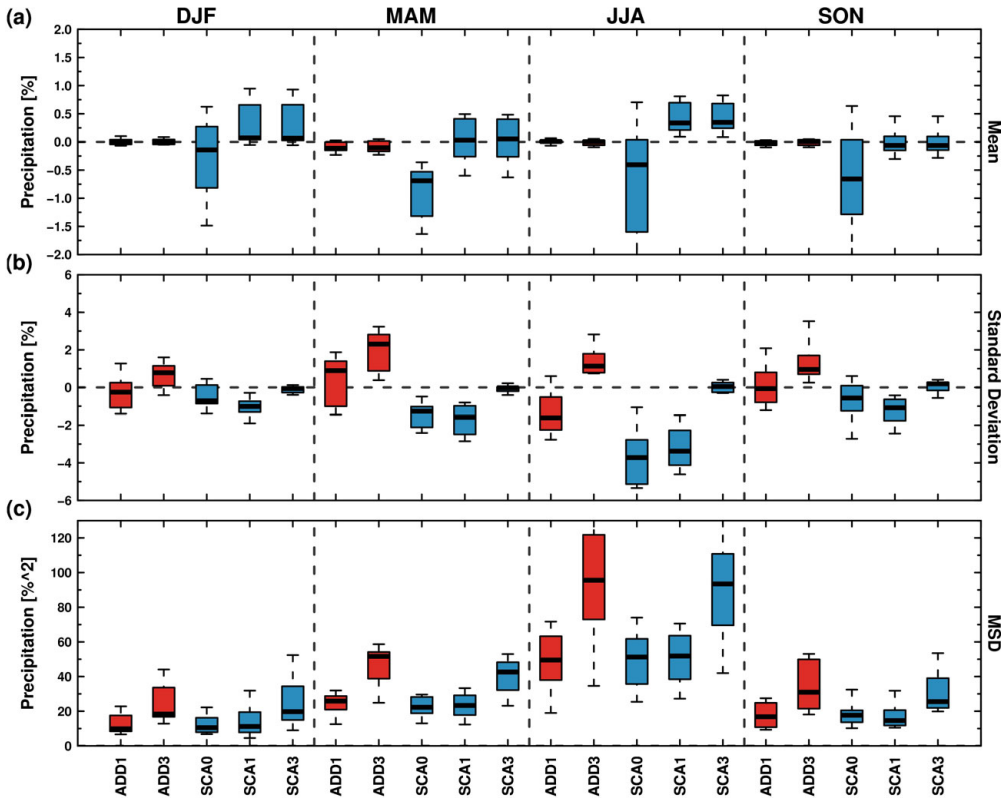

Fig. A 26 Same as Fig. A 25 but for precipitation amount.

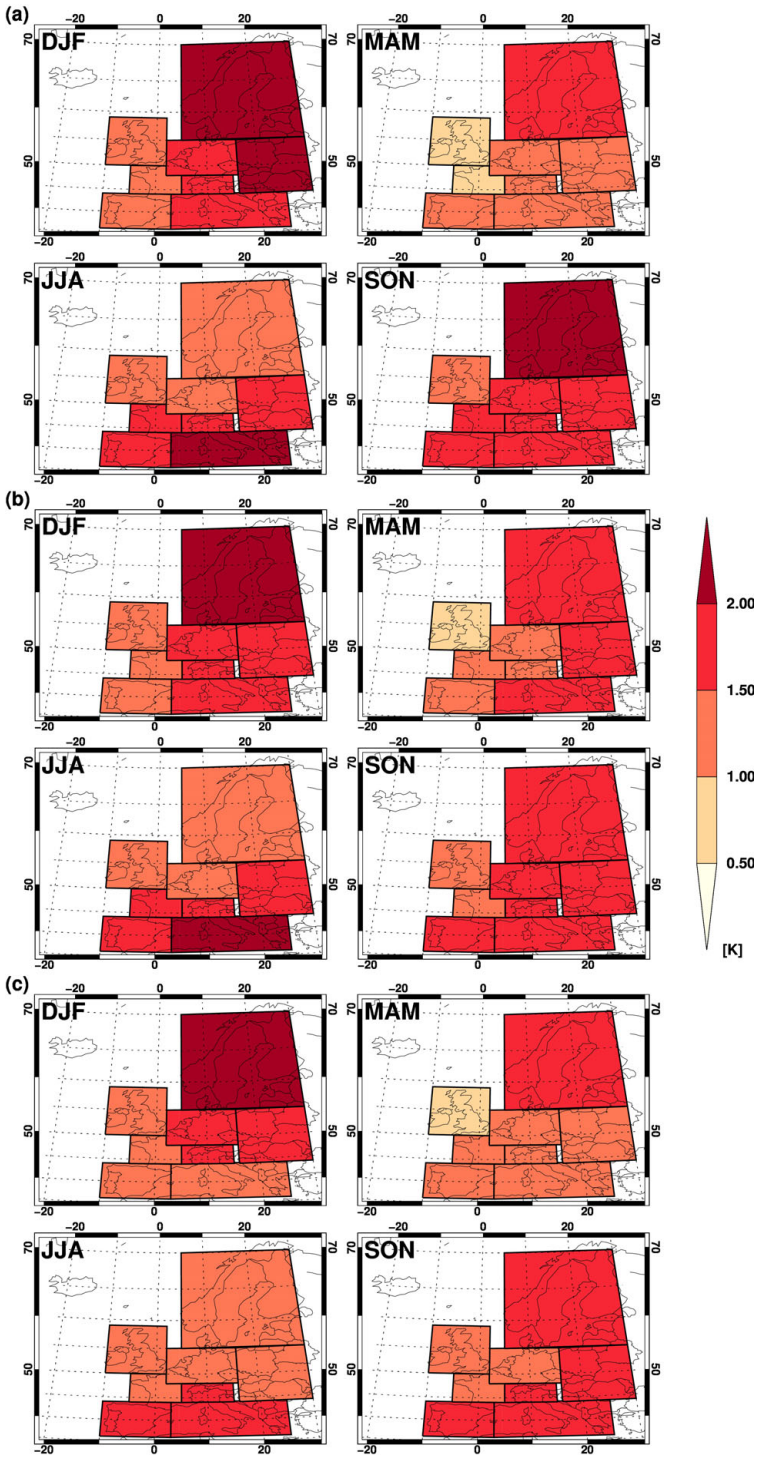

Fig. A 27 Projected seasonal air temperature changes between the two periods of 2021–2050 and 1961–1990 for the original (panel a), filled (panel b), and extended (panel c) ENSEMBLES simulation matrix. In each panel, top-left is DJF, top-right is MAM, bottom-left is JJA, and bottom-right is SON.

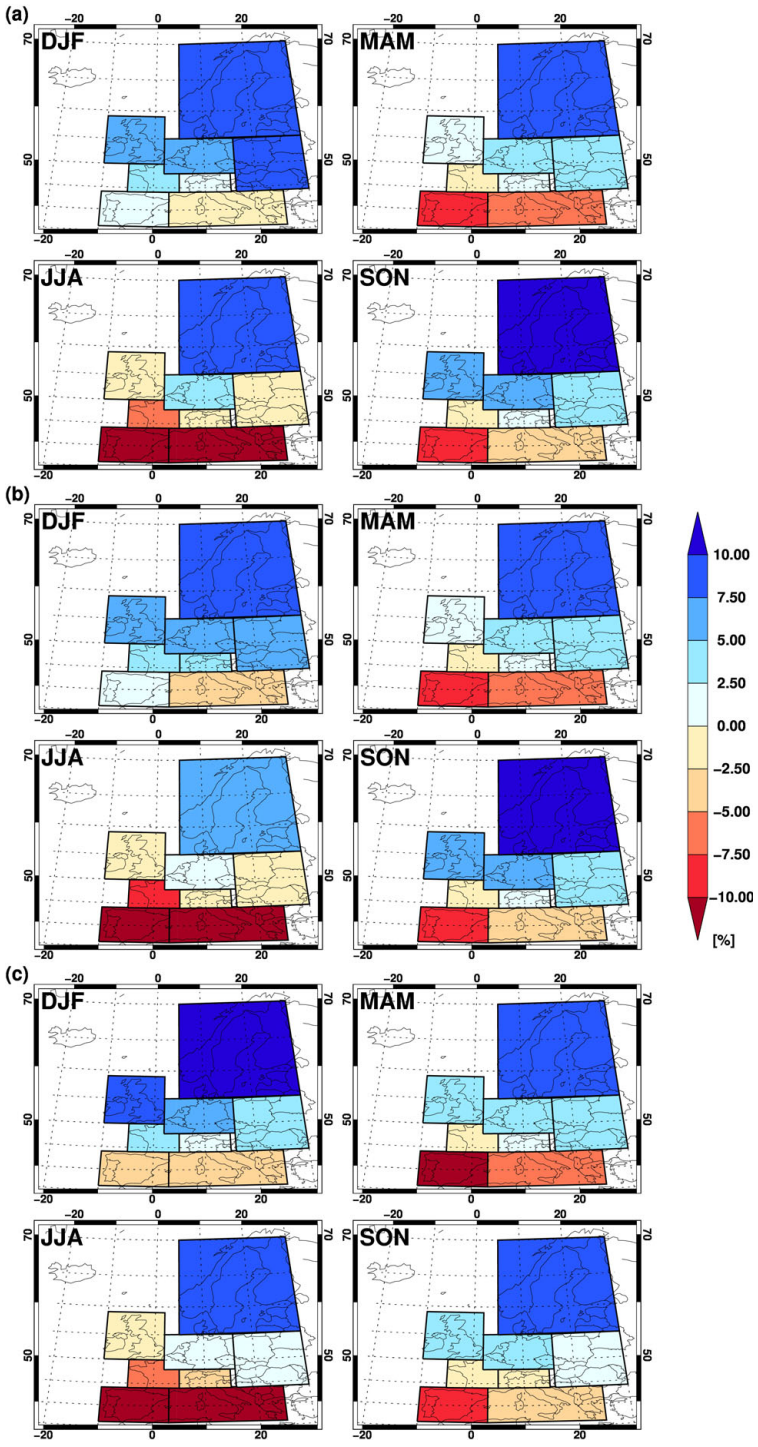

Fig. A 28 Same as Fig. A 27 but for precipitation amount.

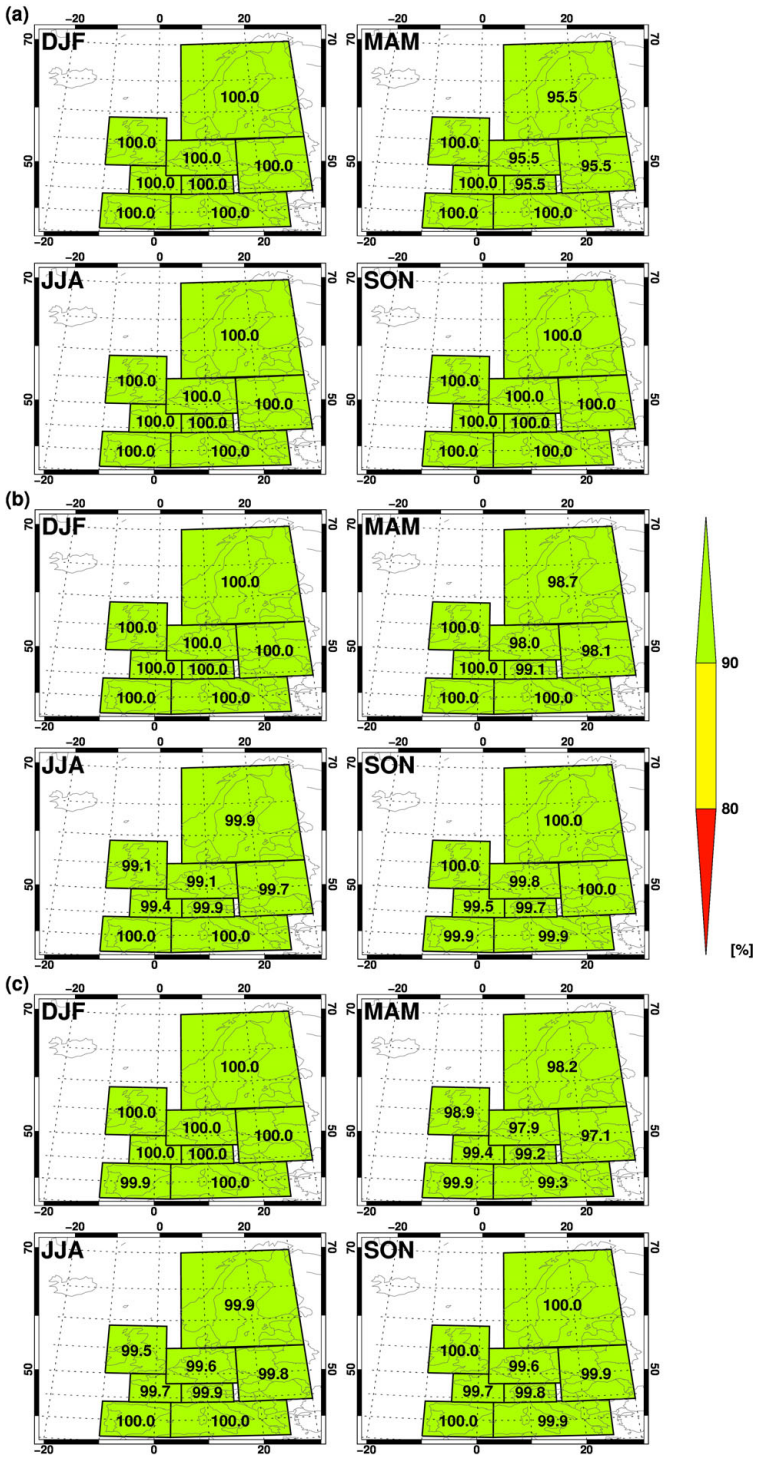

Fig. A 29 Confidence of the projected temperature changes for the original (panel a), filled (panel b), and extended (panel c) ENSEMBLES simulation matrix. Green, yellow, and red colours display very high confidence, high confidence, and medium or no confidence, respectively. The numbers indicate the percentage of models which agree in the sign of the ensemble mean. In each panel, top-left is DJF, top-right is MAM, bottom-left is JJA, and bottom-right is SON.

References

Alexander L. (2011) Climate science: Extreme heat rooted in dry soils. Nature Geoscience 4: 12-13. DOI: 10.1038/ngeo1045.

Buonomo E, Jones R, Huntingford IC, Hannaford J (2007) On the robustness of changes in extreme precipitation over Europe from two high resolution climate change simulations. Q J R Meteorol Soc 133:65–81

Castro CL, Pielke Sr RA, Leoncini G (2005) Dynamical downscaling: assessment of value retained and added using the regional atmospheric modeling system (rams). J Geophys Res 110:1–21

Christensen JH, Christensen OB (2007) A summary of the Prudence model projections of changes in European climate by the end of this century. Clim Change 81:7–30. doi: 10.1007/s10584-006-9210-7

Christensen JH, Rummukainen M, Lenderink G (2010) Formulation of very-high-resolution regional climate model ensembles for Europe. In: van der Linden P, Mitchell JFB (eds.) ENSEMBLES: Climate change and its impacts: Summary of research and results from the ENSEMBLES project. Met Office Hadley Centre, Exeter, UK, pp 47–58

Collins M, Booth BBB, Harris GR, Murphy JM, Sexton DMH, Webb MJ (2006) Towards quantifying uncertainty in transient climate change. Climate Dyn 27:127–147

Collins M (2007) Ensembles and probabilities: a new era in the prediction of climate change. Phil Trans R Soc A 365:1957-1970. doi: 10.1098/rsta.2007.2068

Conover WJ, Johnson ME, Johnson MM (1981) A comparative study of tests for homogeneity of variances, with applications to the outer continental shelf bidding data. Technometrics 23:351–361

Déqué M, Rowell DP, Lüthi D, Giorgi F, Christensen JH, Rockel B, Jacob D, Kjellström E, Castro M, Hurk B (2007) An intercomparison of regional climate simulations for Europe: assessing uncertainties in model projections. Clim Change 81:53–70

Déqué M, Somot S, Sanchez-Gomez E, Goodess CM, Jacob D, Lenderink G, Christensen OB (2012) The spread amongst ENSEMBLES regional scenarios: regional climate models, driving general circulation models and interannual variability. Climate Dyn 38:951–964. doi: 10.1007/s00382-011-1053-x

Déqué M, Somot S (2010) Weighted frequency distributions express modelling uncertainties in the ENSEMBLES regional climate experiments. Climate Res 44:195–209. doi:1 0.3354/cr00866

Feser F, Rockel B, von Storch H, Winterfeldt J, Zahn M (2011) Regional climate models add value to global model data: a review and selected examples. Bull Am Meteorol Soc 92:1181–1192. doi: http://dx.doi.org/10.1175/2011BAMS3061.1

Finger D, Heinrich G, Gobiet A, Bauder A (2012) Projections of future water resources and their uncertainty in a glacierized catchment in the Swiss Alps and the subsequent effects on hydropower production during the 21st century. Water Resour Res 48. doi:10.1029/2011WR010733

Gelman A, Hill J (2009) Data Analysis using regression and multilevel/hierarchical models. Cambridge University Press, New York, USA

Giorgi F, Mearns LO (1991) Approaches to regional climate change simulation: a review. Rev Geophys 29:191–216. doi: 10.1029/90RG02636

Giorgi F, Mearns LO (1999) Introduction to special section: regional climate modelling revisited. J Geophys Res 104:6335–6352. doi: 10.1029/98JD02072

Giorgi F, Coppola E (2007) European climate-change oscillation (ECO). Geophys Res Letter 34:L21703. doi: 10.1029/2007GL031223

Gregory JM, Mitchell JFB, Brady AJ (1997) Summer drought in northern midlatitudes in a time-dependent CO2 climate experiment. J Climate 10:662–686

Harris GR, Sexton DMH, Booth BBB, Collins M, Murphy JM, Webb MJ (2006) Frequency distributions of transient regional climate change from perturbed physics ensembles of general circulation model simulations. Climate Dyn 27:357–375. doi: 10.1007/s00382-006-0142-8

Hawkins E, Sutton R (2009) The potential to narrow uncertainty in regional climate predictions. Bull Am Meteorol Soc 90:p1095. doi: 10.1175/2009BAMS2607.1

Hawkins E, Sutton R (2011) The potential to narrow uncertainty in projections of regional precipitation change. Climate Dyn 37:407–418. doi: 10.1007/s00382-010-0810-6

Heinrich G, Gobiet A (2011a) The future of dry and wet spells in Europe: A comprehensive study based on the ENSEMBLES regional climate models. Int J Climatol. doi: 10.1002/joc.2421

Heinrich G., Gobiet G (2011b) reclip:century 1: Expected climate change and its uncertainty in the Alpine region. WEGC Report to the Austrian Climate Research Program (ACRP) Nr.02/2011, Wegener Center for Climate and Global Change, University of Graz, Austria. Report online available:http://reclip.ait.ac.at/reclip_century/fileadmin/user_upload/reclip_century_files/reclip_century_part_D_Aug_2011.pdf.

Hingray B, Mezghani A, Buishand TA (2007) Development of probability distributions for regional climate change from uncertain global mean warming and an uncertain scaling relationship. Hydrol Earth Syst Sci 11:1097–1114. doi:10.5194/hess-11-1097-2007

Johnson NL, Kotz S, Balakrishnan N (1994) Continuous univariate distributions. John Wiley & Sons, Inc., USA

Jones RG, Murphy JM, Noguer M (1995) Simulation of climate change over Europe using a nested regional-climate model. part i: assessment of control climate, including sensitivity to location of lateral boundaries. Q J R Meteorol Soc 121:1413–1449

Kendon EJ, Jones RG, Kjellström E, Murphy JM (2010) Using and designing GCM–RCM ensemble regional climate projections. J Climate 23:6485–6503. doi: http://dx.doi.org/10.1175/2010JCLI3502.1

Knutti R, Furrer R, Tebaldi C, Cermak J, Meehl GA (2010) Challenges in combining projections from multiple climate models. J Climate 23:2739–2758. doi: http://dx.doi.org/10.1175/2009JCLI3361.1

Laprise R (2003) Resolved scales and nonlinear interactions in limited-area models. J Atmos Sci 60:768–779

Little RJA, Rubin DB (2002) Statistical analysis with missing data. John Wiley & Sons, Inc., Hoboken, New Jersey, USA

Loibl W., Formayer H., Schöner S., Truhetz H., Anders I., Gobiet A., Heinrich G., Köstl K., Nadeem I., Peters-Anders J., Schicker I., Suklitsch S., Züger Z (2011) reclip:century 1: Models, Data, GHG-Scenarios, Simulations. Report to the Austrian Climate Research Program (ACRP), Austrian Institute of Technology (AIT), Vienna, Austria. Report online available: http://reclip.ait.ac.at/reclip_century/fileadmin/user_upload/reclip_century_files/reclip_century_Part_A_Aug_2011.pdf.

Mastrandrea MD, Field CB, Stocker TF et al. (2010) Guidance bote for lead authors of the IPCC fifth assessment report on consistent treatment of uncertainties. Intergovernmental Panel on Climate Change (IPCC), CA, USA

McGregor JL (1997) Regional climate modeling. Meteorol Atmos Phys 63:105–117. doi: 10.1007/BF01025367

Meehl GA, Covey C, Delworth T, Latif M, McAvaney B, Mitchell JFB, Stouffer RJ, Taylor KE (2007) The WCRP CMIP3 multimodel dataset: a new era in climate change research. Bull Am Meteorol Soc, 88:1383-1394

Mitchell JFB., Johns TC, Eagles M, Ingram WJ, Davis RA (1999) Towards the construction of climate change scenarios. Clim Change 41:547–581

Mitchell TD (2003) Pattern scaling: An examination of the accuracy of the technique for describing future climates. Clim Change 60:217–242

Nakicenovic N, Alcamo J, Davis G et al. (2000) IPCC Special Report on Emissions Scenarios. Cambridge University Press, Cambridge, United Kingdom and New York

Prein A, Gobiet A, Truhetz H (2011) Analysis of uncertainty in large scale climate projections over Europe. Meteorol Z 20:383–395. doi: 10.1127/0941-2948/2011/0286

Rowell PR (2005) A scenario of European climate change for the late twenty-first century: seasonal means and interannual variability. Climate Dyn 25:837–849. doi: 10.1007/s00382-005-0068-6

Rubin DB (1987) Multiple imputation for nonresponse in surveys. John Wiley & Sons, Inc., USA

Rummukainen M, Räisänen J, Bjørge D, Christensen JH, Christensen OB, Iversen T, Jylhä K, Ólafsson H, Tuomenvirta H (2003) Regional climate scenarios for use in Nordic water resources studies. Nordic Hydrol 34:399–412

Rummukainen M (2010) State-of-the-art with regional climate models. WIREs Clim Change 1: 82–96. doi: 10.1002/wcc.8

Ruosteenoja K, Tuomenvirta H, Jylhä K (2007) GCM-based regional temperature and precipitation change estimates for Europe under four SRES scenarios applying a super-ensemble pattern-scaling method. Clim Change 81:193–208

Suklitsch M, Gobiet A, Leuprecht A, Frei C (2008) High resolution sensitivity studies with the regional climate model CCLM in the Alpine region. Meteorol Z 17: 467–476

van der Linden P, Mitchell JFB (2009) ENSEMBLES: Climate change and its impacts: summary of research and results from the ENSEMBLES project. Met Office Hadley Centre, Exeter, UK

Wang Y, Leung LR, McGregor JL, Lee DK, Wang WC, Ding Y, Kimura F (2004) Regional climate modeling: progress, challenges and prospects. J Meteorol Soc Jap 82:1599–1628

Wetherald RT, Manabe S (1995) The mechanisms of summer dryness induced by greenhouse warming. J Climate 8:3096–3108

Abstract:
Future climate projections are always affected by uncertainties, whether because of natural variability of the climate system, unknown future greenhouse gas emissions, or approximation errors and simplifications in the applied climate models. However, the resulting uncertainties in climate change scenarios can be assessed by analysing an ensemble of climate simulations, which adequately samples the various sources of uncertainty. In this report, we assess the uncertainty of highly resolved regional climate change scenarios (10 km grid spacing) for the Alpine region as they were generated in the climate research projects reclip:century 1 and reclip:century 2 (reclip.ait.ac.at/reclip_century), funded by the Austrian Climate Research Program (ACRP). By putting these simulations, conducted by the Austrian Institute for Technology (AIT), the Wegener Center for Climate and Global Change (WEGC), and the Central Institute for Meteorology and Geodynamics (ZAMG), into the context of the most recent and comprehensive ensemble of regional climate model (RCM) simulations available for Europe from the EU FP6 project ENSEMBLES (ensembles-eu.org). In this report, we derive the expected climate change of a set of "key climate variables" (temperature, precipitation, global radiation, relative humidity, and wind speed) and assess its associated uncertainty throughout the 21st century. Furthermore, we analyze the ENSEMBLES ensemble with regard to potential sampling biases introduced by the sampling strategy of driving global climate models (GCMs). In this respect, statistical reconstruction methods are applied in order to combine the fine-scale uncertainty of the RCM ensemble with the uncertainty of the much larger coarse-scale ensemble of possible driving GCMs of the CMIP3 project (esg.llnl.gov:8080).

Zum Inhalt:
Klimaprojektionen sind immer von Unsicherheit begleitet, sei es durch die natürliche Variabilität des Klimasystems, unbekannte zukünftige Treibhausgasemissionen oder durch Approximationsfehler und Vereinfachungen in den eingesetzten Klimamodellen. Allerdings kann die resultierende Unsicherheit in Klimaänderungsszenarien durch Verwendung eines Ensembles von Klimasimulationen, welches die verschiedenen Quellen der Unsicherheit adäquat abbildet, bewertet werden. In diesem Bericht analysieren wir die Unsicherheit von hoch aufgelösten Szenarien (10 km Gitterweite) von regionale Klimamodellen (RCMs) für den Alpenraum, wie sie in den Forschungsprojekten reclip:century 1 and reclip:century 2 (reclip.ait.ac.at/reclip_century), gefördert vom Austrian Climate Research Program (ACRP), erstellt wurden. Dabei werden die vom Austrian Institute for Technology (AIT), dem Wegener Center für Klima und Globalen Wandel (WEGC) und der Zentralanstalt für Meteorologie und Geodynamik (ZAMG) durchgeführten Klimasimulationen in den Kontext des neuesten und umfassendsten Ensembles an regionalen Klimasimulationen für Europa vom EU FP6 Projektes ENSEMBLES (ensembles-eu.org) gestellt. Der Bericht fokussiert sich auf erwartete Klimaänderungssignale wichtiger Klimaelemente (Temperatur, Niederschlag, Globalstrahlung, relative Luftfeuchtigkeit und Windgeschwindigkeit) und schätzt deren Unsicherheiten für das 21. Jahrhundert ab. Darüber hinaus wird das RCM Ensemble bezüglich potentieller Verzerrungen aufgrund der limitierten Auswahl von Antriebsdaten durch globale Klimamodelle (GCMs) untersucht. Dabei werden statistische Rekonstruktions-methoden verwendet, um das Ensemble mit allen zur Verfügung stehenden GCM Antriebs-daten vom CMIP3 Projekt (esg.llnl.gov:8080) zu erweitern.

Wegener Center for Climate and Global Change
University of Graz
Brandhofgasse 5
A-8010 Graz, Austria
www.wegcenter.at
ISBN 978-3-9503112-7-3